The Dissertation Committee for Bryan David McCloskey certifies that this is the approved version of the following dissertation:

Novel Surface Modifications and Materials for Fouling Resistant Water Purification Membranes

Committee:

Benny D. Freeman, Supervisor

Donald R. Paul

Isaac C. Sanchez

Mukul M. Sharma

Todd S. Emrick

Novel Surface Modifications and Materials for Fouling Resistant Water Purification Membranes

by

Bryan David McCloskey, B.S.

Dissertation

Presented to the Faculty of the Graduate School of
The University of Texas at Austin
In Partial Fulfillment
of the Requirements
for the Degree of

Doctor of Philosophy

The University of Texas at Austin
December, 2009

Dedication

To my mother and father

ACKNOWLEDGEMENTS

My advisor, Dr. Benny Freeman, has been a wonderful source of information on membranes and life, in general. His guidance throughout my studies here at the University of Texas has been invaluable, and I extend my deepest gratitude to him for all of the opportunities he has presented to me. I would also like to thank Prof. Ho Bum Park of Hanyang University, whose singular brilliance, unbelievable work ethic, and unwavering friendship inspire me every day to achieve greatness. I would also like to thank my committee, Dr. Donald Paul, Dr. Mukul Sharma, Dr. Douglas Lloyd, Dr. Isaac Sanchez, and Dr. Todd Emrick, for their guidance.

I would like to thank all of my co-workers in Dr. Freeman's group over the years. In particular, Mr. Hao Ju has been a wonderful sounding board for many of my ideas, and I thank him for sharing his incredible thoughts with me. I would also like to thank Dr. Alyson Sagle, Dr. Scott Kelman, Dr. Scott Matteucci, Mr. Hua 'Richard' Li, Dr. Claudio Ribeiro, Dr. Victor Kusuma, Dr. Yuan-Hsuan Wu, Ms. Elizabeth Van Wagner, Mr. Daniel Miller and Mr. Brandon Rowe for their friendship and support during my studies. A significant amount of my studies was performed abroad in Prof. Young Moo Lee's and Prof. Heungsoo Shin's laboratories at Hanyang University. My time in Korea was transformative, and I am deeply grateful to Prof. Lee, Prof. Shin and their students, including Dr. Chul Ho Jung, Mr. Sang Hoon Han, Mr. Suresh Mulmi, Ms. So Young Lee, Mr. Hong Gun Kim, Ms. Jae Eun Lee, Mr. Chi Hoon Park, Ms. Eun Kyoung Lee, Mr. Young Min Shin, and Mr. Dong Won Shin. Many foreign visitors to Dr. Freeman's

laboratory provided me a world perspective that I treasure. Among them, I would like to particularly thank Mr. Domenico Foglia, Mr. Alberto Tena, Dr. Roberto Recio, Dr. Angel Lozano, Mr. Julien Wicker, Mr. Stephane Fredon, and Dr. Maria-Chiara Ferrari. Dr. Nathan Miller of the Jackson School of Geosciences at the University of Texas has helped collect all of the Inductively Coupled Plasma Mass Spectrometry data found in this thesis, and I appreciate his candor and quick responses to my requests.

I would also like to thank all of my friends and family who have encouraged and supported me during my studies. Last, but not least, no words can express the gratitude I owe my mother, Mrs. Debbie McCloskey, and my father, Mr. David McCloskey. Without them, my graduate studies would have been impossible, as the guidance they have given me has kept me grounded and focused.

The National Science Foundation (Graduate Research Fellowship, grant #CBET 0553957, Center for Layered Polymer Systems, grant #DMR0423914) and Advanced Hydro, Inc. provided generous financial support that I greatly appreciate.

NOVEL SURFACE MODIFICATIONS AND MATERIALS FOR FOULING RESISTANT WATER PURIFICATION MEMBRANES

Publication No._____

Bryan David McCloskey, Ph. D.

The University of Texas at Austin, 2009

Supervisor: Benny D. Freeman

A major challenge facing widespread implementation of membrane-based water purification is fouling, which results in increased operating costs and reduced membrane lifetime. This thesis focuses on various methods, including novel membrane surface modifications and polymers that resist degradation when exposed to oxidizing agents used as disinfectants, to alleviate membrane fouling.

Fouling-resistant ultrafiltration membrane coatings were prepared from poly(ethylene glycol) diglycidyl ether-crosslinked chitosan (chi-PEG hybrid). Composite membranes were prepared for oil-water emulsion filtration by coating the most promising chi-PEG hybrid onto a polysulfone ultrafiltration membrane. Optimization of the coating layer thickness led to composite membranes that exhibited water flux values more than 5

times higher than that of uncoated membranes after one day of oily-water crossflow filtration. The organic rejection of the coated membranes was also higher than that of the uncoated polysulfone membranes.

Polydopamine (PDOPA) deposition was discovered to reduce fouling in water purification membranes. PDOPA was found to deposit from solution onto virtually any surface. When deposited on water purification membranes, PDOPA rendered the membrane more hydrophilic and less susceptible to fouling. Moreover, covalent binding of other molecules, such as amine-terminated poly (ethylene glycol) (PEG), to PDOPA is simple and performed using benign chemicals and conditions. Commercially-available polymeric membranes were modified with polydopamine, and all showed improved fouling resistance while filtering oil-water emulsions. To demonstrate the versatility and ease of PDOPA modification scalability, PDOPA was deposited on entire membrane modules, and the resulting modified module exhibited improved fouling resistance.

Finally, high ion rejection, chlorine-tolerant sulfonated polysulfone thin-film composite membranes were prepared and characterized. Interestingly, freestanding thick sulfonated poly(arylene ether sulfone) (BPS) films exhibit nearly neutral electrostatic charge, even though sulfonation introduces fixed negative charge into the polymer structure. As a result, charge exclusion ion partitioning is not a dominant rejection mechanism in these films. However, composite membranes prepared from a BPS coating layer and a porous Udel polysulfone support exhibit a negatively charged surface and,

presumably, charge exclusion would be a more important partitioning mechanism for these membranes. Therefore, thick BPS films do not exhibit certain drawbacks, such as reduced salt rejection of mixed-valence feeds, that are observed in BPS thin-film composite membranes.

TABLE OF CONTENTS

List of tables **xv**

List of figures **xvii**

1. Chapter 1: Introduction- water scarcity and membrane technology **1**

1.1 Freshwater scarcity 1

1.2 Water purification technologies 3

1.3 Water purification membranes 3

1.4 Goals and organization of this dissertation 7

2. Chapter 2: Background- fouling and fouling alleviation **8**

2.1 Membrane purification of non-conventional water sources 8

2.2 Membrane fouling: a major challenge 10

2.3 Combating fouling in conventional water purification membranes 12

2.4 Biofouling and biofouling control 19

2.5 Modeling mass transport in membranes 21

2.5.1 Membrane pure water flux 21

2.5.2 Resistances in series model 23

3. Chapter 3: Materials and experimental methods **29**

3.1 Materials 29

3.1.1 Chitosan-PEG hydrid coating materials 29

3.1.2 PDOPA and PDOPA-g-PEG materials 29

3.1.3 Sulfonated poly(arylene ether sulfone) materials 30

3.1.4 Materials common to all studies 31

3.2 Methods 31

3.2.1 Preparation of PEG-Chitosan hybrid prepolymerization solution 31

3.2.2 Preparation of freestanding PEG-chitosan hybrid films 32

3.2.3 Preparation of PEG-Chi hybrid-coated UF membranes 32
3.2.4 PDOPA deposition on flat membrane sheets and subsequent PEG attachment 33
3.2.5 PDOPA modification of TW30 membrane modules 34
3.2.6 Sulfonated poly(arylene ether sulfone) synthesis 35
3.2.7 BPS thin film composite preparation 36
3.2.8 Pure water flux measurement 38
3.2.9 Salt rejection (single and mixed valence) analysis 42
3.2.10 Arsenic rejection analysis for BPS membranes 43
3.2.11 Crossflow emulsified oil fouling experiments: NF, RO, and PEG-chitosan hybrid composite membranes 43
3.2.12 Emulsified oil fouling measurements: UF and MF flat sheet membranes 44
3.2.13 Emulsified oil fouling experiments: TW 30 membrane modules 45
3.2.14 Irreversible fouling determination 46
3.2.15 BSA adhesion measurements 47
3.2.16 Static bacterial adhesion 48
3.2.17 PDOPA leaching from TW30 membrane modules 50
3.2.18 Molecular weight cutoff/solute rejection properties 52
3.2.19 Scanning electron microscopy (SEM) 53
3.2.20 Fourier transform infrared spectroscopy (FTIR) 53
3.2.21 Contact angle measurements 54
3.2.22 Streaming zeta potential measurements 54
3.2.23 Atomic force microscopy (AFM) measurements 55
3.2.24 PDOPA deposition thickness measurements on polysulfone 55

4. Chapter 4: Composite membranes based on a selective chitosan-poly(ethylene glycol) hydrid layer: synthesis, characterization, and performance in oil-water purification 57

4.1 Summary 57

4.2 Introduction 58

4.3 Results and Discussion 60

4.3.1 Freestanding film characterization 60

4.3.2 Composite membrane characterization 64

4.3.3 Oil fouling experiments 69

4.4 Conclusions 72

5. Chapter 5: A universal, biofouling-inspired surface modification to increase water purification membrane fouling resistance 74

5.1 Summary 74

5.2 Introduction 74

5.3 Results and Discussion 78

5.3.1 Effect of PDOPA deposition on membrane flux and surface property characteristics 78

5.3.2 PDOPA leaching from a TW30 Dow Filmtec RO membrane module 86

5.3.3 Oil emulsion fouling on unmodified, PDOPA modified and PDOPA-g-PEG modified membranes 88

5.3.4 Irreversible oil emulsion fouling of unmodified and PDOPA-modified membranes 95

5.3.5 Positively-charged DTAB-decane emulsion fouling of XLE RO membranes 96

5.3.6 Protein and bacterial adhesion to unmodified and PDOPA-modified membranes 99

5.3.7 Oil emulsion fouling of TW30 Dow Filmtec RO membrane modules 102

5.4 Conclusions 105

6. Chapter 6: Influence of polydopamine deposition conditions on pure water flux and foulant adhesion resistance of Reverse osmosis, ultrafiltration, and microfiltration membranes 106

6.1 Summary 106

6.2 Introduction 107

6.3 Background 109

6.3.1 Hydraulic resistance of PDOPA and PDOPA-g-PEG modified membranes 109

6.4 Results and Discussion 111

6.4.1 Polydopamine modification of XLE RO, PS-20 and PSF A1 UF, and PVDF MF membranes: pure water flux 111

6.4.2 PEG grafting to PDOPA modified XLE RO, PS-20 UF, and PVDF MF membranes 116

6.4.3 BSA adhesion resistance 127

6.4.4 Correlation between BSA adhesion resistance and total flux loss due to PDOPA or PDOPA-g-PEG. 134

6.5 Conclusions 136

7. Chapter 7: Probing ion partitioning via charge exclusion in sulfonated polysulfone materials 138

7.1 Summary 138

7.2 Introduction 139

7.2.1 Sulfonated polysulfone as a chlorine-tolerant desalination membrane candidate 139

7.2.2 BPS dense film and thin film composite salt rejection 141

7.2.3 Ion partitioning mechanisms in membranes with fixed charges 142

7.3 Results and Discussion 143

7.3.1 Support membrane pretreatment to prevent pore collapse 143

7.3.2 Solvent selection for BPS TFC membrane preparation 146

7.3.3 BPS thin film composite characterization: Water flux and NaCl rejection 147
7.3.4 Surface charge and salt passage of post-polymerization sulfonated polysulfone and BPS dense films 150
7.3.5 Arsenic speciation and rejection in polyamide RO and BPS dense films 156
7.3.6 Surface charge and salt passage of BPS thin-film composite membranes 159
7.4 Conclusions 163
8. Chapter 8: Conclusions and recommendations 165
8.1 Conclusions 165
8.2 Recommendations 169
9. References 174
VITA 190

LIST OF TABLES

Table 2.1: Comparison of energy requirements and costs between evaporation and membrane processes. The numbers in parenthesis indicate the percent increase in total solids as a result of the concentration process. Adapted from [10] 9

Table 2.2: Selected studies using polymer coatings to enhance membrane fouling resistance. 19

Table 4.1: Pure water permeance of membranes at 60 psi (4.1 atm) before and after using the membranes to filter oil/water emulsions for one day. 70

Table 5.1 Commercial membranes used in this study. 76

Table 5.2: Influence of PDOPA deposition time on captive *n*-decane-in-water contact angles of PSF A1 UF membranes. 82

Table 5.3: Captive n-decane-in-water (XLE RO) or air-in-water (PVDF MF) bubble contact angles. 83

Table 5.4: Common bond rupture forces for selected bonds. 88

Table 5.5: Relative fluorescent intensity (λ_{em}=575 nm) of rhodamine-tagged BSA on a variety of membrane surfaces. 101

Table 5.6: Initial salt rejection and irreversible fouling data for TW30 unmodified and modified modules. The salt rejection was measured with no organics in the feed solution. 104

Table 6.1: Membranes used in this study. 108

Table 6.2: Influence of PDOPA deposition on membrane hydraulic resistance. 115

Table 6.3: Modification parameters for membranes numbered in Figure 6.8. 136

Table 7.1: Comparison of NaCl rejection of BPS materials in freestanding dense film form and thin-film composite (TFC) form. 142

Table 7.2: Surface tensions and boiling points of liquids used in the pretreatment of Udel polysulfone supports during composite membrane preparation. Surface tension values from [149]. Boiling point values from Sigma Aldrich. 144

Table 7.3: Water uptake, ion exchange capacity (IEC), and zeta potential (pH=7) for BPS-20H, 20K, and 32K freestanding films. Water uptake and ion exchange capacity data are from [22]. 156

Table 7.4: Salt rejection values for BPS TFC membranes. 162

LIST OF FIGURES

Figure 1.1: Water scarcity index. An area with water scarcity index of 0.4 or higher is considered highly water-stressed.[1] 2

Figure 1.2: Membrane classifications and filtration capabilities.[11] Human serum albumin is abbreviated HSA. 4

Figure 2.1: a. A schematic of particulate fouling in porous water purification membranes.[17] b. The influence of protein fouling on permeance vs. time in a conventional MF membrane in crossflow protein filtration. Filtration parameters: 1 g/L BSA in pH=7.4 phosphate buffered saline, 25 cm/s crossflow velocity, transmembrane pressure difference (TMP)=10 bar, 0.2 μm nominal pore size PVDF membrane (Pall Corp, hydrophilic PVDF, Port Washington, NY). 12

Figure 2.2: Crossflow filtration and resulting shear stress on a membrane surface. 13

Figure 2.3: A conventional MF membrane in backpulsed and non-backpulsed crossflow filtration. Conditions: 0.2 μm nominal pore size PVDF membrane (Pall Corp., hydrophilic PVDF, Port Washington, NY), 1350 ppm soybean oil, 150 ppm DC193 surfactant oil-water emulsion, 25 cm/s crossflow, TMP=10 bar. Backpulse conditions: backpulse frequency= 0.1 min^{-1}, backpulse duration= 10 s. 15

Figure 2.4: Hydrophilic grafting and coating onto conventional polymer membranes to improve fouling resistance. 16

Figure 2.5: A schematic of a resistance in series model for a fouled membrane. 25

Figure 2.6: Schematic describing protocol to characterize mass transfer resistance associated with fouling. J_s and $J_{s,f}$ (the salt water fluxes of a non-fouled and fouled membrane, respectively) are measured only in membranes that reject ions (*i.e.*, NF and RO membranes). All measurements are performed at the same TMP and temperature (25 °C). The water rinsing cycle is discussed in Chapter 3. 26

Figure 3.1: Structure of Jeffamine M-1000. 30

Figure 3.2: Schematic of PDOPA modification apparatus for TW30 Dow Filmtec modules. The module's feed and retentate ports (NPT 1/8") were connected to flexible tubing which led to the beaker containing the

PDOPA solution. PDOPA deposition was visibly present on the tubing and the membrane module after ~30 min deposition time. 35

Figure 3.3: The sulfonated polysulfone copolymers (BPS series) used in this study (n=20-50%). M^+ can be either a K^+ or Na^+ counterion or a free acid (H^+). 36

Figure 3.4: a) Dead-end filtration cell and b) ultrafiltration, nanofiltration, and reverse osmosis crossflow system. 39

Figure 3.5: UV absorbance at λ=280nm of aqueous solutions containing various concentrations of PDOPA. 52

Figure 4.1: Synthesis of a chitosan-PEG hybrid network 60

Figure 4.2: (a). Surface SEM images of films made from a 1.4 PEGDGE/chitosan prepolymerization solutions, and (b). 2.0 PEGDGE/chitosan prepolymerization solutions. 62

Figure 4.3: (a). Pure water permeability vs. film thickness for a series of chitosan/PEG hybrids. The pure water permeability of the nonporous films are: 1.33 PEG/chitosan ratio=31.7±5.8 L μm m^{-2} hr^{-1} atm^{-1}, 0.66 PEG/chitosan ratio=3.8±0.5 L μm m^{-2} hr^{-1} atm^{-1}. (b). PEG rejection curves for films made from 0.66, 1.33, and 2.0 PEGDGE/chitosan solutions. The numbers next to the curves indicate the PEGDGE/chitosan ratio of the film's prepolymerization solution. 63

Figure 4.4: SEM cross sectional image of a PSf membrane coated with a 1.4 PEG crosslinker to chitosan ratio solution (1.5 wt% chitosan). Approximate solution coating thickness was 80 μm, leading to a final coating thickness of ~0.7 μm. 65

Figure 4.5: ATR FTIR spectra of an uncoated PSf membrane, a 1.4 PEGDGE/chitosan film, and three composite membranes (a-c) using the following coating solution concentrations: a. 1.0 wt% chitosan, b. 1.25 wt% chitosan, c. 1.5 wt% chitosan. All coating layers were formed from a 1.4 PEGDGE/chitosan ratio solution. The spectra were displaced vertically for easier viewing. 67

Figure 4.6: Pure water permeance as a function of pressure for three PSf/chi-PEG hybrid composite membranes. The numbers above the bars on the far right hand side of the graph represent the weight percent chitosan in the prepolymerization solution. The bars of similar shading at other

pressures correspond to samples of these same chitosan concentrations. All coating solutions had a 1.4 PEGDGE/chitosan ratio. Error bars were calculated using the standard deviation of three 3.5 cm^2 and one 14.6 cm^2 diameter membranes cut from the same membrane sample. 69

Figure 4.7: (a). Permeate flux as a function of time for the filtration of an oil/ water emulsion (1350 ppm vegetable oil, 150 ppm DC193 surfactant) at 6.8 atm and a crossflow flowrate of 1.3 L/m (Re~1400). (b). Total organic rejection as a function of time. (♦) 1.5 composite, (●) 1.25 composite, (▲) 1.0 composite, and (○) uncoated PSf membranes. 71

Figure 5.1: An illustration of emulsified oil membrane fouling and PDOPA-g-PEG membrane modification to improve fouling resistance of a porous membrane. PDOPA modification (indicated by the brown outlines) is uniform and ultra-thin (~5 nm), leading to a conformal coating of the membrane surface and pore structure. PEG grafting to the PDOPA layer is achieved using aqueous-based chemistry. Many PDOPA and PDOPA-g-PEG-modified membranes exhibit improved fouling resistance, including a poly(vinylidene fluoride) MF membrane (PVDF MF), whose unmodified and PDOPA-g-PEG modified oil emulsion filtration fluxes are presented here. Rejection values were measured at the end of the filtration (t=1h). Filtration conditions: 1350 ppm soybean oil, 150 ppm DC193 (Dow Corning) surfactant, 2 L/m crossflow (Re~2600), ΔP=0.3 atm. 77

Figure 5.2: Pure water permeance as a function of PDOPA deposition time on a polysulfone ultrafiltration membrane (PSF A1 UF), and PDOPA deposition thickness as a function of PDOPA deposition time on Udel polysulfone thin films.[80] 79

Figure 5.3: Effect of PEG molecular weight on rejection by an unmodified PSF A1 UF membrane. From these data, the molecular weight cutoff is approximately 92.5 kDa. Adapted from [55] 80

Figure 5.4: Streaming zeta potential, ζ, of an unmodified, PDOPA-modified, and PDOPA-g-PEG modified XLE RO membrane. A 60 min PDOPA deposition time and 60 min PEG (5 kDa) grafting time were used in the respective modifications. Lines were drawn to guide the eye. 85

Figure 5.5: Atomic force microscopy images of unmodified and PDOPA-modified PSf A1 UF, NF-90, and XLE RO membranes. The root-mean-square roughness of each image is listed below each image. 86

Figure 5.6: Total leaching of PDOPA from a TW30 membrane module while being rinsed with ultrapure water. PDOPA leaching was measured using UV absorbance. Line was drawn to guide the eye. 88

Figure 5.7: Effect of filtration time on membrane flux using unmodified, PDOPA-modified, and PDOPA-g-PEG-modified: a) polysulfone ultrafiltration (PS-20 UF) , b) PTFE MF, c) NF-90, and d) XLE RO membranes to filter an oil/water emulsion. Rejection values (organic rejection for MF and UF membranes, salt rejection for NF and RO membranes) were measured at the end of the filtration (t= 1 h for UF and MF membranes, t=24 h for NF and RO membranes). A 1350 ppm soybean oil, 150 ppm DC193 non-ionic surfactant emulsion was used as the organic foulant in this study.....91

Figure 5.8: Effect of filtration time on membrane flux using unmodified, PDOPA-modified, and PDOPA-g-PEG-modified: a) PES UF, b) PVDF MF, and c) PP MF membranes to filter an oil/water emulsion. Organic rejection values were measured at the end of the filtration (t= 1h). A 1350 ppm soybean oil, 150 ppm DC193 non-ionic surfactant emulsion was used as the organic foulant in this study.....92

Figure 5.9: Dow Water Solutions a) NF-90 and b) XLE RO membrane NaCl rejection before oil emulsion filtration (hollow markers) and during an oil emulsion filtration (filled markers). 2000 ppm NaCl solution was used for all experiments. An oil emulsion (1350 ppm soybean oil and 150 ppm DC193 surfactant) was added to the membrane feed after "pure" salt water rejection was measured. 95

Figure 5.10: Irreversible fouling in PS-20 UF, PTFE MF, NF-90, and XLE RO membranes. $P_{w,f}$ is the pure water permeance following the filtration experiments in Figure 5.7a-d, and $P_{w,o}$ is pure water permeance before the filtration experiments. After the fouling experiments, all membranes were rinsed by circulating ultrapure water through the crossflow system before measuring $P_{w,f}$. Membrane characteristics (i.e., pore sizes, nominal fluxes, manufacturers, etc.) are listed in Table 5.1.....96

Figure 5.11: DTAB- decane positively-charged emulsion fouling experiments performed on unmodified, PDOPA-modified, and PDOPA-g-PEG-modified XLE RO membranes. a) Flux as a function of time, and b) post-fouling pure water permeance and the irreversible fouling seen in each membrane tested in Figure 5.11a. $P_{w,f}$ is the pure water permeance following the filtration experiments in Figure 5.11a, and $P_{w,o}$ is pure water permeance before the filtration experiments. After

the fouling experiments, all membranes were rinsed by circulating hot (50 °C) ultrapure water through the crossflow system before measuring $P_{w,f}$. Filtration conditions: ΔP= 150 psi, 3.8 L/min crossflow (Re~4900), 15 ppm DTAB, 135 ppm decane, 2000 ppm NaCl. 98

Figure 5.12: Rhodamine-tagged BSA adhesion on PES UF and PP MF membranes. Fluorescent microscopy images were recorded at 1 ms (exposure time insets are 80 ms) for PES membranes and 5 ms (insets are 500 ms) exposure time for PP membranes....100

Figure 5.13: *P aeruginosa* adhesion (as measured by the bacteria's luminescence) to unmodified, PDOPA-modified and PDOPA-g-PEG-modified membranes. A 60 min PDOPA deposition time and a 60 min PEG grafting time was used for all modifications....102

Figure 5.14: Effect of filtration time on permeate water flow rate, normalized by the transmembrane pressure difference, for an unmodified TW30 membrane module, a PDOPA-modified module, and a PDOPA-g-Jeffamine-modified module filtering an oil/water emulsion. Rejection values are for NaCl measured following 24 hours of filtration. Filtration conditions: 3.8 L/min feed flowrate, ΔP= 3.4 bar (50 psi), 25 °C. The feed was an aqueous solution containing 1350 ppm soybean oil, 150 ppm DC193 surfactant, 250 ppm NaCl and had a pH of 7.3.....104

Figure 6.1: The influence of PDOPA deposition time on the ratio of PDOPA-modified membrane pure water flux (J_{PDOPA}) to unmodified membrane pure water flux (J_o). Error bars represent standard deviations from at least 3 separate experiments....113

Figure 6.2: The ratio of pure water flux of PDOPA-g-PEG modified membranes, J_{PEG}, to the pure water flux of PDOPA-modified membranes, J_{PDOPA}, as a function of: a) PEG grafting temperature, b) PEG grafting time, and c) PEG-NH_2 concentration in the grafting solution. A 60 min PDOPA deposition (2 mg/mL dopamine, 15mM tris, pH=8.8, ambient conditions) was used for all membranes prior to PEG grafting. All PEG grafting was performed using 5 kDa PEG-NH_2 in 15 mM tris buffer at pH=8.8.....117

Figure 6.3: PEG grafting density on PDOPA-modified PS-20 UF membranes as a function of: a) PEG-NH_2 grafting time, and b) PEG-NH_2 concentration in the grafting solution. Grafting conditions for a): 1 mg/mL 5 kDa PEG-NH_2, 60 °C, 15 mM tris buffer (pH=8.8), and b): 60 min grafting time using 5 kDa PEG-NH_2, 60 °C, 15 mM tris buffer (pH=8.8). All

values were obtained via gravimetric analysis. A 60 min PDOPA deposition (2 mg/mL dopamine, 15mM tris, pH=8.8, ambient conditions) was used for all membranes prior to PEG grafting. 121

Figure 6.4: Hydraulic resistance of PEG grafted to PDOPA-modified: a) PVDF MF, b) PS-20 UF, and c) XLE RO membranes as a function of PDOPA deposition time and PEG-NH_2 molecular weight. PDOPA deposition conditions: 2 mg/mL dopamine in tris buffer (15 mM, pH=8.8) at ambient conditions. PEG grafting conditions: 60 min (PVDF MF and PS-20 UF) or 30 min (XLE RO) PEG grafting time using $2x10^{-4}$ mol/L PEG-NH_2, 60 °C, tris buffer (15 mM, pH=8.8). Standard errors were (in m^{-1}): $1.2x10^{9}$ (PVDF MF), $1.6x10^{10}$ (PS-20 UF), and $1.0x10^{13}$ (XLE RO). Standard errors were calculated from at least 2 replicate trials of 4 data points for each membrane. 125

Figure 6.5: PEG grafting density as a function of PDOPA deposition and PEG-NH_2 molecular weight on: a) PVDF MF, b) PS-20 UF, and c) XLE RO membranes. All values were obtained via gravimetric analysis. PDOPA deposition conditions: 2 mg/mL dopamine in tris buffer (15 mM, pH=8.8) at ambient conditions. PEG grafting conditions: 60 min (PVDF MF and PS-20 UF) or 30 min (XLE RO) PEG grafting time using $2x10^{-4}$ mol/L PEG-NH_2, 60 °C, tris buffer (15 mM, pH=8.8). Error bars are the standard error of at least two replicate trials. 126

Figure 6.6: Influence of PDOPA deposition time on normalized fluorescent intensity of BSA adhered to: a. PVDF MF, b. PS-20 UF, and c. XLE RO membranes. Rhodamine-tagged BSA was used, and the intensity of the BSA adhered to the membrane was measured using $\lambda_{ex}/\lambda_{em}$=525 nm/575 nm and a plate reader. All intensities were normalized to the adhered BSA intensity measured on an unmodified membrane. 130

Figure 6.7: Influence of a. PEG grafting time and b. PEG-NH_2 conentration in the grafting solution on normalized fluorescent intensity of BSA adhered to PVDF MF, PS-20 UF, and XLE RO membranes. Prior to PEG grafting, these membranes were first PDOPA-modified using a 60 minute PDOPA deposition time at ambient conditions and the following dopamine solution: 2 mg/mL, 15mM tris, pH=8.8. 134

Figure 6.8: BSA adhesion reduction as a function of the ratio of modified membrane flux, J_T, to the unmodified membrane flux, J_o. 135

Figure 7.1: A typical polyamide crosslinked structure and the sulfonated polysulfone copolymers (BPS series) used in this study (n=20-50%). M+ can be either a K+ or Na+ counterion or a free acid (H+). 140

Figure 7.2: a. Influence of pretreatment solution content on ultrapure water flux (ΔP=1.4 atm) of porous Dow Water Solutions polysulfone support membranes. * indicates that the membranes were not dried before water flux measurements; essentially no water flux was observed in these two membranes following drying. The drying process was to maintain the membrane at ambient conditions for 2 hours. b. Water flux after drying under vacuum for 2 hours at various temperatures. 145

Figure 7.3: SEM images of BPS-20K (a) and BPS-20H (b) thin film composite membranes on a polysulfone support. The BPS layer is clearly seen on the surface of the support membrane. Both membranes were prepared using a 0.2% BPS coating, followed by three 0.1% BPS coatings. Adapted from[150]. 148

Figure 7.4: Salt passage through a post-polymerization sulfonated polysulfone membrane (Hi-Flux CP, ▲ and ■) and two BPS dense films in the presence of Ca^{2+} ions. Hi-Flux CP data from[151]. 151

Figure 7.5: Streaming zeta potential of XLE polyamide RO membrane and Udel, Radel, and post-polymerization sulfonated Radel polysulfone. 10 mM NaCl in water was used as the reference solution and a pressure ramp of 300 mbar was used for each measurement. 153

Figure 7.6: Streaming zeta potential of acid (left) and potassium (right)-form BPS materials compared to Radel and post-polymerization sulfonated Radel. 10 mM NaCl in water was used as the reference solution and a pressure ramp of 300 mbar was used for each measurement. 156

Figure 7.7: As(V) and As(III) rejection by an RO membrane (ES-10, Nitto Denko). Adapted from [156]. 158

Figure 7.8: a. As(V) and b. As(III) rejection of BPS dense films 159

Figure 7.9: Streaming zeta potential of selected BPS dense films and TFCs in (a.) acid and (b.) potassium salt form. 10 mM NaCl in water was used as the reference solution and a pressure ramp of 300 mbar was used for each measurement. 160

Figure 7.10: Sodium ion passage in BPS dense films and BPS thin-film composites. Testing conditions for the TFCs: 3.8 L/min crossflow, ΔP=400 psi, T=25 °C, pH= 6.7, 380 ppm NaCl (150 ppm Na^{+}). 161

Figure 7.11: Arsenate (As(V)) and arsenite (As(III)) rejection at various pH using a BPS-32K TFC membrane. 3.8 L/min crossflow, ΔP=400 psi, T=25 °C, 10 mM NaCl. 163

Figure 8.1: Synthesis of PEG-NH_2 from low cost PEG-OH. 172

1. CHAPTER 1: INTRODUCTION- WATER SCARCITY AND MEMBRANE TECHNOLOGY

1.1 Freshwater scarcity

Water scarcity is one of the largest concerns facing modern society. Although water covers nearly two-thirds of the earth's surface, only 2.5% of this water is fresh, and most freshwater is found in glaciers and deep groundwater that is not easily accessible.[1] Furthermore, in developing countries, biological pollutants introduced by human activities into existing freshwater rivers, streams, lakes, and irrigation canals decrease the total available freshwater even further and increase the risk of waterborne diseases.[2] In 2002, 2.6 billion people lived in unacceptable sanitary conditions. By 2025, this number is projected to be around 3.5 billion.[3, 4] Because of poor water quality in many third world countries, almost 5000 children die *per day* due to diarrheal diseases. As population increases and developing nations become more industrially advanced, demand for freshwater will increase. This demand has made many areas of the world highly water-stressed, and future projections show escalating water scarcity throughout the world.

This problem is exacerbated by the uneven distribution of freshwater throughout the world, and large populations live in areas that are arid. Figure 1.1 is a map of the Water Scarcity Index (defined as the total human withdrawal of freshwater from renewable freshwater supplies divided by the total renewable freshwater supplies available) throughout the world.[1] Areas with a Water Scarcity Index of 0.4 or higher are

considered highly water-stressed. As can be seen, freshwater supply is a major problem in regions of the world where rainfall is short and populations are high, such as parts of the Middle East, Africa, China, India, and even the United States.

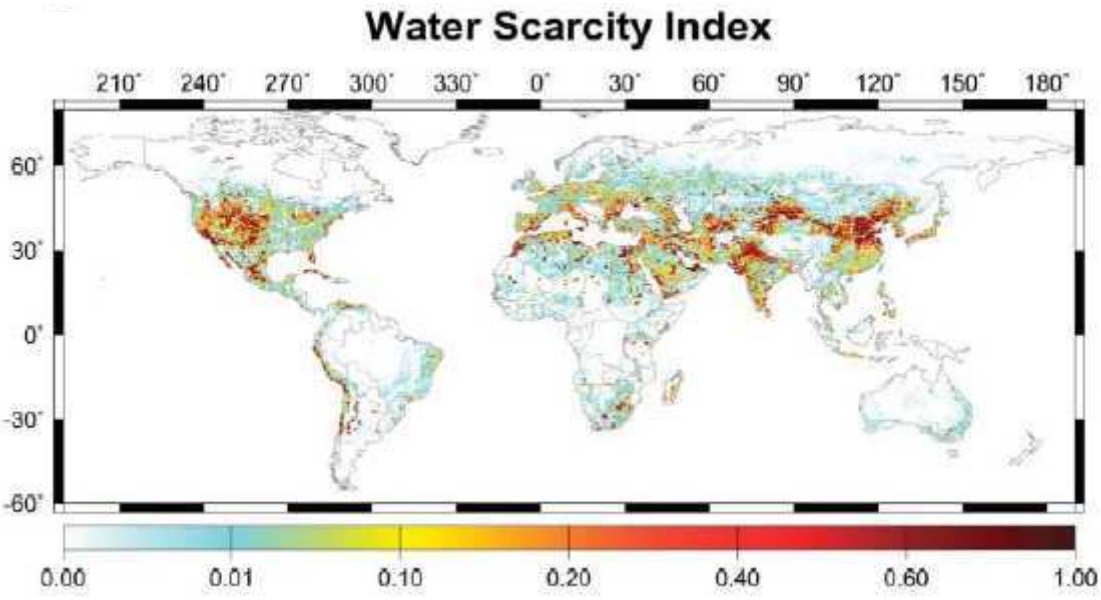

Figure 1.1: Water scarcity index. An area with water scarcity index of 0.4 or higher is considered highly water-stressed.[1]

In the next few decades, a water crisis could potentially affect the United States - more specifically the western, more arid regions of our Nation - due to an explosion of population, already over-allocated aquifers, and aging water treatment facilities.[5, 6] The demand for freshwater in municipal and agricultural applications is ever increasing. Meeting future water demands will be a challenge, especially since United States Environmental Protection Agency (EPA) requirements protect many sensitive aquatic environments that will be affected by depleting our high-quality water sources.[6] Therefore, both the EPA and the Department of the Interior have proposed updating and expanding our nation's current water treatment infrastructure to address anticipated future

water supply problems. Potential water sources, such as seawater and produced water from oil and natural gas processing, are often located near highly arid and densely populated regions.[1, 7] If such water could be economically purified, immediate relief could be provided in water-scarce areas.

1.2 Water purification technologies

There are many water purification technologies available, each having a relatively specialized application. These include activated carbon filters for removal of organic compounds and chlorine, ultraviolet radiation and chlorine treatment for sterilization of microorganisms such as bacteria and viruses, distillation for removal of nonvolatile contaminants, and deionization (or ion exchange) for desalination.[8] However, none of these technologies can completely purify water alone (*e.g.*, carbon filters cannot remove bacteria or ions from water, distillation cannot remove volatile organic compounds, UV cannot kill cysts and does not remove any other contaminants, etc.). Furthermore, distillation, probably the most common water purification technology other than membrane technology, is highly energy intensive and is, therefore, not as economically viable in many cases as membranes.[9] Membranes are an attractive solution to water purification based on their versatility (*i.e.*, membranes can remove nearly all water contaminants), small footprint and inherent economic advantages over other alternatives.

1.3 Water purification membranes

A membrane can be defined as a barrier to mass transport in which transport of certain molecules or particles is either completely or partially restricted.[10] Synthetic

industrial membranes are used to either purify or enrich a feed stream and are often size-selective. That is, larger particles or molecules will have more limited transport through the membrane than smaller molecules. Liquid purification membranes are usually divided into two large categories, porous and nonporous, and multiple subcategories: microfiltration (MF), ultrafiltration (UF), nanofiltration (NF), and reverse osmosis (RO). Figure 1.2 provides a brief description of the size-sieving capabilities of each membrane class, each of which is discussed in more detail below.

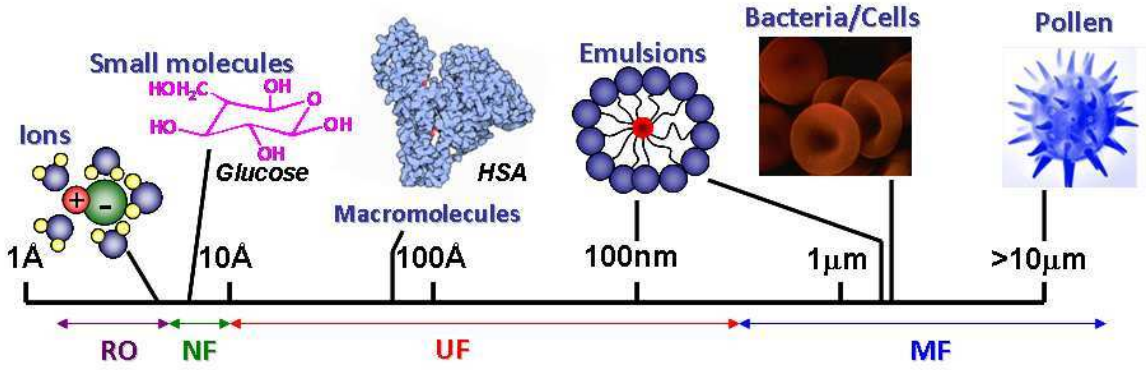

Figure 1.2: Membrane classifications and filtration capabilities.[11] Human serum albumin is abbreviated HSA.

Microfiltration membranes are used to purify liquid streams containing particles with effective hydrodynamic diameters ranging from 0.1 μm to 10 μm. They are often applied to separations involving bacteria, virus or cell (all of which usually have a hydrodynamic diameter in between 0.1 μm and 5 μm) removal in food and pharmaceutical industries, as well as drinking water treatment.[10, 12] Wastewater treatment, in which particulates and colloidal matter are the primary contaminants, can also be accomplished using MF membranes.[10, 13] Microfiltration membranes are typically

fabricated from polymers such as polyethylene, polypropylene, poly(tetrafluoroethylene), and poly(vinylidene fluoride).[10]

Ultrafiltration membranes are commonly used to purify liquid streams containing macromolecules (*e.g.*, proteins and polysaccharides) and particles with effective diameters ranging from 1 nm to 100 nm.[10] For example, UF membranes are used to separate lactose and water from milk proteins in cheese production and other dairy processes, clarify fruit juices, remove organics in highly stable oil-water emulsions, and concentrate and purify valuable pharmaceutical products from fermentation operations in biotechnology applications.[13] They also have enormous potential to treat wastewater streams containing small colloidal particles and organic matter, such as end-product wastewater in latex emulsion processing plants, poultry farms, metalworking facilities, food and beverage processing plants, textile plants, and sewage waters.[10] Ultrafiltration membranes are typically fabricated from hydrophobic polymers such as polysulfone, polyethersulfone, and poly(vinylidene fluoride), although polyacrylonitrile and other somewhat more hydrophilic polymers are also used to prepare UF membranes.[10] Furthermore, both MF and UF membranes are being explored as possible candidates to replace conventional flocculation/sedimentation/clarification pretreatment for RO-based seawater desalination.[14-16] Membrane pretreatment requires smaller amounts of costly flocculants (such as ferric chloride), and the pretreated water quality is much higher when using membrane filtration.[10] In other words, membranes remove more organic

contaminants from seawater than conventional pretreatment, which, in turn, reduces fouling of the desalting RO membranes (fouling will be discussed in Chapter 2).

MF and UF membranes are similar in that they are both porous membranes in which particles are rejected based on their size relative to the membrane's pore size. In reverse osmosis (RO) membranes, the "pore" size is on the order of the membrane's polymer chain mobility (on the order of a few angstroms).[17] Therefore, these membranes are generally considered to be nonporous. Molecular transport through RO membranes obeys a solution-diffusion mechanism[18, 19]. In other words, molecules are separated by differences in their solubility and diffusivity in the membrane. Furthermore, most RO processes are used mainly for desalting sea and brackish water, with approximately 50% of RO systems being used for this application.[13] Other applications for RO include producing ultrapure water for the electronics and pharmaceutical industries and wastewater treatment.[13]

NF membranes are often used to purify water containing divalent ions or dissolved organic solutes with molecular weights around 100.[10, 13, 18, 20] NF membranes have small permanent pores that are approximately one order of magnitude larger than atomic dimensions, but are still much smaller than UF membrane pores.[21] They have higher flux than RO membranes and can, therefore, be used at lower operating pressures. However, they have lower rejection of small ions, such as sodium and chloride, than RO membranes.[18] The RO and NF market is dominated by interfacially polymerized

polyamide membranes, because traditional cellulose acetate membranes are much more prone to biological attack and are not as competitive with respect to water flux or salt rejection.[22]

1.4 Goals and organization of this dissertation

The main focus of this dissertation is aimed at exploring surface modification strategies to control membrane fouling. Additionally, some studies were also performed on new chlorine-tolerant desalination membranes. In this regard, the thesis is organized around the following main topics:

1.) Surface modification of UF membranes using hydrogel-based coatings (Chapter 4).

2.) Surface modification of membranes using novel bioinspired polymer deposition (Chapter 5 and 6) to reduce oil emulsion, protein, and bacterial fouling.

3.) Preparation and characterization of chlorine-resistant reverse osmosis membranes based on sulfonated polysulfones (Chapter 7).

Chapter 2 provides basic concepts of fouling and strategies to control fouling in membranes. Chapter 3 presents the experimental methodology used throughout the subsequent chapters. Conclusions and recommendations for future studies are provided in Chapter 8.

2. CHAPTER 2: BACKGROUND- FOULING AND FOULING ALLEVIATION

2.1 Membrane purification of non-conventional water sources

Amid growing water scarcity and depleted freshwater supplies, there has been significant interest in purifying various "non-conventional waters." These "non-conventional waters" include seawater, brackish water[23], and various wastewaters, such as produced water[24] and sewage.[25-27] Recent advances have made membrane technology competitive compared to other purification processes. For example, purified water from the RO seawater desalting plant in Ashkelon, Israel costs approximately $0.52/m^3, [4, 28] whereas evaporative desalting processes such as multi-stage flash and multi-effect distillation consume nearly 10 times more energy,[4] contributing to a much larger carbon footprint, and cost as much as $1.00-1.40/m^3 of purified water.[29] As shown in Table 2.1, membranes can also have lower energy and capital costs than evaporative technologies for concentrating processes. Membrane bioreactor (MBR) treatment of wastewaters has also captured significant market share from conventional flocculation/clarification technologies.[25] In 2005, MBR purification of municipal wastewaters was valued at $217 million and was growing 10.9% per year, which was faster than any other treatment method.[25]

Table 2.1: Comparison of energy requirements and costs between evaporation and membrane processes. The numbers in parenthesis indicate the percent increase in total solids as a result of the concentration process. Adapted from [10].

Concentration Process	Evaporation	Membrane
Whole Milk (2.2x)	136 kcal/kg	17 kcal/kg
Corn Steep Liquor (8x), 300 gpm	$1.2M/yr	$390K/yr
Gelatin (9x), 20 tons/h	$516K/yr	$186K/yr

As discussed in section 1.3, different membranes have been developed to treat various types of water. For example, MF and UF membranes are generally used in applications involving removal of large (>10 nm) organic contaminants because they have sufficient rejection of these contaminants while maintaining high flux. Therefore, these membranes are typically used in MBRs[26, 27], seawater RO pretreatment[16], and food and beverage concentration processes.[10] Typical contaminants in MBR and seawater treatment include bacteria, polysaccharides, proteins, soluble inorganic salts (such as sodium, arsenic, and boron salts), particulates, and natural organic matter.[26] Other wastewaters, such as produced water from oil and gas production and wastewaters from many industrial processes, contain surfactants and emulsified oil.[30] All of these contaminants (with the exception of soluble salts), can lead to membrane fouling.

This thesis focuses primarily on fouling by emulsified oil because of the aggressive fouling nature of oils and the problem posed by management of water produced from oil and natural gas recovery, as well as purification of oil-water emulsions from other manmade sources. Produced water is the single largest waste stream from oil and gas operations, with 7 cubic meters of water produced for every cubic meter of equivalent oil or gas.[24] An estimated 340 million barrels (bbl) of produced water are

handled every year in the US alone.[7] Typical contaminants include residual hydrocarbons, heavy metals, radionuclides, inorganic salts, suspended emulsions, and surfactants, many of which are aggressive foulants.[24] To protect surface waters and soil from contamination, subsurface re-injection is the usual disposal method for produced water, which costs an estimated $0.50/bbl to $1.75/bbl due to the large capital required for drilling.[7] However, membrane treatment to purify ~80% of this water for beneficial use, such as irrigation or livestock consumption, is estimated to cost only $0.08-$0.10/bbl.[7] However, membrane fouling is an issue that must be remedied before membranes can be widely implemented for produced water purification. Furthermore, other wastewaters that could be purified for beneficial use, such as those produced from metalworking operations, can contain significant amounts of oil contaminants.[10, 31] Additionally, oil emulsion fouling of membranes is a key problem in membrane-based purification of bilgewater aboard ships.[32]

2.2 Membrane fouling: a major challenge

A key concern facing water purification membranes is fouling. When filtering a solution with two or more components, membranes usually reject one or more of these components to a greater extent than the others. For example, when filtering oil-water emulsions, UF membranes will generally reject a large percentage of the organic components while allowing water to permeate preferentially. As the feed solution approaches the surface of the membrane, a buildup of the rejected emulsified oil droplets occurs, creating a concentration gradient near the membrane surface. The buildup of such rejected solutes near the surface of the membrane, due to the balance of convective

transport towards and diffusive transport away from the membrane surface, is called concentration polarization (CP).[12, 13, 33, 34] Because of CP, the concentration of solutes at a membrane surface can be as much as 20-50 times higher than in the bulk feed.[13] If the concentration of an organic solute reaches a critical level, a "gel-layer" will form.[12] This gel-layer provides an additional resistance (in addition to the membrane itself) to water permeation and, therefore, water flux decreases.

Fouling is the deposition of matter in a membrane's pores (internal fouling) or on its surface (external fouling) that leads to a change in membrane transport characteristics, such as flux and selectivity.[12] Figure 2.1 presents a schematic of fouling in porous membranes. Fouling occurs when water containing organic contaminants (*e.g.*, particulate, colloidal, or macromolecular material) is filtered through a membrane. As the water is filtered, the contaminants deposit inside the porous structure by adsorption to the pore walls or physical entrainment. Contaminants also deposit on and adhere to the surface of the membrane, creating a "cake layer" which strongly reduces water flux and affects overall membrane rejection. An example of membrane fouling occurs when filtering protein solutions and emulsified oil (both have been identified as key foulants in wastewaters [12, 35]). Porous ultrafiltration membranes show a significant and largely irreversible decline in water flux after only a few minutes of operation when filtering water containing these contaminants, yet rejection of these contaminants only slightly increases with time. Figure 2.1 presents a typical flux curve for a microfiltration membrane filtering a protein (bovine serum albumin) solution. After only 10 hours of

operation, the membrane's permeance, which is flux divided by the transmembrane pressure difference (TMP), has been reduced by three orders of magnitude. This large flux reduction illustrates the impact of fouling on membrane performance and shows how fouling could result in large cost increases in membrane operation due to required membrane cleaning, periodic membrane replacement and increased energy needed to maintain high flux operation.

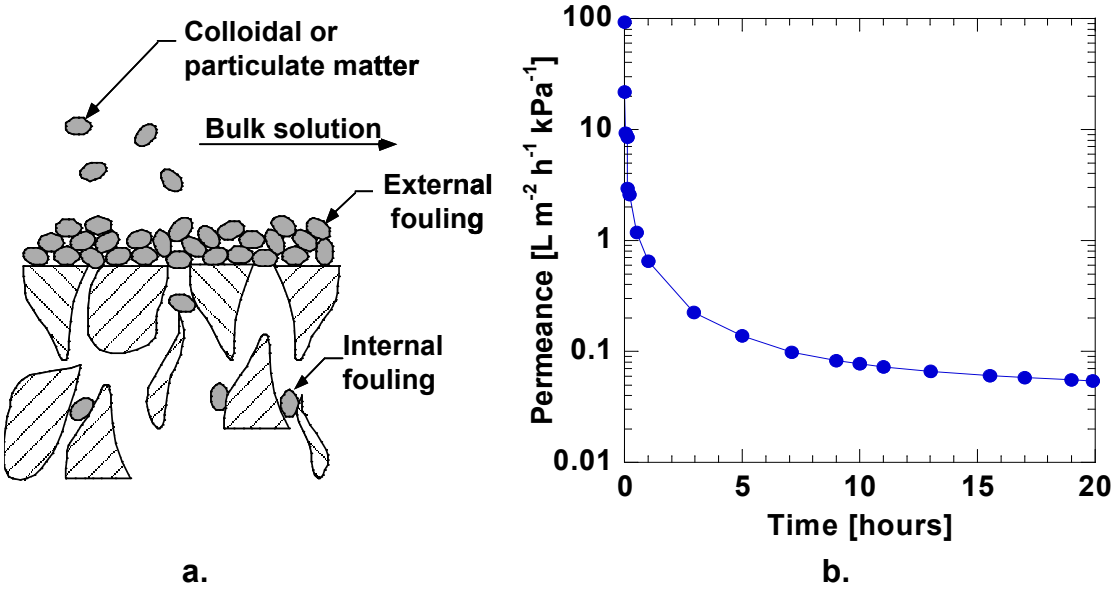

Figure 2.1: a. A schematic of particulate fouling in porous water purification membranes.[17] b. The influence of protein fouling on permeance vs. time in a conventional MF membrane in crossflow protein filtration. Filtration parameters: 1 g/L BSA in pH=7.4 phosphate buffered saline, 25 cm/s crossflow velocity, transmembrane pressure difference (TMP)=10 bar, 0.2 μm nominal pore size PVDF membrane (Pall Corp, hydrophilic PVDF, Port Washington, NY).

2.3 Combating fouling in conventional water purification membranes

There are multiple hydrodynamic properties and membrane modifications that have been proposed to reduce membrane fouling. Introducing hydrodynamic instabilities in the membrane feed stream can reduce CP and fouling.[36-39] For example, crossflow filtration (Figure 2.2) is widely used in commercial applications.[10] By feeding

contaminated water parallel to the membrane surface, a shear stress is introduced, which helps remove foreign material from the membrane surface.

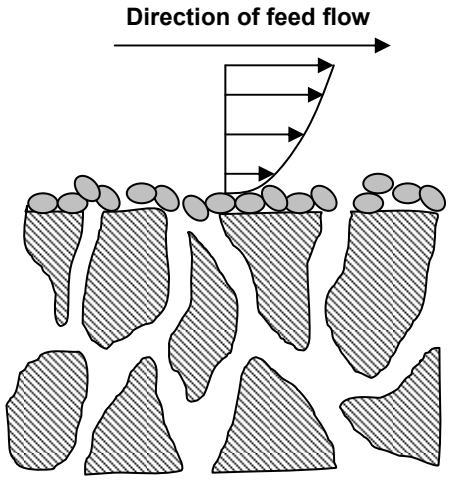

Figure 2.2: Crossflow filtration and resulting shear stress on a membrane surface.

Membrane module designs are, therefore, important for promoting useful crossflow shear rates. Many membrane module designs, including spiral-wound, hollow fiber, and flat-sheet configurations, are currently used.[13] However, besides some membrane bioreactor applications[40], flat-sheet "plate-and-frame" modules are seldom used because of their high cost, low surface area per volume, and problems with gasket sealing.[13] Spiral wound modules are made by wrapping a sealed membrane envelope/membrane spacer assembly around a perforated collection tube. Feed water is introduced through the membrane assembly tangential to the membrane surface. Such modules are most common for reverse osmosis and ultrafiltration, as high pressures can be easily achieved.[13] Hollow fiber modules consist of many "straw-like" membrane fibers. The end of a fiber bundle is sealed in an epoxy resin which is then cut to expose the fiber lumen. Contaminated water can then be passed either through the fiber lumen or

outside the fibers. Many MF, and several UF, applications employ hollow fiber modules, such as membrane bioreactors and RO pretreatment.[14, 15, 40]

Other hydrodynamic cleaning processes have been explored to reduce membrane fouling. The most common are backpulsing and air sparging.[36] Air sparging works by introducing gas bubbles in the feed stream. These bubbles increase fluid turbulence and therefore reduce CP and fouling.[26, 37, 41] Backpulsing involves intermittently reversing the transmembrane pressure so that accumulated foulants on the membrane surface will be convectively removed and carried back into the bulk feed.[42] Backpulsing is effective at reducing cake layer formation and surface fouling. For example, Figure 2.3 presents permeance as a function of time for a 0.2 μm nominal pore size poly(vinylidene fluoride) MF membrane (Pall Corp., hydrophilic PVDF, Port Washington, NY) filtering an aqueous solution of emulsified oil in crossflow filtration and in crossflow filtration with a 10 second backpulse every 10 minutes. The permeance and, therefore, flux of the backpulsed membrane is more than two times higher than the flux of the non-backpulsed membrane after 6 hours of filtration.

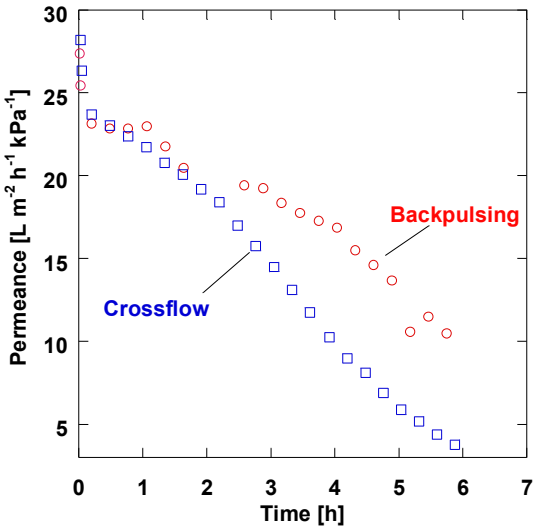

Figure 2.3: A conventional MF membrane in backpulsed and non-backpulsed crossflow filtration. Conditions: 0.2 μm nominal pore size PVDF membrane (Pall Corp., hydrophilic PVDF, Port Washington, NY), 1350 ppm soybean oil, 150 ppm DC193 surfactant oil-water emulsion, 25 cm/s crossflow, TMP=10 bar. Backpulse conditions: backpulse frequency= 0.1 min^{-1}, backpulse duration= 10 s.

Although introduction of hydrodynamic instabilities may reduce CP and fouling to a certain extent, not all fouling is alleviated, and internal membrane fouling is still an irreversible problem. Therefore, most current research has focused on improving inherent membrane anti-fouling properties. Grafting hydrophilic monomers to the surface of conventional membranes and coating membranes with thin hydrogel (hydrophilic crosslinked polymer network) layers are two surface modification methods being explored to combat membrane fouling (Figure 2.4). Both methods decrease attractive forces between foulants and the membrane. Increasing membrane hydrophilicity[26] and reducing membrane roughness[43] have been employed in various studies to reduce fouling.

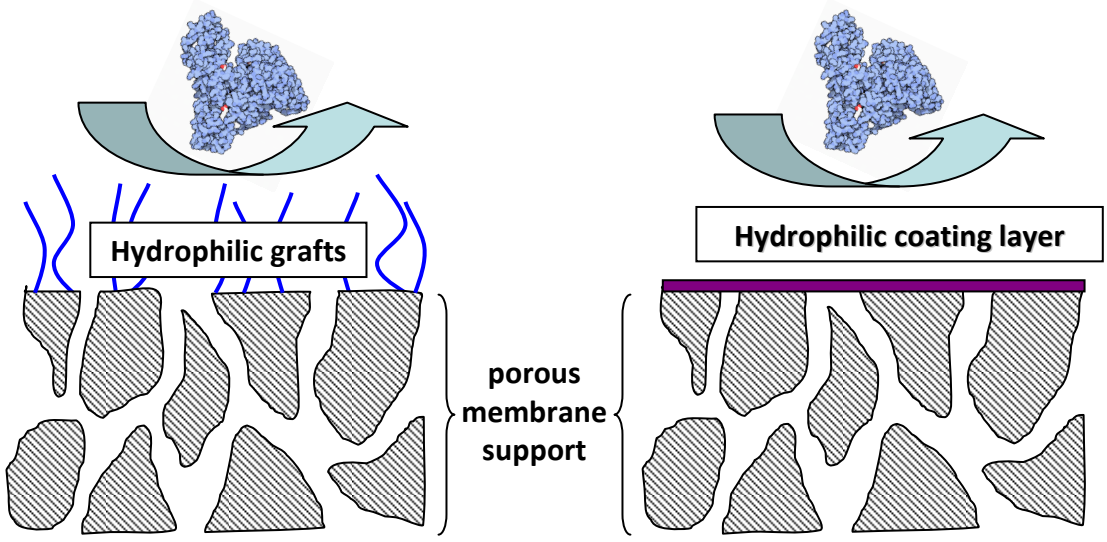

Figure 2.4: Hydrophilic grafting and coating onto conventional polymer membranes to improve fouling resistance.

Grafting hydrophilic monomers to already-formed membranes is a popular method to reduce membrane fouling. Grafting is performed by introducing reactive sites in the membrane through a variety of different treatments, including UV irradiation[44-46], plasma treatment[47-49], treatment with redox reagents[50, 51], or other chemical modifications.[52] These approaches usually induce free radicals in the membrane polymer backbone that are highly reactive with vinyl monomers, which are widely available and provide many different functionalities. Most research has focused on using poly(ethylene glycol) macromer grafts due to PEG's well-documented low fouling characteristics.[53, 54]

Membrane surface coatings have also been explored as possible modification candidates because, using this method, internal membrane fouling can potentially be eliminated.[17] These coated membranes consist of two layers: 1) a dense, thin (< 1 μm)

hydrogel network, and 2) a conventional UF membrane that serves as a porous support for the hydrogel. Figure 2.4 presents a schematic of a standard ultrafiltration membrane coated with an thin hydrogel layer to form a composite membrane. Composite membranes will always have a lower flux than their conventional UF counterparts when filtering *pure water.* However, if the hydrogel layer is made sufficiently thin and the hydrogel has an inherently high permeability, the composite membranes can have higher flux than porous UF membranes when filtering contaminated water.[17, 55] This result is due to several inherent properties of the hydrogel network. First, it can act as a selective barrier, allowing high water permeability while rejecting nearly all organic foulants. This feature reduces or eliminates the entrainment of foulants in the porous membrane structure, thereby reducing or eliminating internal fouling. Second, the hydrophilicity of the hydrogel reduces adsorption of organic moieties to the membrane and, therefore, reduces surface fouling. Additionally, successful surface modification often reduces membrane surface roughness and increases surface hydrophilicity, and both of these properties have been linked to reduced membrane fouling.[26, 43]

As shown in Table 2.2, several studies report the application of coatings to membranes as a route to enhance fouling resistance. For example, Li and Barbari spin-coated crosslinked poly(vinyl alcohol) (PVA) onto regenerated cellulose UF membranes and found the composite membrane to be highly resistant to protein (*i.e.*, BSA) fouling.[56] Wang *et al*., Myung *et al*., and Kim *et al*. also used a PVA coating layer on various porous membranes to reduce fouling.[57-59] Hyun *et al.* coated PSf UF membranes with

polymerized methyl methacrylate/poly(ethylene glycol) (PEG) methyl ether methacrylate and observed a strong reduction in biofouling.[60] Yoon *et al.* created an electrospun nanofiber poly(acrylonitrile) support for a chitosan coating and obtained high flux and high organic rejection for the resulting composite membranes when used in oil-water emulsion filtration.[61] Ju *et al*. coated crosslinked PEG diacrylate networks onto PSf UF membranes and observed a large water flux increase over that of uncoated membranes when filtering oil-water emulsions.[55] A similar PEG network was used by Sagle *et al.* to improve ionic emulsified oil fouling resistance of polyamide RO membranes.[62] Nunes *et al.* coated PVDF UF membranes with a polyether-block-polyamide (PEBAX) copolymer and tested their fouling characteristics.[63] Further studies on PEBAX-based fouling-resistant membrane coatings for PVDF MF membranes and RO membranes were reported by Freeman and Pinnau and Louie *et al.*[17, 64]

Table 2.2: Selected studies using polymer coatings to enhance membrane fouling resistance.

Coating material	Support membrane	Application	Reference
PEBAX	UF, poly(vinylidene fluoride)	Oil-water emulsion	17
PVA	UF, regenerated cellulose	BSA solution	56
PVA	Electrospun PVA	Oil-water emulsion	57
PVA	NF, RO	Dyeing wastewater	58, 59
PEG methyl ether methacrylate-based comb polymer	UF, polysulfone	BSA, alginate, and cell-lysate solutions	60
Chitosan	Electrospun poly(acrylonitrile)	Oil-water emulsion	61
Crosslinked PEG diacrylate	UF, polysulfone	Oil-water emulsion	55
Crosslinked PEG diacrylate	RO, polyamide	Ionic oil-water emulsion	62
PEBAX	UF, poly(vinylidene fluoride)	Oil-water emulsion	63
PEBAX	RO, polyamide	Oil-water emulsion	64
Chitosan-PEG hybrid	UF, polysulfone	Oil-water emulsion	Chapter 4

2.4 Biofouling and biofouling control

Biofouling is a problem in water purification and in membrane bioreactors.[26, 27] Biofouling is the adsorption of polysaccharides, proteins, bacteria, and other biological matter to a membrane surface, usually resulting in the development of a biofilm.

Biofilms typically develop in a series of five stages:[65]

1. A conditioning film comprised of proteins and other organic matter forms on the surface.
2. Bacteria are brought close to the surface by fluid flow.
3. Bacteria adhere to the conditioned surface.
4. The microorganisms grow and divide, colonizing the surface and producing extracellular matrix polymers.
5. Detachment to the planktonic state to colonize other locales.

Membrane biofouling results not only in reduced flux, but also in reduced salt rejection in desalination processes as a result of biofilm-enhanced concentration polarization.[13, 66, 67] Although membrane modification and introduction of hydrodynamic instabilities in the fluid flow across the membrane surface may reduce fouling caused by these contaminants (as will be demonstrated for polydopamine-based modifications discussed in Chapters 5 and 6), fouling cannot be completely avoided without further chemical cleaning, so it is common to clean membranes on a regular basis.[13] Common cleaning reagents include acids, alkalis, chelatants, detergents, and sterlizers.[13, 68] Among these, sodium hydroxide, disodium ethylene diamine tetraacetate (Na-EDTA), and sodium dodecyl sulfate (SDS) are the most common cleaning agents for organic-fouled membranes.[68] Citric acid, hydrochloric acid, nitric acid, surfactants, and enzymes are used to remove proteins from membrane surfaces.[69] The most common biocidal reagent is chlorine (e.g. sodium hypochlorite) due to its low cost and high effectiveness against

most bacteria.[22, 70] Because many different chemicals are used to clean membranes, membrane polymers must be robust to withstand such cleaning cycles.

However, such chemical stability is not always present in membrane polymers. For example, polyamide RO membranes are susceptible to chlorine degradation, even at very low chlorine concentrations (*e.g.,* a few ppm).[22, 70] Therefore, chlorine-pretreated water is usually dechlorinated prior to being fed to RO membranes by adding bisulfates, which results in hypochlorite ions being reduced to chloride ions, and then rechlorinated after RO treatment for distribution.[22, 71] Due to the additional cost of chlorine removal, chlorine-resistant RO membranes would be a significant step forward in the battle against biofouling, because then chlorinated water could be fed directly to RO membranes. To this end, a new class of sulfonated polymers, discussed in Chapter 7, was investigated as potential chlorine-resistant materials for desalination applications.

2.5 Modeling mass transport in membranes

2.5.1 Membrane pure water flux

One model to describe water flux through porous, non-coated membranes, in the absence of foulants, is derived by assuming all flow through the membrane occurs via laminar flow through circular pores. In this case, a modified version of the Hagen-Poiseuille equation is used to describe water flux through the membrane[12]:

$$J_i = \frac{\varepsilon \pi d^4 \Delta p}{32 \mu l \theta} \tag{1}$$

where J_i is the membrane's pure water flux, ε is the membrane's surface porosity, d is the effective pore diameter, Δp is the transmembrane pressure difference, μ is the water viscosity, θ is the pore tortuosity factor, and l is the membrane thickness. Thus, a membrane's flux is directly proportional to the transmembrane pressure difference and inversely proportional to fluid viscosity. However, measuring membrane surface porosity and pore tortuosity is tedious and not required for the work in this thesis. It is conventional to group the constants and membrane-specific terms in equation (1) together and to use the following simplified version of equation (1) to characterize pure water flux:

$$J_i = \frac{\Delta p}{\mu R_i} \tag{2}$$

where R_i (with units of inverse length) is the intrinsic hydraulic (pure water) resistance to flow. Equation (2) is also known as Darcy's Law.[13] UF membranes commonly have a hydraulic resistance on the order of 10^{11}-10^{13} m^{-1}, whereas MF membranes have hydraulic resistances less than 10^{11} m^{-1}.[72]

The solution-diffusion model is used to characterize water transport through nonporous membranes. In this study, the solution-diffusion model is particularly useful in determining hydrogel thickness in composite (*i.e.*, coated) membranes, although reverse osmosis membranes also obey this mechanism:[19, 62]

$$J_i = \frac{P}{l}(\Delta p - \Delta \pi) \tag{3}$$

where P is the hydrogel/membrane permeability constant, l is the hydrogel/membrane thickness and $\Delta\pi$ is the osmostic pressure difference between the feed and permeate. P depends on several membrane characteristics, such as water diffusivity and solubility in the membrane, and it is empirically measured for hydrogels by measuring pure water flux of thick, freestanding films of known thickness:

$$P = \frac{V \cdot l}{a \cdot t \cdot \Delta p} \tag{4}$$

where V is the permeate volume collected over a time period t, using a film of area a and thickness l. Reverse osmosis membrane permeance (*i.e.,* pressure normalized flux), A, is commonly measured empricially:[22, 62]

$$A = \frac{P}{l} = \frac{V}{a \cdot t \cdot \Delta p} \tag{5}$$

The osmotic pressure difference in pure water filtration is zero. Therefore, by comparing equation (3) to equation (2) (and redefining R_i as R_h for a hydrogel film or as R_m for an uncoated membrane), the hydraulic resistance to flow of a nonporous membrane can be defined as:

$$R_i = \frac{l}{\mu P} = \frac{1}{\mu A}. \tag{6}$$

2.5.2 Resistances in series model

Darcy's law can be modified to include mass transport resistances in series (such as the resistance associated with fouling and the inherent membrane resistance):[55]

$$J_t = \frac{\Delta p}{\mu\left(R_m + R_{ir} + R_r\right)} \tag{7}$$

where J_t is the membrane flux at the end of a fouling experiment, R_m is the uncoated membrane's intrinsic hydraulic resistance to flow, and R_{ir} and R_r are the added mass transfer resistances associated with irreversible and reversible fouling, respectively. The CP resistance is lumped into the reversible fouling term in this model. This model assumes that fouling, CP, and the intrinsic membrane mass transfer resistance are additive resistances in series. Figure 2.5 presents a schematic of a fouled membrane and the mass transfer resistances associated with water flux. Surface fouling and CP can result in reversible increases in mass transfer resistance, although strongly adsorbed surface foulants may also contribute to irreversible increases in mass transfer resistance.[13, 17] Therefore, Figure 2.5 is a simplified illustration of the resistance in series model. Internal fouling largely contributes to the membrane's irreversible mass transfer resistance. While this model is simplistic and does not provide a detailed mechanism for flux reduction, it is straightforward to use and provides a tool to characterize the extent of fouling.

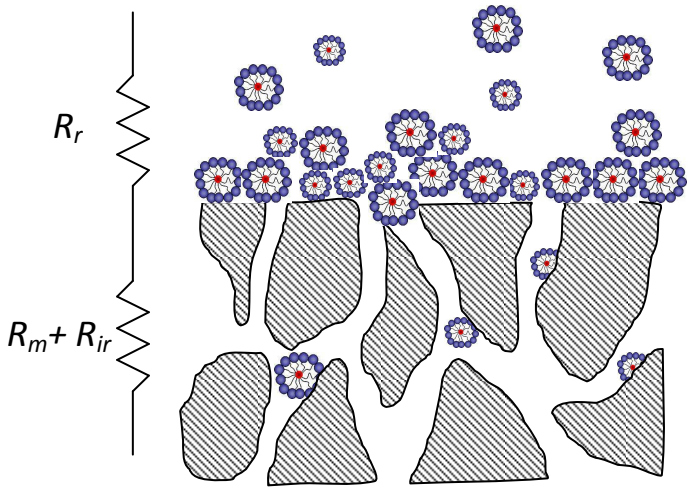

Figure 2.5: A schematic of a resistance in series model for a fouled membrane.

Using equation (2), R_m is readily determined by measuring the pure water flux as a function of TMP. Irreversible mass transfer resistance, R_{ir}, can be determined by measuring the pure water flux of a membrane before and after a fouling experiment:

$$R_{ir} = \frac{(J_w - J_f)\mu}{\Delta p} \tag{8}$$

where J_w is the membrane's pure water flux before fouling, and J_f is the membrane's pure water flux after a fouling experiment. Figure 2.6 presents the protocol used in this thesis to determine J_t and J_f. The fractional flux recovery after a fouling experiment can be calculated as $R_m/(R_m+R_{ir})$, and it is an indicator of a membrane's cleaning efficiency (*i.e.*, a high ratio indicates that the membrane is easier to clean).

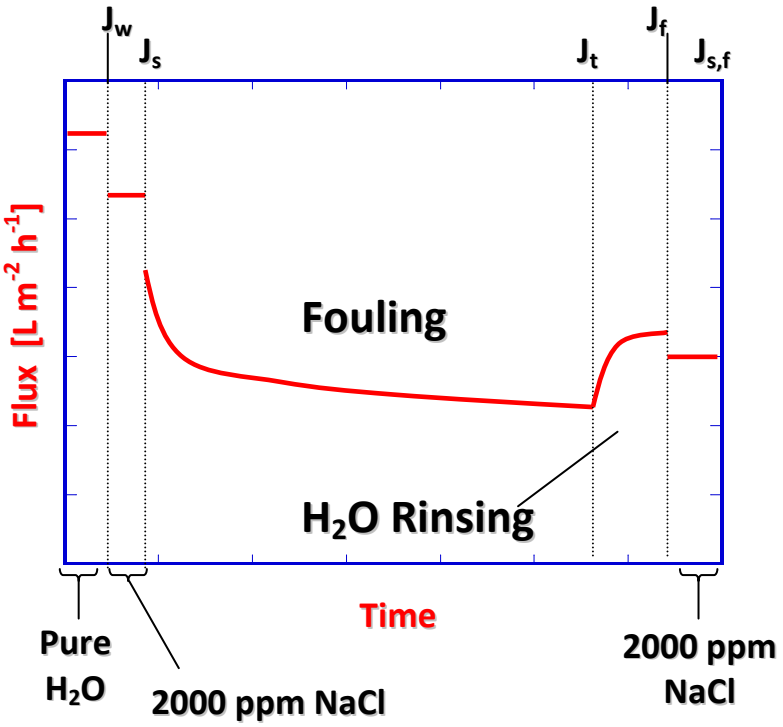

Figure 2.6: Schematic describing protocol to characterize mass transfer resistance associated with fouling. J_s and $J_{s,f}$ (the salt water fluxes of a non-fouled and fouled membrane, respectively) are measured only in membranes that reject ions (*i.e.*, NF and RO membranes). All measurements are performed at the same TMP and temperature (25 °C). The water rinsing cycle is discussed in Chapter 3.

If a hydrogel coating layer or polydopamine deposition layer (discussed in chapters 4-6) is used to modify a membrane, the pure water flux typically decreases due to an increase in the total membrane mass transfer resistance. To accurately characterize the flux loss due to such membrane modifications, equation (7) is modified by adding the mass transfer resistance associated with the modification:

$$J_t = \frac{\Delta p}{\mu\left(R_m + R_h + R_f\right)} \tag{9}$$

where R_h is the total hydraulic resistance of the surface modification, and $R_f = R_r + R_{ir}$, which is the total mass transfer resistance due to fouling and concentration polarization.

As indicated earlier, R_m can be determined from pure water flux measurements of an unmodified membrane. After modifying the membrane, R_h can be determined by measuring the pressure dependence of the pure water flux (in this case, R_f=0):

$$R_h = \frac{\mu}{\Delta p}(J_{um} - J_{\mathrm{mod}}) \tag{10}$$

where J_{um} is the pure water flux of the unmodified membrane, and J_{mod} is the pure water flux of the analogous modified membrane. The flux loss due to modification is an important parameter, since some membrane modifications may reduce a membrane's pure water flux to the point where any benefit in fouling resistance is outweighed by its low initial flux. Ideally, the ratio R_m/R_h should be as high as possible, and the modification should still provide as low a fouling mass transfer resistance, R_f, as possible.

Equation (9) may be used to characterize the effective thickness of a modification layer on a membrane in the case where, for example, a uniform thickness hydrogel coating is applied to the membrane surface. In pure water filtration experiments, R_f=0, and equation (9) reduces to:

$$J_t = \frac{\Delta p}{\mu\left(R_m + R_h\right)}. \tag{11}$$

By measuring R_m for an unmodified membrane, J_t for the composite membrane, and the permeability of a freestanding hydrogel film, the effective hydrogel coating thickness can be determined by combining equations (6) and (11):

$$J_t = \frac{\Delta p}{\mu\left(R_m + \frac{l}{\mu P}\right)} \tag{12}$$

Although fouling reduces membrane flux and, consequently, increases membrane operating costs, surface modifications have been effective at remediating fouling. In this chapter, a simple model (the series resistance model) was introduced to describe water transport through unmodified and modified membranes. In subsequent chapters, this model will be used to identify the dominant mass transfer resistances in the filtrations and characterize the effectiveness of the membrane modifications.

3. CHAPTER 3: MATERIALS AND EXPERIMENTAL METHODS

3.1 Materials

3.1.1 Chitosan-PEG hydrid coating materials

High molecular weight chitosan (M_V~350,000) was purchased from Aldrich (St. Louis, Mo.). Its degree of deacetylation (DD, defined as the ratio of free amino groups to amino and N-acetyl groups) was 76% as determined based on UV-spectroscopy according to a method reported in the literature. [73] Its viscosity average molecular weight was determined via capillary viscometry in a 0.3M sodium acetate/0.2M acetic acid solution. The resulting data were analyzed using the Mark-Houwink-Sakurada equation with the following parameters: $K=7.5x10^{-4}$ dL/g and a=0.76. [74] Glacial acetic acid, poly(ethylene glycol) diglycidyl ether (PEGDGE, M_w~526), and various molecular weight linear poly(ethylene glycol) (PEG) samples were purchased from Aldrich and used without further purification.

3.1.2 PDOPA and PDOPA-g-PEG materials

Dopamine hydrochloride, Trizma hydrochloride (tris buffer), sodium hydroxide, sodium chloride, dimethyl sulfoxide, glycine buffer, and bovine serum albumin (BSA) were purchased from Sigma Aldrich (St. Louis, MO, USA) and used as received. Rhodamine N-hydroxyl succinimide (R-NHS), and slide-a-lyzers were purchased from Pierce Biotechnology. Sephadex columns were purchased from GE Life Sciences. Flat-sheet XLE reverse osmosis (XLE RO) and NF-90 nanofiltration (NF-90) membranes were kindly provided by Dow Water Solutions (FilmTec Corp., Edina, MN, USA).

Polypropylene (PP MF, average pore diameter of 0.1 μm) and PTFE (PTFE MF, average pore diameter of 0.22 μm) microfiltration membranes were purchased from GE Water and Process Technologies. Poly(vinylidene fluoride) (PVDF MF, average pore diameter of 0.22 μm) microfiltration membranes were purchased from Millipore Corp. Methyl-terminated poly(ethylene glycol) amine (mPEG-NH_2, Mw=5kDa) was purchased from JenKem, USA, Inc. Jeffamine (Figure 3.1) was kindly provided by Huntsman Corp. (The Woodlands, TX, USA).

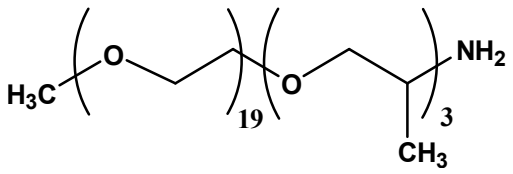

Figure 3.1: Structure of Jeffamine M-1000.

3.1.3 Sulfonated poly(arylene ether sulfone) materials

Di-sulfonated random copolymers used in this study were synthesized by Akron Polymer Systems (Akron, OH, USA) from commercially available 4,4′-dichlorodiphenyl-sulfone (DCDPS) and 4,4′-biphenol (BP). DCDPS was directly sulfonated to obtain a di-sulfonated monomer (3,3′-disulfonate-4,4′-dichlorodiphenylsulfone, SDCDPS).[22, 75-77] The support membrane, composed of micro-porous Udel® and non-woven fabric, was obtained from Dow Water Solutions (FilmTec Corporation, Edina, MN, USA) and used after an appropriate pretreatment process. Di(ethylene glycol) (Di(EG)), glycerin, isopropanol, calcium chloride, arsenic (III) oxide, and sodium arsenate dibasic hydrate were purchased from Aldrich Chemical Co. (St. Louis, MO, USA) and used as received.

3.1.4 Materials common to all studies

Ultrapure water (18.2 MΩ-cm, 1 ppb TOC) was produced from an A10 gradient/RiOs Millipore Corporation water purification system. Wesson vegetable oil was used to prepare oil/water emulsions, and DC193 non-ionic surfactant was purchased from the Dow-Corning Chemical Company. Polysulfone ultrafiltration membranes (PSf A1) were kindly provided by GE Water and Process Technologies (Minnetonka, MN, USA).

3.2 Methods

3.2.1 Preparation of PEG-Chitosan hybrid prepolymerization solution

Chitosan was dissolved in an aqueous acetic acid solution such that the ratio of chitosan to acetic acid was 3:1. Chitosan concentrations of 1.0, 1.25 and 1.5 wt% were used in this study. The solution was filtered through a 7 micrometer particle filter to remove any undissolved chitinous material and then degassed in a round-bottom flask. The final chitosan concentration was determined by placing 5 g of solution on a silicon wafer and evaporating the solvent first at 90 °C for 30 minutes and then at 120 °C overnight under vacuum. The resulting chitosan film was weighed, and its weight was divided by the solution weight to obtain the mass of chitosan per unit mass of solution. Water was added to the solution to give the final desired chitosan concentration. Once the exact concentration was known, the chitosan solution was vigorously mixed with PEGDGE using a stirbar at 4 °C to form a homogeneous solution (this step usually took 1-3 minutes of mixing depending on the viscosity of the chitosan solution). The

PEGDGE/chitosan ratio (wt/wt) in the prepolymerization solution was the primary variable in this study.

3.2.2 Preparation of freestanding PEG-chitosan hybrid films

The prepolymerization solution was cast onto a Si-wafer using a 3" diameter glass ring as a solution retainer. The films were placed under an IR light at 70° C for 1.5 h to crosslink the film and evaporate the solvent. After the crosslinking step, the Si-wafer was placed in water to remove the resulting film (the film will detach from the plate due to swelling). The films were stored in water before use.

3.2.3 Preparation of PEG-Chi hybrid-coated UF membranes

A 4.5"x4.5" PSf A1 membrane was first immersed in a 20 wt% glycerol/isopropanol solution for at least 30 minutes. The surface of the membrane was wiped dry using Kimwipes and allowed to dry at ambient conditions (approximately 15-20 minutes). The membrane was then taped to a glass plate, taking special care to ensure it was as flat as possible. A bead of prepolymerization solution was placed on the edge of the membrane, and the solution was spread across its surface using a "draw down" method with a smooth metal rod (Gardco Company, Pampano Beach, FL). The tape acts as a spacer to produce a coating solution thickness of ~80 micrometers (the exact thickness depends on the thickness of the tape). Once the prepolymerization solution was coated on the membrane, the membrane was placed under an IR lamp and heated to ~70 °C for 30 minutes to crosslink the chitosan. The membrane was covered by a Petri dish to minimize evaporation of the water in the preopolymerization solution. The Petri dish

was then removed, and the coating was allowed to dry at 70 °C for 30 minutes. The resulting composite membrane was stored overnight at ambient conditions and tested within 24 hours of preparation.

3.2.4 PDOPA deposition on flat membrane sheets and subsequent PEG attachment

The protocol described in this section was used to modify membranes characterized in Chapter 5. The membranes characterized for BSA adhesion in Chapter 6 were also modified using the protocol described here. However, membranes characterized for pure water flux in Chapter 6 used the modification protocol described in Section 3.2.8b.

Membranes were prepared for PDOPA modification by immersion in isopropyl alcohol for at least 10 min to wet the membrane pores, then in ultrapure water for at least 30 minutes to completely replace the alcohol in the membrane pores. The membrane was then taped to a glass plate and a glass ring was secured to the membrane surface. A 2mg/ml dopamine solution (15 mM Tris-HCl, pH=8.8 buffer) was placed in the glass ring (in contact with the membrane surface) and constantly stirred. After the desired immersion period, the modified membrane was removed from the glass plate and thoroughly rinsed under running ultrapure water. Membranes were stored in ultrapure water. A 1 hour PDOPA immersion time was chosen as a standard for MF membranes modified in this study; a 45 minute immersion time was used for UF membranes, and a 30 minute immersion time was used for the NF and RO membranes. These immersion

times ensured that: 1. all modified membranes retained at least 80% of their respective unmodified membrane pure water flux and 2. significant increases in membrane surface hydrophilicity (i.e., contact angle) were observed. The membrane was allowed to rinse in ultrapure water for several hours before testing or PEG conjugation.

PEG conjugation was accomplished by immersion in a PEG-NH_2 solution (i.e., PDOPA-g-PEG modification, 15 mM Tris-HCl, pH=8.8 buffer) at the desired PEG-NH_2 concentration, temperature, and grafting time. Unless otherwise stated, all PEG grafting was accomplished using a $2x10^{-4}$ mol/L PEG-NH_2 solution (i.e., 0.2 g/L 1 kDa PEG, 1 g/L 5 kDa PEG-NH_2, or 4 g/L 20 kDa PEG-NH_2) at 60 °C. A Boekel Scientific incubator (Cat. # 133000, Feasterville, PA, USA) was used to keep the membrane and contiguous solution at constant temperature during the PEG grafting step. The standard grafting time was 60 minutes for MF and UF membranes and 30 minutes for RO membranes. The membrane was removed from the solution and thoroughly rinsed under running ultrapure water and stored in ultrapure water until it was used.

3.2.5 PDOPA modification of TW30 membrane modules

TW30-1812-36 Dow Filmtec membrane modules (along with the polypropylene module housings) were purchased from waterfilters.net. Ultrapure water was circulated through the module using a peristaltic pump for approximately 10 minutes before modification (see Figure 3.2 or a schematic of the modification procedure). 400 mL of 2 mg/mL dopamine in tris buffer (15 mM, pH=8.8) was then circulated through the module at approximately 1 L/min. at ambient conditions. After 30 minutes, the module was

rinsed using ultrapure water for approximately 1 h. To further modify the membrane, a 0.25 w% Jeffamine solution was circulated through the module for 30 minutes at 50 °C, after which the module was rinsed using ultrapure water.

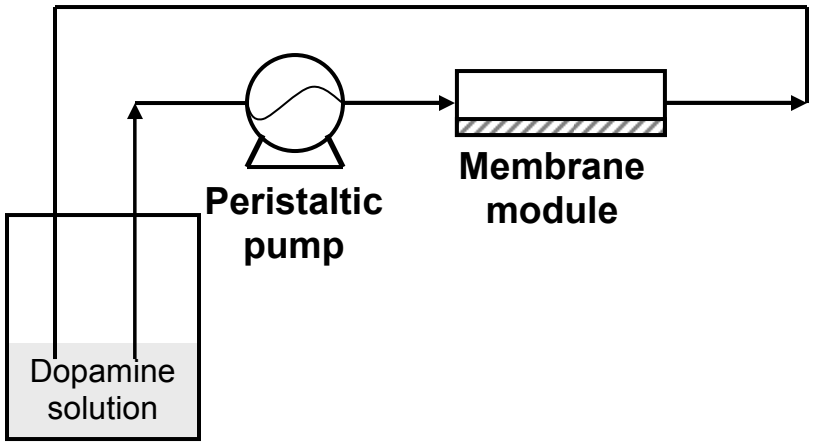

Figure 3.2: Schematic of PDOPA modification apparatus for TW30 Dow Filmtec modules. The module's feed and retentate ports (NPT 1/8") were connected to flexible tubing which led to the beaker containing the PDOPA solution. PDOPA deposition was visibly present on the tubing and the membrane module after ~30 min deposition time.

3.2.6 Sulfonated poly(arylene ether sulfone) synthesis

Random sulfonated polysulfone copolymers were synthesized by polymerization of a disulfonated monomer (3,3'-disulfonato-4,4'-dichlorodiphenyl sulfone (SDCDPS)) with an analogous non-sulfonated monomer (4,4'-dichlorodiphenyl sulfone (DCDPS)). For this study, all polymers are discussed using the same nomenclature in Park et al., namely BPS-XXM, where BPS is the random copolymer shown in Figure 3.3, XX is the molar percentage of sulfonated monomer in the polymer, and M is the sulfonated polymer counterion (either 'H' for the free acid form of the polymer, or 'N' or 'K' for the sodium or potassium sulfonate form, respectively). For example, BPS-20N is the

polymer shown in Figure 3.3 when n=20 and 'M' is sodium. Other hydrophobic segments were studied by Park et al., but were not considered in this thesis.

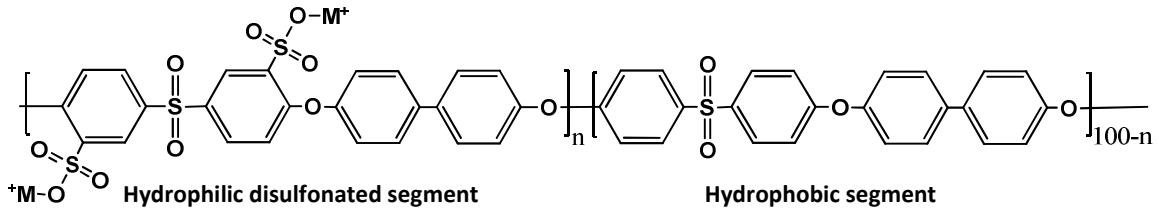

Disulfonated poly(arylene ether sulfone) copolymer, BPS

Figure 3.3: The sulfonated polysulfone copolymers (BPS series) used in this study (n=20-50%). M^+ can be either a K^+ or Na^+ counterion or a free acid (H^+).

3.2.7 BPS thin film composite preparation

Park et al. initially prepared thin-film composite membranes from BPS-40H and an Udel polysulfone support provided by GE (GE A1 support, GE Water and Process Technologies). BPS-40H was dissolved (0.5 w/v%) in 96% formic acid (Sigma-Aldrich, St. Louis, MO) and degassed. Using a fine painter's brush (Performance Select Gold Series, Home Depot, USA) the BPS solution was coated onto a polysulfone support membrane. Because of formic acid's relatively low boiling point (~100.8 °C[78]), the solvent quickly evaporated from the membrane surface using infrared heat lamps. Fast solvent evaporation resulted in minimal penetration of the polymer solution into the porous structure of the support membrane. This procedure yielded a BPS skin layer of approximately 0.7-1.2 μm that, according to Park et al., was defect-free.[22]

Di(EG) was used in this study as the BPS solvent because BPS materials with low sulfonation degree were partially insoluble in formic acid. BPS-20, 32, 40, and 50 in acid

or potassium sulfonate form were dissolved in Di(EG) at a slightly elevated temperature (50 °C). Udel polysulfone support membrane, provided by Dow Water Solutions, was pretreated via immersion in an 85% isopropanol (IPA), 15% glycerin (Gly) mixture for at least 30 minutes. This pretreatment mixture was chosen because it was shown to most effectively preserve the membrane's pore structure after a drying procedure: the optimization of this pretreatment procedure will be discussed later. The support membrane was removed from the IPA/Gly mixture and patted dry using tissue paper. Drying the membrane surface was essential to form defect-free coatings, because any residual glycerin (which has a high boiling point and will, therefore, not readily evaporate) on the membrane surface could result in small skin layer defects. The membrane was then allowed to dry at room temperature for approximately 30 minutes, or until all IPA had evaporated.

The membrane was then taped to a glass plate using masking tape, taking special care to insure that the membrane lay as flat as possible. A bead of BPS solution was placed on one edge of the membrane and drawn down the membrane surface using a painter's brush. The BPS solution concentration ranged from 0.1 w% to 1 w%. Within 30-60 seconds of the casting procedure, the support membrane was visibly wetted by the Di(EG) solution, indicating that polymer solution pore penetration occurred. The membrane was placed in an oven at 90 °C and dried under vacuum. This drying procedure was necessary due to Di(EG)'s high boiling point and, therefore, low vapor pressure at ambient conditions. During the drying process, a significant amount of

condensation on the oven glass window was observed. Therefore, the oven was intermittently opened and the window was wiped dry to speed the drying process. At least two hours of drying was needed to evaporate the solvent. Condensation of a liquid (assumed to be Di(EG)) was observed between the glass plate and the membrane, even after the membrane appeared to be dry, indicating that a large amount of the coating solution permeated through the membrane pores during the drying process. Di(EG) is water-soluble and would wash away to leave defects in the coating layer if not completely removed. To decrease possible defects in the BPS layer, a second and third coating procedure could be repeated. These extra coating steps were performed using a brush coating technique similar to that used in the first coating step. Support membrane wetting was also observed during these extra coating steps.

3.2.8 Pure water flux measurement

a) PEG-chitosan hybrid pure water flux measurement

To determine pure water permeability of PEG-chitosan hybrid freestanding films and composite membranes, cylindrical stirred dead-end cells (c.f., Figure 3.4a) were used. In this mode of filtration, the whole feed stream is allowed to challenge the membrane, making it ideal for testing pure water permeation. Pure water flux tests were conducted for each membrane at three transmembrane pressures: 20, 40 and 60 psi (1.4, 2.7 and 4.1 bar), respectively. Two dead-end cell sizes with effective filtration areas of 3.5 cm^2 (UHP25, Advantec MFS, Inc., Dublin, CA) and 14.6 cm^2 (HP4750, Sterlitech Corp., Kent, WA), were used in this study. Water flux, J_i, was calculated from the

volume of water, V, that permeated through a membrane of area, a, during a time interval, t:

$$J_i = \frac{V}{a \cdot t}. \tag{1}$$

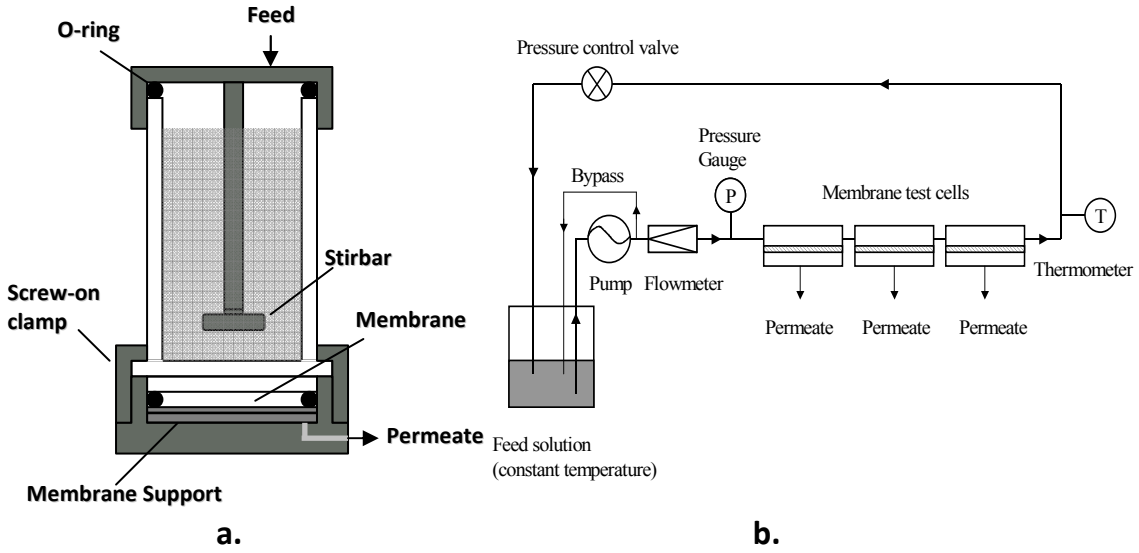

Figure 3.4: a) Dead-end filtration cell and b) ultrafiltration, nanofiltration, and reverse osmosis crossflow system.

Permeance, p_i, is calculated by dividing the membrane flux by the transmembrane pressure, Δp:

$$p_i = \frac{J_i}{\Delta p} \tag{2}$$

Permeability, P_i, of dense polymer films is calculated by multiplying the film's permeance by its thickness, l:

$$P_i = p_i \cdot l \tag{3}$$

b) Water flux measurement on unmodified, PDOPA, and PDOPA-g-PEG modified membranes

Pure water flux was characterized in dead-end filtration cells (UHP43, Advantec MFS, Dublin, CA for MF and UF membranes; CF042, Sterlitech Corp., Kent, WA for RO membranes). Unmodified membranes were cut to the size appropriate for the dead-end cell to be used (UF and MF: 4.3 cm diameter, RO: 5.1 cm diameter) and immersed in IPA for at least 30 minutes prior to a flux measurement. The IPA soak insured that any extractable components (e.g., glycerin) were removed and that the porous structure of the UF and MF membranes was completely wetted. Membranes were then placed in dead-end cells immediately after the IPA soak and rinsed with ultrapure water. Approximately 100 mL of ultrapure water was allowed to permeate through the MF and UF membranes and 30 mL through the RO membranes to rinse the IPA from the membrane structure before the water flux was measured. The transmembrane pressure differences used in this study were as follows: MF membranes: 3 psi (0.2 atm), UF membranes: 10 psi (0.7 atm), and RO membranes: 150 psi (10.2 atm). Steady-state water flux, J_i, was calculated using equations (1) and (2).

After the unmodified membrane's pure water flux was measured, PDOPA modification was performed on each membrane in the dead-end cells. 5-10 mL of dopamine solution (2 mg/mL, 15 mM tris buffer, pH=8.8, ambient conditions) was added to each dead-end cell after any remaining ultrapure water used in the flux experiments was decanted. Using magnetic stir bars, the dead-end cells were stirred intermittently during the PDOPA deposition process. After deposition, the membranes were carefully

removed from the dead-end cells and rinsed with ultrapure water. They were then soaked in IPA, again for 30 minutes, to remove any unbound or loosely-bound PDOPA. The membranes were then placed in dead-end cells, and their pure water flux was measured as described previously. The membranes were then removed from the dead-end cells and modified by immersion in a PEG-NH_2 solution (i.e., PDOPA-g-PEG modification, 15 mM Tris-HCl, pH=8.8 buffer) at the desired PEG-NH_2 concentration, temperature, and grafting time. Following PEG grafting, the membrane was removed from the solution and thoroughly rinsed under running ultrapure water. Afterwards, the water flux of the PDOPA-g-PEG membrane was recorded using the protocol described previously.

Stirred dead-end filtration is a poor technique to effectively analyze salt rejection of an RO membrane, because concentration polarization may lower rejection values.[79] Therefore, salt rejection was not measured in this study. Dead-end filtration was used instead of the more common crossflow filtration because it allows faster screening of many samples, and the PDOPA modification could be performed easily inside the dead-end cell. However, in a previous study, where salt rejection was measured in crossflow filtration, PDOPA deposition was found to have little effect on XLE RO salt rejection, whereas the PDOPA-g-PEG modification increased membrane salt rejection.[80]

c) Support membrane for sulfonated poly(arylene ether sulfone) thin film composite pure water flux measurement

To determine the pure water flux of the Udel support membrane after various pretreatments, the methods described in Section 3.2.8 a) were used with a transmembrane pressure of 1.4 atm (20 psi).

3.2.9 Salt rejection (single and mixed valence) analysis

All salt rejection analysis was performed using crossflow filtration (c.f., Figure 3.4b) similar to that used by Park et al. (3.8 L/min (Re~4900), T=25 °C, pH=6.5).[22] BPS material characterization was performed at a transmembrane pressure difference of 27.2 atm, and XLE RO and NF-90 characterization was performed at a transmembrane pressure difference of 10.2 atm. The feed was allowed to circulate for at least 1 h before permeate samples were collected. Single salt rejection values were performed either at 2000 ppm NaCl or 416 ppm $CaCl_2$ (150 ppm Ca^{2+}), unless otherwise stated. For single salt rejection analysis, conductivity of the feed and permeate streams were recorded using an Oakton CON 110 conductivity meter (Oakton Instruments, Vernon Hills, IL). The salt concentration was calculated from a calibration curve and equation (4) was used to calculate salt rejection:

$$R = (1 - \frac{C_p}{C_f}) \times 100\% \quad (4)$$

where R is rejection, C_p is the salt concentration in the permeate, and C_f is salt concentration in the feed.

Mixed valence salt rejection explored using BPS materials was performed at 150 ppm Na^+ (380 ppm NaCl) and various amounts of Ca^{2+}. Inductively coupled plasma mass spectroscopy (ICP-MS, Agilent 7500ce Quadrupole) was employed to analyze the Na^+ and Ca^{2+} concentrations in the feed and permeate.

3.2.10 Arsenic rejection analysis for BPS membranes

Sodium arsenate dibasic hydrate was dissolved in ultrapure water to make a 1 g/L stock solution. A sufficient amount of the stock solution was added to a crossflow feed containing 10 mM NaCl to make a final As(V) ion concentration of 200 ppb. The feed pH was adjusted to the desired pH using 1N NaOH or 1N HCl. Typically, rejection at high pH (i.e., ~10) would be analyzed first, and then the pH would be decreased. The feed was allowed to circulate for at least 1 h before permeate samples were collected at each pH. After As(V) rejection analysis was completed at each pH, the crossflow system was drained and rinsed using ultrapure water before the same experimental protocol were followed for As(III) rejection. As_2O_3 was dissolved in 3N HCl to make a 1 g/L stock solution. 200 ppb As(III) feed was also used in this study. ICP-MS was used to measure the feed and permeate concentrations of each As species.

3.2.11 Crossflow emulsified oil fouling experiments: NF, RO, and PEG-chitosan hybrid composite membranes

The crossflow filtration unit used to test oil fouling in NF, RO, and PEG-chitosan hybrid composite membranes was purchased from Separations Systems Technologies (Figure 3.4b, San Diego, CA). This apparatus was equipped with three filtration cells, each with an effective filtration area of 7.8 cm x 2.5 cm (19.4 cm^2) and a flow channel

depth of 3.1 mm. The membranes were tested at a crossflow rate of 3.8 L/min (Re~4900) and 10.2 atm transmembrane pressure difference for NF and RO membranes. A crossflow rate of 1.3 L/min (Re~ 1700) and 6.8 atm transmembrane pressure difference was used for the PEG-chitosan hybrid composite membranes. The permeate of each membrane was collected in a beaker placed on an electronic balance. The balances were connected to a computer and weight measurements were collected every 60s by a Labview (National Instruments, Austin, TX) program. Organic rejection was calculated using equation (4), where C_p is the organic concentration in the permeate, and C_f is organic concentration in the feed. C_p and C_f were measured using a Total Organic Carbon Analyzer (TOC5050, Shimadzu Corp., Japan).

The oil-water emulsion was prepared by blending 4.5 g DC193 surfactant and 40.5 g soybean oil in 3 L of water using an industrial-sized blender (Waring LBC15, Torrington, CT) for 3 minutes at the blender's highest speed (~20,000 rpm).[55] This mixture was then diluted to a total volume of 30 L using ultrapure water (the final organic concentration was 1500 ppm). DTAB-decane emulsions were also prepared in a similar fashion: 0.5 g DTAB and 4.5 g decane was blended with 3 L of water using a blender and then diluted to 30 L using ultrapure water (the final concentration of a DTAB-decane emulsion was 150 ppm).

3.2.12 Emulsified oil fouling measurements: UF and MF flat sheet membranes

The system used in the NF and RO fouling employed a diaphragm pump (Wanner Hydra Cell, Minneapolis, MN, USA) whose flow rate and pressure were stable above

approximately 3 atm. Therefore, to test UF and MF membranes at lower pressures, a similar system was built using a peristaltic pump (Cole Parmer, USA). The same cell used in the RO system was used in these experiments; however, the UF and MF system was equipped with only one test cell. The MF membranes were tested at a crossflow rate of 2.0 L/min (Re~2600) and 0.3 atm (5 psi) transmembrane pressure difference. To test the UF membranes, a diaphragm pump head was used on the peristaltic pump motor drive to achieve higher pressures with stable flow rates. The UF membranes were tested at 2.1 atm (30 psi) transmembrane pressure difference and 0.8 L/min crossflow rate (Re~1000). Permeate weight measurements were collected every 10 seconds for these experiments.

The same emulsified oil mixture that was used for RO membranes was used for UF and MF membranes, although the feed tank for the UF/MF apparatus contained 8 L of fluid, rather than 30 L.

3.2.13 Emulsified oil fouling experiments: TW 30 membrane modules

Both Jeffamine and PDOPA-modified modules were tested in a fashion similar to that of the flat-sheet membranes. The flat sheet cells were removed from the crossflow system and replaced with two modules. The feed and retentate pressures were monitored to account for any pressure losses through the modules. Before a fouling experiment, the pure water flux of the modules was determined at 3.4 atm transmembrane pressure difference and 3.8 L/min crossflow. Salt water flux and rejection (with no organics present) were determined immediately after the pure water flux (concentrated salt water

was added to the feed until the total feed concentration of salt was 250 ppm). A fouling experiment was then performed using the 1500 ppm emulsified oil mixture described earlier. After the fouling experiment, the crossflow system was flushed with ultrapure water at least three times, after which water was allowed to circulate through the system. The post-fouling pure water flux was recorded after the rinsing cycle.

3.2.14 Irreversible fouling determination

Irreversible fouling was determined by comparing the pure water permeance of a membrane before and after a fouling experiment and uses a protocol similar to that shown in Figure 2.6. Before a fouling experiment, the pure water flux of a membrane was determined at the same transmembrane pressure difference and crossflow rate at which the fouling experiment took place (e.g., 2.1 atm and 0.8 L/min for a UF membrane). For NF and RO membranes, salt water flux and rejection (with no organics present) were determined immediately after the pure water flux (concentrated salt water was added to the feed until the total salt concentration in the feed solution was 2000 ppm). A fouling experiment was then performed on the membranes (for the NF and RO membranes, the fouling experiment lasted 24 hours, for the UF and MF membranes, fouling experiments were conducted for 1 hour). After the fouling experiment, the crossflow system was flushed with ultrapure water at least three times, after which water was allowed to circulate through the system for 10 minutes (the rinsing cycle took a total of one hour to complete for the NF and RO membranes and 20 minutes for the UF and MF membranes). The post-fouling pure water flux was recorded immediately after the rinsing cycle. The same procedure was used for both non-ionic oil emulsion and DTAB-decane positively-

charged emulsion fouling experiments for XLE RO membranes, except hot water (50 °C) was used to rinse the membranes after DTAB-decane fouling.

3.2.15 BSA adhesion measurements

Protein adhesion experiments were performed using a fluorimetric assay of tagged bovine serum albumin (BSA). R-NHS-tagged BSA, rather than fluorescein-tagged BSA, was used in this study because the polyamide desalination membranes exhibited a significant fluorescent signal at approximately the same excitation/emission spectrum as fluorescein. The fluorescent tagging of BSA was accomplished using a common approach.[81] Briefly, 40 mg BSA was dissolved in 5 mL of ultrapure water, and 8 mg of R-NHS was dissolved in 175 μL of dimethyl sulfoxide. 150μL of the R-NHS solution was added to the BSA solution and incubated at room temperature for 1h, after which the reaction was quenched by adding 50 μL of glycine buffer. The reaction mixture was purified by eluting through sephadex columns and then dialysis against ultrapure water using Slide-A-Lyzers (15-20 hour dialysis time was typical). The final concentration and fluorescent tags per BSA molecule were analyzed using UV spectrophotometry.[81] There were approximately 3.5 rhodamine molecules per BSA molecule.

2.5 cm (1 in.) diameter samples were cut from flat-sheet membranes. The circular samples were placed in dead-end cells (Advantec MFS, #UHP 25) having an effective surface area of 3.5 cm^2 and washed several times with ultrapure water. R-NHS-tagged BSA solution (0.1 mg/mL in ultrapure water) was then added to the cells. After 30

(Chapter 6) or 60 (Chapter 5) minutes, the protein solutions were decanted and the membrane surface was washed repeatedly with ultrapure water. The membranes were then air dried, and their fluorescence intensity was measured using either a fluorescent microscope (Leica DM IRBE, Bannockburn, IL, USA) or a plate reader (Tecan Sapphire II, Mannedorf, Switzerland).

3.2.16 Static bacterial adhesion

Bacterial static adhesion experiments, similar to the protein adhesion experiments described above, were performed with *Pseudomonas aeruginnosa*. Naturally-occurring biofilms are typically a comprised of a poorly-understood complex of many bacterial species. In these studies, one common model bacterium, *Pseudomonas aeruginosa*, was selected for study. This gram-negative, rod-shaped organism can be found in nearly all natural waters, including drinking reserves. It is widely known to prolifically foul surfaces, forming robust biofilms due to its rapid rate of reproduction.[82]

A freezer stock of *P. aeruginosa* was a generous gift of Dr. Marvin Whiteley's laboratory. The bacteria were genetically modified by the Whiteley lab from the PA14 strain of *P. aeruginosa* containing the pQF50 parent plasmid. Plasmids are extra-chromosomal DNA molecules expressed by the cell. Plasmids, which occur naturally in bacteria, are also able to replicate independent of the chromosomal DNA. The lux operon (a sequence of five genes) of *Photorabdus luminescens* is responsible for the light-producing ability of this bacterium. The lux operon from *P. luminescens* was

cloned into the pQF50 plasmid of *P. aeruginosa* to produce the pQF50-lux plasmid. This alteration allows *P. aeruginosa* to luminesce.

Cells were grown (by the procedures described below) from the freezer stock in the presence of carbenicillin antibiotic. The pQF50-lux plasmid contains genes which give the bacteria resistance to the carbenicillin antibiotic. Light production is a very energy-intensive process. If the genes responsible for luminescence are contained on a plasmid, the cell will readily discard the plasmid to avoid the energetic requirements of such. However, if the same plasmid containing the lux operon also provides resistance to an antibiotic in the growth media, the cell will retain the plasmid, thus retaining its luminescent quality.

Cells were grown by streaking a bit of the freezer stock on a culture plate and incubating overnight at 37°C. A single colony was picked from the plate and grown in liquid media (containing 100μg/mL carbenicillin) overnight at 37°C with shaking. A 0.5mL aliquot of the liquid culture was diluted with 4.5mL fresh LB media without antibiotic and grown for about two hours at 37°C with shaking, until the optical density at 600nm was in the range of 0.3 – 0.5. This dilution/growth procedure ensures that the bacteria are in log-phase growth during the experiment for maximum attachment and luminescence. The liquid culture was diluted with more fresh media to an optical density of OD_{600} = 0.1, corresponding to 10^8cells/mL (a standard cell concentration for bacteriological assays).

Unmodified, PDOPA-modified, and PDOPA-g-PEG-modified 1”-diameter membranes were loaded in dead-end cells. The bacteria suspension was dispensed into the dead-end cells (2mL) and incubated at 37°C for one hour. After one hour, the bacteria suspension was removed and the membranes were gently rinsed with ~10mL deionized water. Four ¼”-diameter samples were cut out of each membrane and loaded into an opaque white 96-well plate. 100μL fresh LB broth (no antibiotic) was dispensed into each cell to ensure that the bacteria would luminesce during the assay. Luminescence was measured in a Biotek Synergy HT plate reader running KC4 software. High luminescence indicates high bacterial adhesion. Relative luminescence was calculated using the following equation:

$$RL = \frac{1000}{L_p} \cdot (L_m - L_n) \tag{5}$$

where RL is the membrane’s relative luminescence, L_p is the luminescence of a positive control (100 μL of OD=0.1 liquid culture), L_m is the luminescence of a bacteria-fouled membrane, and L_n is a negative control of an non-fouled membrane.

3.2.17 PDOPA leaching from TW30 membrane modules

Dopamine and PDOPA absorb UV light at two wavelengths, 200 nm and 280 nm. However, the peak at 280 nm is linear with respect to PDOPA concentration over a concentration range of 1-40 ppm (see Figure 3.5). This absorbance provides an easy route to track PDOPA leaching from membrane modules. The PDOPA in Figure S3a was prepared by placing 50.0 mg of dopamine HCl in 25.0 mL of 15mM tris buffer

(pH=8.8) and allowing the polymerization reaction to take place for 45 min. The reaction was quenched by adjusting the pH to 6.5 using a few drops of 3M HCl. Dilutions using ultrapure water were used to make the standard solutions in Figure 3.5.

TW30 membrane modules[83, 84] were modified by placing 250 mL of a 2mg/mL dopamine HCl in 15mM tris buffer (pH=8.8) in the feed-side of the module and sealing the feed and retentate ports. The module was agitated manually for 45 min. to insure uniform modification. The module was then rinsed by placing ultrapure water in the feed-side of the module and intermittently shaking the sealed module over the course of ~24 h. (the water was replaced at least five times during the course of the rinsing cycle). The rinsing water was then replaced with 200 mL of ultrapure water. The module was agitated intermittently for 2 h., after which the UV absorbance of the water at 280 nm was measured and the PDOPA concentration (and therefore total PDOPA) was calculated from the calibration curve presented in Figure S3a. The water was immediately replaced after taking the UV absorbance measurement and the module was agitated again for 2 h., after which the water's UV absorbance was tested. This process was repeated over the course of 12 h. (6 total water replacements). The total PDOPA leaching per day (in mg/day) was determined as twice the total amount of PDOPA leaching over the 12 h. period. However, leaching of a polyamide membrane synthesis byproduct was also found in TW30 membranes. The byproduct had a maximum UV absorbance at 286 nm and, therefore, the same leaching procedure was performed on an unmodified TW30

membrane, and the results of this leaching procedure were subtracted from the PDOPA leaching results.

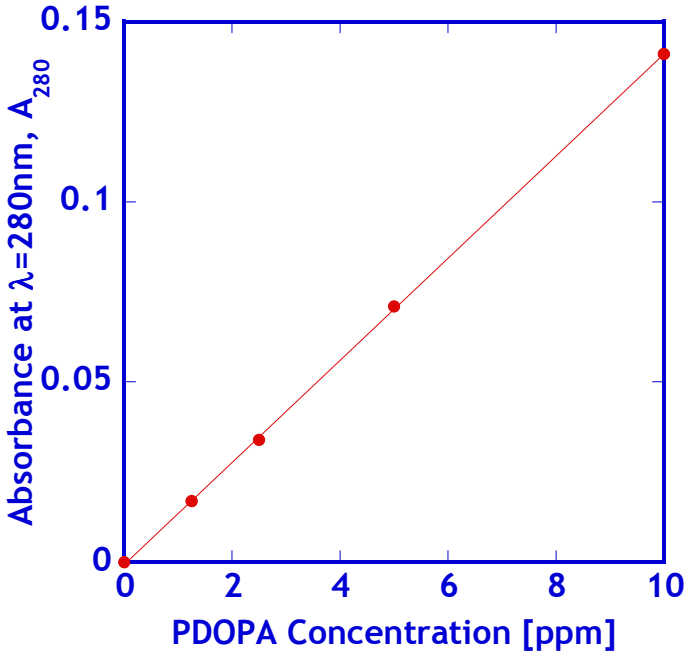

Figure 3.5: UV absorbance at λ=280nm of aqueous solutions containing various concentrations of PDOPA.

3.2.18 Molecular weight cutoff/solute rejection properties

14.6 cm^2 dead-end cells were used to test solute rejection characteristics of freestanding films and composite membranes. All solute rejection was accomplished by feeding an aqueous solution of PEG (~0.5 wt% PEG) to the cell at low pressure (usually around 1.4 atm). The low pressure insures that concentration polarization is negligible and does not affect the actual solute rejection properties of the membrane. Multiple solutions with varying PEG molecular weight (ranging from 400 to 1,000,000 g/mol) were used to elucidate the solute sieving properties of the freestanding films and

composite membranes. The rejection of PEG was calculated from permeate and feed concentrations measured using a total organic carbon analyzer according to equation (4).

The molecular weight cutoff (MWCO) of a particular membrane was reported as the PEG molecular weight that has a rejection of 90%. The membrane's mean pore diameter was taken to be equal to the Stokes diameter of the PEG exhibiting 50% rejection, which could be calculated from the molecular weight of the PEG using equation (6):[85]

$$d = 33.46 \times 10^{-3} M_w^{0.557} \quad (6)$$

where d (nm) is the Stokes diameter of PEG of molecular weight M_w.

3.2.19 Scanning electron microscopy (SEM)

Membrane cross sections were prepared by a freeze-fracturing method. Composite membranes were rinsed in ethanol to remove glycerol from the pore structure. Once dried, the membranes were cut into 0.5 cm x 2 cm strips and immersed in liquid nitrogen for 5 minutes. Once thoroughly frozen, the membrane was quickly bent, resulting in a clean fracture. The samples were imaged using a Hitachi S-4500 field emission scanning electron microscope with a working distance of 10 mm and an accelerating voltage of 5 kV. The samples were coated with gold before imaging.

3.2.20 Fourier transform infrared spectroscopy (FTIR)

Attenuated Total Reflectance (ATR) FTIR (ZnSe crystal, 45° angle of incidence) was used to characterize the surface chemistry of composite and unmodified membranes.

A Nicolet 6700 FTIR spectrometer with OMNIC software was used to collect data. Before testing, all membranes were initially rinsed in ethanol, air-dried for one hour, and then dried at elevated temperature (~80 °C) overnight.

3.2.21 Contact angle measurements

Contact angle measurements were performed using a captive n-decane bubble in water, as described previously[55]. A membrane was cut into a 5 mm wide strip and placed face down in a custom-made holder. The membrane-holder assembly was placed in a small, clear water bath such that the membrane was fully immersed in water. A computer-controlled camera was focused on the membrane surface and at least five decane bubbles were placed on the membrane surface using a syringe with a hooked needle. Images of the bubbles were analyzed using software from First Ten Angstroms (Portsmouth, VA, USA). The values reported in this study are the average and standard deviation of at least five measurements.

3.2.22 Streaming zeta potential measurements

Streaming zeta potential of XLE RO membranes was analyzed using a SurPASS Electrokinetic Analyzer (SurPASS, Anton-Paar USA, Ashland, VA). Membranes were soaked in 10 mM NaCl for at least 30 minutes prior to analysis. Membranes were loaded in a clamping cell and the SurPASS was rinsed with 10 mM NaCl prior to analysis. 10 mM NaCl was used as the reference solution, and a 300 mbar pressure ramp was used during characterization. The solution pH was adjusted to ~10 using sodium hydroxide at the beginning of the experiment. An automatic titration was performed by the SurPASS

using 0.1 N HCl was used to adjust the pH during the analysis. The Fairbrother-Mastin approximation was used to evaluate the measured streaming potentials.[86]

3.2.23 Atomic force microscopy (AFM) measurements

Membranes were soaked in IPA and cleaned using pressurized, filtered air to remove any PDOPA microparticles from the membrane surface. The membranes were taped to a silicon wafer prior to analysis. All membranes were tested dry. Images were collected using a Veeco Dimension 3100 AFM with a Nanoscope controller (Version 5.30, Veeco, Plainview, NY). A 2 x 2 μm image size was collected at 1 Hz (256 scans). Root-mean-square roughnesses were calculated by the Nanoscope software on the 2 x 2 μm image.

3.2.24 PDOPA deposition thickness measurements on polysulfone

To quantify the amount of PDOPA deposited on a polymer surface as a function of immersion time, ellipsometry was employed on thin, nonporous films of UDEL polysulfone from Solvay Solexis (Alpharetta, GA). Thin films (~150 nm) of polysulfone were created by spin coating a 3 wt% polysulfone solution in cyclopentanone onto silicon wafers at 1000 rpm. Thickness was measured using a variable angle spectroscopic ellipsometer manufactured by J.A. Woollam Co., Model 2000D and methods described in previous studies.[87, 88] A polysulfone-coated wafer was then immersed in a stirred dopamine solution similar to that used to modify membranes to deposit PDOPA on the film's surface. After a given deposition time, the film was rinsed in running ultrapure water and air-dried. The coated polysulfone film was then re-measured using

ellipsometry, and the PDOPA layer thickness was determined using a Cauchy model.[88] For the unmodified polysulfone films, a 3-layer model was used to represent the system of a silicon substrate, a native silicon oxide layer, and the polysulfone film. A 4-layer model was used for the PDOPA-modified polysulfone films, where the 3 previously mentioned layers' properties were fixed based on the initial ellipsometry scan and the 4th layer was used to model the PDOPA coating.

4. CHAPTER 4: COMPOSITE MEMBRANES BASED ON A SELECTIVE CHITOSAN-POLY(ETHYLENE GLYCOL) HYDRID LAYER: SYNTHESIS, CHARACTERIZATION, AND PERFORMANCE IN OIL-WATER PURIFICATION

4.1 Summary

A series of poly(ethylene glycol) diglycidyl ether-crosslinked chitosan (chi-PEG hybrid) films were prepared to elucidate their potential as fouling-resistant ultrafiltration (UF) membrane coating layers. Water permeability increased as the poly(ethylene glycol) diglycidyl ether to chitosan ratio in the prepolymerization mixture increased due to increased porosity in the polymer matrix resulting from phase separation during polymerization. Composite membranes for oil-water emulsion filtration were prepared by coating an optimized member of the chi-PEG hybrid family onto a commercial polysulfone ultrafiltration membrane. Scanning electron microscopy (SEM), attenuated total reflectance Fourier transform infrared spectroscopy (FTIR), and pure water permeance measurements indicated that, depending on the concentration of chitosan in the coating solution, the coating layer thickness could be controlled, so water permeance could be optimized. These composite membranes exhibited water flux values more than 5 times higher than that of uncoated membranes after one day of oily-water crossflow filtration, indicating that the hydrophilic polymer coating significantly enhanced the fouling resistance of the underlying polysulfone membrane. The organic rejection of the coated membranes was also slightly higher than that of the uncoated polysulfone membranes.

4.2 Introduction

This study focuses on improving oil-fouling resistance of polysulfone ultrafiltration (PSf UF) membranes via surface coating with an ultra-thin (<1 μm), nonporous, hydrophilic polymer. This thin-film coating method is advantageous for two reasons: 1. irreversible internal membrane fouling can be greatly reduced or even eliminated, and 2. organic adhesion to the hydrophilic membrane surface will be lower than that of a more hydrophobic surface, which may reduce external fouling. [17] In this study, new coating materials based on the biopolymer chitosan and poly(ethylene glycol) (PEG), two highly hydrophilic materials with desirable coating properties, are used to form thin (<1 μm) coatings on PSf UF membranes to increase their fouling resistance. To the best of our knowledge, this report is the first example of PEG-crosslinked chitosan being used for this application.

Chitosan, or partially deacetylated poly(N-acetyl glucosamine), whose structure is presented in Figure 4.1, is derived from chitin (poly(N-acetyl glucosamine)), which is a primary ingredient in crustacean seashells and is, therefore, an abundant and low-cost polymer.[89-91] Chitosan has many characteristics that make it a promising candidate for water purification membrane coatings. These characteristics include high hydrophilicity (for high water throughput and low interaction energy with hydrocarbons), excellent heavy metal chelating properties (high affinity to bind and, therefore, reject heavy ions such as lead and mercury), well-documented anti-bacterial properties (to reduce many forms of biofouling), and ease of forming ultra-thin, yet strong films.[90, 91] PEG-based

monolayers and coatings have also exhibited excellent anti-fouling properties.[54, 55, 60] Here, chitosan was mixed with a bifunctional PEG molecule, PEG diglycidyl ether, and heated to produce a crosslinked structure as shown in Figure 4.1. This crosslinker serves as either a grafting or crosslinking agent depending on whether one or both of the functional epoxide groups reacts with the free amine groups in chitosan (Figure 4.1).[92] PEG "brushes," which are formed by grafting, have been shown in recent studies to reduce protein adhesion to various surfaces.[54] Such PEG brushes could reduce the protein and other biomacromolecular (such as polysaccharides) fouling susceptibility of chitosan coatings, although biomacromolecule fouling *per se* is outside the scope of this work. By using PEG as a crosslinking and grafting agent, chitosan is rendered insoluble in acidic media and its swelling in water is reduced, which may help eliminate possible coating layer delamination in composite membranes.

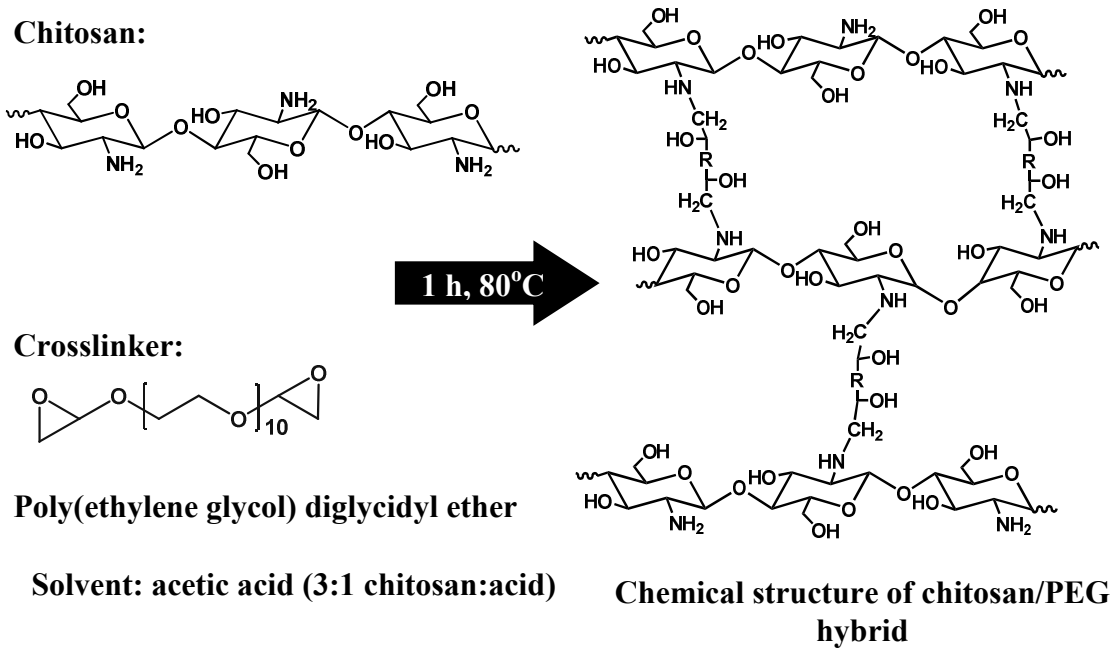

Figure 4.1: Synthesis of a chitosan-PEG hybrid network

In this study, the hydraulic permeability and solute rejection properties of a series of PEG-chitosan hybrid materials are reported. The PEG crosslinker to chitosan ratio in the prepolymerization solution was varied to optimize transport properties (*i.e.*, to obtain high water permeability and high solute rejection). The most promising member of this PEG-chitosan series was selected as a model coating material for commercial polysulfone membranes. Fouling and rejection characteristics of these composite membranes are reported.

4.3 Results and Discussion

4.3.1 Freestanding film characterization

Freestanding films were made from a 1.5 w% chitosan solution and PEGDGE/chitosan wt/wt ratio of 0.66, 1.33, 2.00, 2.66, and 3.33. Figure 4.2 presents the

surface scanning electron microscope (SEM) image of a film made from a 1.33 (a) and 2.00 (b) PEGDGE/chitosan ratio solution. Between these two ratios, macroscopic pore formation occurs during the crosslinking process. In other words, films made from solutions containing a PEGDGE/chitosan ratio above approximately 1.4 exhibit pore formation. This pore formation is attributed to phase separation during the crosslinking process, which is common when a linear polymer (such as chitosan) is crosslinked in the presence of a diluent (in this case, PEGDGE acts as both the crosslinker and diluent).[93] Once the crosslinking process is complete and the film is rinsed, any water-soluble, unreacted PEGDGE or other components not bound to the polymer network (*i.e.*, sol) will wash away, leaving the porous, crosslinked chitosan phase. Pore formation was not observed using SEM analysis in the 1.33 PEGDGE/chitosan ratio films. MWCO presented later also indicates that these films are nonporous. All films were insoluble in a 3 wt% acetic acid solution (a common solvent for chitosan), indicating that the crosslinking reaction was indeed effective.

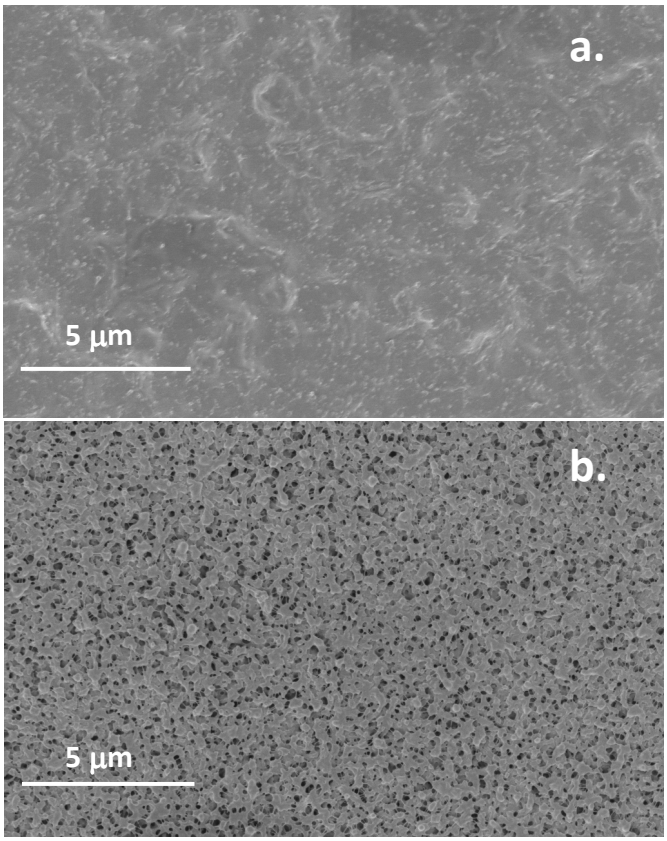

Figure 4.2: (a). Surface SEM images of films made from a 1.4 PEGDGE/chitosan prepolymerization solutions, and (b). 2.0 PEGDGE/chitosan prepolymerization solutions.

Figure 4.3a presents the influence of film thickness (which ranges from 10 to 60 microns) on pure water permeability. The number next to each curve represents the PEGDGE/chitosan ratio in the prepolymerization solution. Water permeability decreases with increasing film thickness for all samples above a PEGDGE/chitosan ratio of 1.4. The trend of decreasing permeability with increasing film thickness is ascribed to macroscopic pore formation in these films (as seen from the SEM images). Pore tortuosity and intrinsic film porosity may vary with film thickness, which would

contribute to the observed decreases in permeability with increasing thickness. However, films formed from solutions with a PEGDGE/chitosan ratio of 1.4 or below show constant permeability with respect to film thickness, which is expected of films that exhibit no macroporous morphology. Interestingly, a general increase in permeability is seen with increasing crosslinker content. This permeability increase is most likely due to two phenomena. First, as PEGDGE content increases in the prepolymerization solution, its role as a diluent also increases, and therefore likely creates more free volume in the network structure. Second, as the PEGDGE content increases, there is a decreasing probability that both epoxy groups in each molecule covalently bind to the chitosan, thereby making PEG grafting more prevalent than crosslinking.

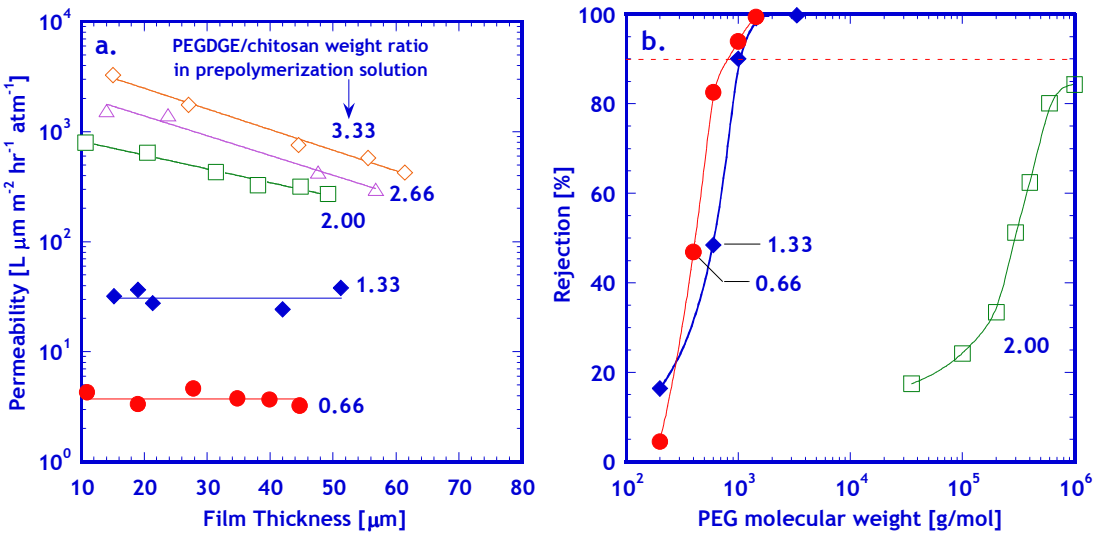

Figure 4.3: (a). Pure water permeability vs. film thickness for a series of chitosan/PEG hybrids. The pure water permeability of the nonporous films are: 1.33 PEG/chitosan ratio=31.7±5.8 L µm m^{-2} hr^{-1} atm^{-1}, 0.66 PEG/chitosan ratio=3.8±0.5 L µm m^{-2} hr^{-1} atm^{-1}. (b). PEG rejection curves for films made from 0.66, 1.33, and 2.0 PEGDGE/chitosan solutions. The numbers next to the curves indicate the PEGDGE/chitosan ratio of the film's prepolymerization solution.

Figure 4.3b presents the molecular weight cutoff curves for PEG in different films (all with an approximate thickness of 15 microns). The curves below a PEGDGE/chitosan ratio of 1.4 show high rejection for relatively small PEG molecules. For example, the molecular weight cutoffs of films prepared from 0.66 and 1.33 PEG/chitosan solutions are approximately 900 and 1000, respectively, whereas the higher PEGDGE/chitosan ratio film has a MWCO greater than 1,000,000, which was the highest PEG molecular weight considered in this study. These results, coupled with SEM images presented earlier, indicate that pore formation occurs at a PEGDGE/chitosan ratio greater than about 1.4 and that the films formed from lower PEGDGE/chitosan ratio are more suitable for UF coatings.

4.3.2 Composite membrane characterization

Composite membranes formed by coating a solution having a PEGDGE/chitosan ratio of 1.4 and containing 1.0 wt% chitosan will be named "1.0 composite membrane". Similar composite membranes formed from 1.25 wt% and 1.5 wt% chitosan concentrations (with the same 1.4 PEGDGE/chitosan ratio) will be referred to as "1.25 composite membrane" and "1.5 composite membrane," respectively. Freestanding films made from solutions with different chitosan concentrations but the same PEGDGE/chitosan ratio were found to exhibit statistically similar water permeability and solute rejection over the range of chitosan concentrations used in this study.

Figure 4.4 presents a cross-sectional SEM image of a 1.5 composite membrane. This image shows that a dense PEG-chi hybrid layer has been formed on the surface of

the support membrane. The coating layer thickness is approximately 0.7 micrometers. However, other images show that the coating layer thickness varies from approximately 0.4 to 0.9 micrometers. Images for coatings made from lower concentration coating solutions showed similar results with thinner coatings. For example, a 1.0 composite membrane had a coating layer thickness that ranged from 0.2 to 0.45 micrometers, and a 1.25 composite membrane had a thickness that ranged between 0.4 and 0.6 micrometers. The variability of the coating thickness can be attributed to the support membrane not being completely flat during the coating procedure, and hence, producing solution coatings that are thinner in some regions than in others.

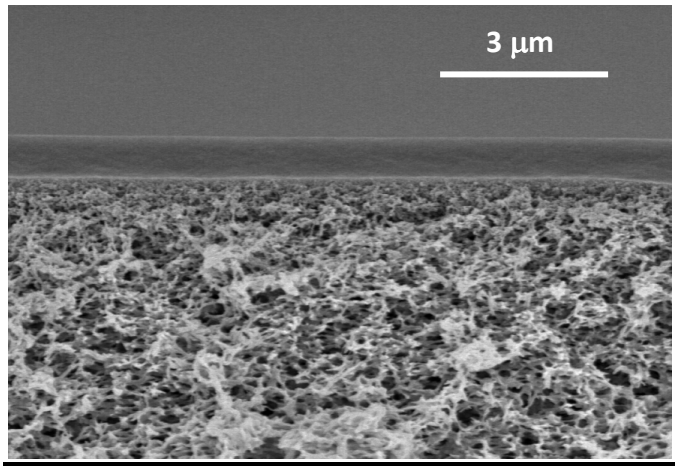

Figure 4.4: SEM cross sectional image of a PSf membrane coated with a 1.4 PEG crosslinker to chitosan ratio solution (1.5 wt% chitosan). Approximate solution coating thickness was 80 μm, leading to a final coating thickness of ~0.7 μm.

ATR-FTIR was used to examine the composite membrane surface chemistry. Figure 4.5 presents the ATR-FTIR surface spectra for an uncoated PSf membrane, a 1.0, 1.25, and 1.5 composite membrane, and a 1.4 PEG-chi hybrid film. In the PSf spectrum, the peak heights were normalized to the highest intensity peak, which was located at

~1240 cm^{-1}. The peak heights in the spectra of the composite membranes and freestanding films were normalized to the large peak at 1070 cm^{-1}. Characteristic peaks of both the PEG-chi hybrid and PSf are observed in the composite membranes. For example, in the 1.0 composite membrane, characteristic PSf peaks appear at 1585, 1490, 1240, 1151, and 825-880 cm^{-1}, while the rest of the peaks are attributable to the PEG-chi hybrid coating. Peaks of both the PEG-chi hybrid and the PSf support were observed due to the PEG-chi thickness being smaller than that of the penetration depth of the FTIR beam. Based on the FTIR crystal properties (ZnSe crystal, n=2.4), the angle of incidence of the beam (Θ=45°), and by assuming that the film's refractive index is similar to that of chitosan (n=1.56[94]), the penetration depth was calculated to vary between approximately 0.3 μm at high wavelengths and 1.5 μm at low wavelengths. [95] The FTIR data indicate that a PEG-chi hybrid coating is present on the surface of the PSf membrane.

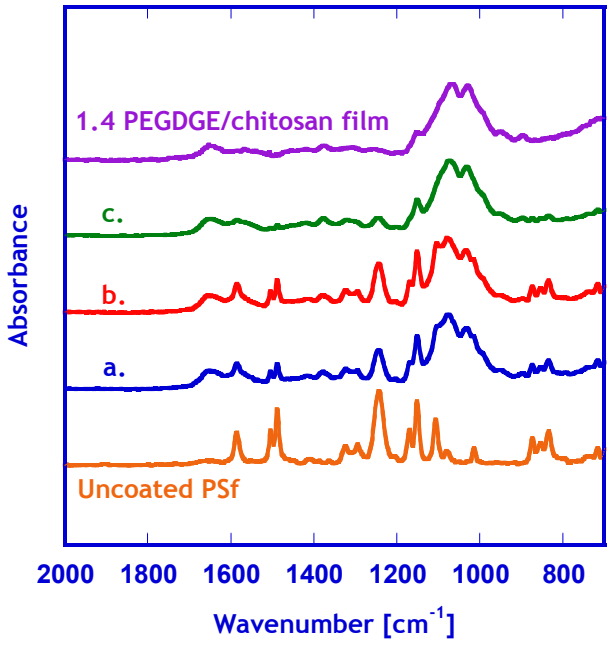

Figure 4.5: ATR FTIR spectra of an uncoated PSf membrane, a 1.4 PEGDGE/chitosan film, and three composite membranes (a-c) using the following coating solution concentrations: a. 1.0 wt% chitosan, b. 1.25 wt% chitosan, c. 1.5 wt% chitosan. All coating layers were formed from a 1.4 PEGDGE/chitosan ratio solution. The spectra were displaced vertically for easier viewing.

Figure 4.6 presents pure water permeance (*i.e.*, pressure normalized flux) as a function of pressure for the three composite membranes discussed above. A general increase in permeance is observed with decreased coating solution concentration. However, variability in permeance increases significantly as coating solution concentration decreases. This variability was measured using the standard deviation of three 3.5 cm^2 and one 14.6 cm^2 diameter membranes cut from the same composite membrane. Large differences in the coating layer thickness and possible pinhole defects from sample-to-sample are the most probable cause for the variability observed in the 1.0 composite membrane, which forms samples with the thinnest coatings. However, less variability was observed in the 1.25 and 1.5 composite membranes, suggesting that these

membranes have more uniform coating thicknesses and/or fewer defects, especially compared to the 1.0 composite membrane. Additionally, the water permeance for each membrane remains statistically equal at different pressures, which would be expected of nonporous crosslinked polymers. [96] Based on the water permeability (31.0 L μm m^{-2} hr^{-1} atm^{-1}) of a thick, dense 1.4 PEG/Chitosan ratio films, the effective thicknesses of the thin skin layer range from 0.7 μm for the 1.0 composite to 1.9 μm for the 1.5 composite, which are slightly higher than the values observed in the SEM images. A previous study exploring PEG hydrogels as possible coating materials observed a similar difference between the effective and actual coating thickness and attributed it to slight pore penetration.[55] Although no significant pore penetration was observed in the SEM images, the lengthy crosslinking step used in this study could lead to solution wicking into the pore structure. Different coating techniques, such as spin coating or brush coating, may lead to more consistent coatings with less pore penetration.

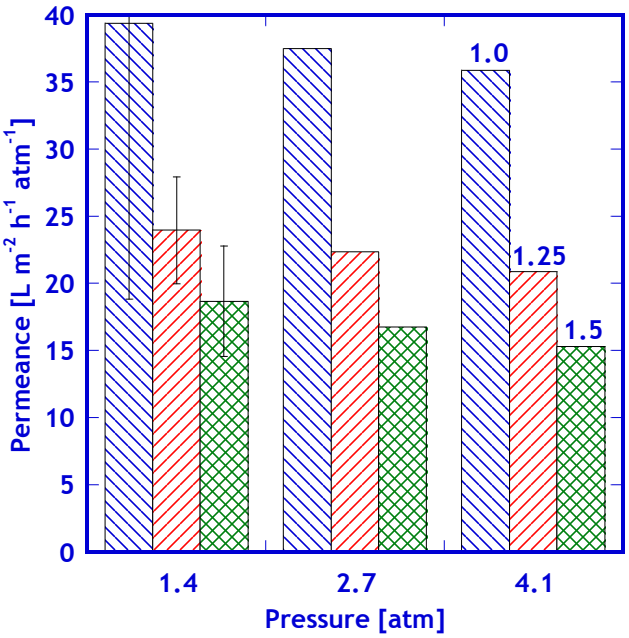

Figure 4.6: Pure water permeance as a function of pressure for three PSf/chi-PEG hybrid composite membranes. The numbers above the bars on the far right hand side of the graph represent the weight percent chitosan in the prepolymerization solution. The bars of similar shading at other pressures correspond to samples of these same chitosan concentrations. All coating solutions had a 1.4 PEGDGE/chitosan ratio. Error bars were calculated using the standard deviation of three 3.5 cm^2 and one 14.6 cm^2 diameter membranes cut from the same membrane sample.

4.3.3 Oil fouling experiments

To test the PEGDGE/chitosan hybrid layer's fouling resistant capabilities, crossflow filtration of an oil-water emulsion was performed on both coated and uncoated membranes. This oil-water emulsion has been used in previous studies.[55, 61]

Figure 4.7 presents flux and rejection of the composite membranes and, for comparison, an uncoated PSf membrane. After one day of operation, the 1.5 composite membrane exhibited a flux of approximately 70 $Lm^{-2}h^{-1}$, which was 5 times higher than the average flux of three uncoated membranes, which was approximately 13 $Lm^{-2}h^{-1}$. The 1.0 and 1.25 composite membranes had higher initial fluxes (136 and 113 $Lm^{-2}h^{-1}$,

respectively) but both fouled to a greater extent than the 1.5 composite membrane during the filtration experiment (decreasing to 88 and 77 $Lm^{-2}h^{-1}$, respectively). Nevertheless, their fluxes still remained higher than that of the 1.5 composite membrane after one day of operation. Furthermore, the rejection capabilities of the coated membranes are better than those of the uncoated membrane (as seen in Figure 4.7b). Rejection for the coated membranes remained constant (~98%) over the course of one day. However, the uncoated membrane's rejection slightly increases from ~96.7% to 97.7%, and it was always less than that of the coated membranes. Although in this experiment the composite membranes were not run "side-by-side" with an uncoated membrane, previous experiments always showed uncoated membranes with a lower rejection and a lower flux than the composite membranes run with it. Clearly, the thin PEG-chi hybrid coating increases membrane efficiency when filtering oil/water emulsions.

Table 4.1: Pure water permeance of membranes at 60 psi (4.1 atm) before and after using the membranes to filter oil/water emulsions for one day.

	Water Permeance [L m^{-2} h^{-1} atm^{-1}]		
Membrane	Before oil/water filtration, P_{BF}	After oil/water filtration, P_{AF}	P_{AF}/P_{BF}
1.0 Composite	35.9	25.1	0.7
1.25 Composite	20.9	17	0.82
1.5 Composite	15.3	14	0.91
Uncoated	367	10.7	0.03

NOTE: The oil/water filtration experiment was conducted according to the conditions given in Figure 4.7.

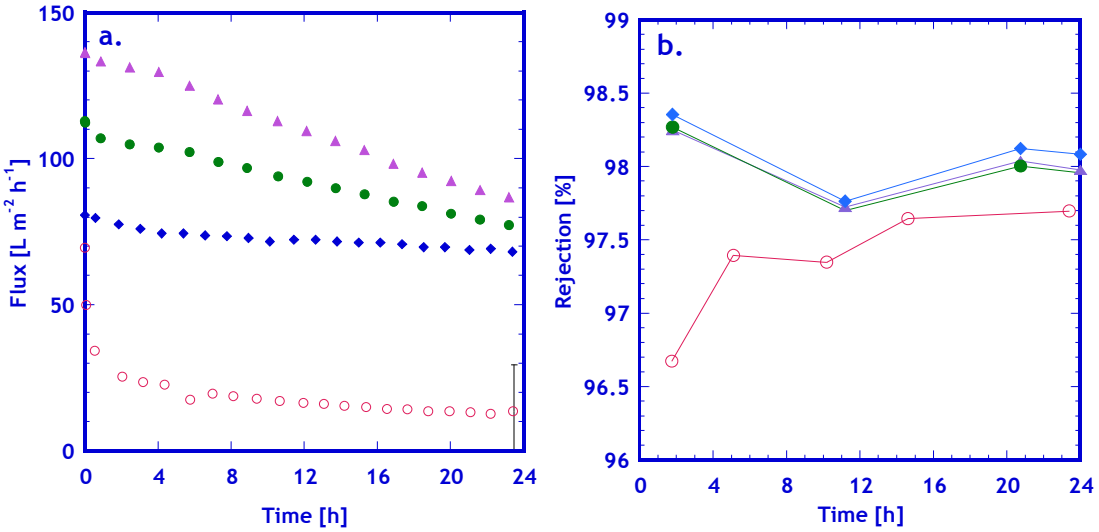

Figure 4.7: (a). Permeate flux as a function of time for the filtration of an oil/ water emulsion (1350 ppm vegetable oil, 150 ppm DC193 surfactant) at 6.8 atm and a crossflow flowrate of 1.3 L/m (Re~1400). (b). Total organic rejection as a function of time. (♦) 1.5 composite, (●) 1.25 composite, (▲) 1.0 composite, and (○) uncoated PSf membranes.

Further evidence of the fouling-resistant capabilities of the PEG-chi hybrid coatings can be observed when comparing irreversible fouling of the composite membranes to that of the unmodified PSf. To elucidate the extent of irreversible fouling, once a crossflow fouling experiment was finished, the membranes were carefully removed from their crossflow cells and thoroughly rinsed in ultrapure water to insure that all external foulants had been removed. Due to the effective filtration area of each membrane (3" x 1"), three circular disks with 1" diameters were cut from each sample and were tested for pure water permeation in 3.5 cm^2 dead-end cells. These "after filtration" water permeance results were compared to the pure water permeance of "before filtration" membranes. Table 4.1 compares pure water permeance data for membranes before and after being used to filter the oil/water emulsion. The after filtration membranes were those used in the crossflow experiments presented in Figure

4.7. In other words, they were membranes that underwent oil-emulsion crossflow filtration for 24 h. As expected, irreversible fouling of the composite membranes decreases as the coating thickness increases, as observed by comparing the ratio of pure water permeance in the before and after filtration samples. This decrease in irreversible fouling is most likely due to the increased integrity of the coated membranes: fewer defects leads to less internal irreversible fouling. The fouling resistance of the coating layer is indicated by comparing the composite membrane's before and after filtration permeance with that of an uncoated membrane. The uncoated membrane only retains 3% of its original pure water permeance after filtration, whereas the composite membranes retain from 70-91% of their original water permeance. By eliminating a significant amount of irreversible fouling, membrane cleansing cycles may prove to be more efficient at restoring flux to levels consistent with those observed in the membranes prior to exposure to fouling mixtures such as oil/water emulsions.

4.4 Conclusions

A series of hydrogels based on chitosan and a bifunctional PEG crosslinker were synthesized. Their characteristic morphologies, transport properties and solute rejection properties were characterized using various methods. Based on these findings, a 1.4 PEGDGE/chitosan ratio solution was found to be the most promising coating candidate for UF membranes. Therefore, composite membranes were synthesized by coating a 1.4 PEGDGE/chitosan solution on a conventional UF PSf membrane via a "draw-down" method. SEM, FTIR, and pure water permeance measurements indicated that, depending on the concentration of chitosan in the coating solution, the coating layer thickness could

be controlled, and therefore water permeance could be optimized. However, thin composite coating layers led to more defects, as indicated by variability in their pure water permeance. This PEG-chi hybrid coating layer can significantly increase a polymer membrane's resistance to fouling. In this study, the thin PEG-chi hybrid coating increases membrane efficiency (*i.e.*, an increase in both rejection and water flux) significantly when filtering oil/water emulsions. Furthermore, these PEG-chi hybrid coatings sharply reduce irreversible internal fouling, which could make membrane cleaning cycles more efficient at restoring flux following fouling. When comparing the fouling performance of composite membranes, the thin coating layer (*i.e.*, 1.0 composite membrane) composite membrane's flux remained higher during the fouling experiment than that of a composite membrane with a thicker coating layer (*i.e.*, 1.25 or 1.5 composite membrane). However, the 1.0 composite membrane fouled to a greater extent than the other two composite membranes, suggesting that the thinner coating has more defects and therefore more internal fouling. On the other hand, the 1.5 composite membrane maintained a slightly lower flux, but showed high resistance to fouling (only 8% decrease in flux during a one day oil/water emulsion filtration experiment).

5. CHAPTER 5: A UNIVERSAL, BIOFOULING-INSPIRED SURFACE MODIFICATION TO INCREASE WATER PURIFICATION MEMBRANE FOULING RESISTANCE

5.1 Summary

Here we report membrane surface modification methods to remarkably reduce fouling in all common classes of membranes used in water purification applications. Polydopamine was recently found to non-selectively deposit from solution onto virtually any surface. When deposited on water purification membranes, polydopamine renders the membrane surfaces more hydrophilic and less susceptible to fouling. Moreover, it can serve as a primer layer to permit additional chemical modification of membrane surfaces with other fouling-resistant moieties, such as poly(ethylene glycol) (PEG). Various polymeric membranes were modified with polydopamine, and all showed improved fouling resistance while filtering an aggressive foulant: oil-water emulsions. PEG ad-layers were easily applied to polydopamine-modified membrane surfaces to further improve fouling performance in many cases. Finally, this strategy was applied to entire membrane modules, thereby rendering all wetted parts resistant to fouling. The simplicity, versatility, and broad applicability of polydopamine deposition on membranes provide distinct advantages over other common modification strategies to reduce fouling.

5.2 Introduction

Bioinspired materials, by mimicking Nature, have been used to produce materials having a wide variety of interesting properties, including reversible attachment polymers (Gecko-like adhesion)[97], self-cleaning surfaces (lotus and rice leaf morphologies)[98, 99] and

other stimuli-responsive (i.e., thermo-, pH-, photo-responsive, etc.) materials[100]. In this regard, mussels are notorious maritime foulants that adhere to virtually any surface, including traditional non-stick materials such as PTFE,[101] by secreting a sticky, proteinaceous compound known as mussel adhesive plaque. A recent study reports that dopamine (4-(2-aminoethyl)benzene-1,2-diol) self-polymerizes under mild (pH~8.5, tris buffer) aqueous conditions and adheres to virtually any surface.[101] The resulting polymer, polydopamine (PDOPA), mimics *Mytilus edulis* foot protein 5 (Mefp-5) by incorporating two chemical groups (catechols and amines) prevalent in Mefp-5, which is a key component of *M. edilus'* adhesive plaque.[101] PDOPA adhesion was particularly strong on organic surfaces, many of which are used in water purification membranes. PDOPA treatment of even highly hydrophobic surfaces, such as PTFE, renders them very hydrophilic, based on contact angle measurements, and membranes with hydrophilic surfaces are reported to resist fouling by hydrophobic solutes, such as emulsified oil droplets.[55, 101]

In this study, we used PDOPA to modify common liquid filtration membranes, including polypropylene (PP) microfiltration (MF), PTFE MF, PVDF MF, PES ultrafiltration (UF), polysulfone (PSf) UF, polyamide (PA) nanofiltration (NF), and PA RO. Detailed information regarding membrane specifications are provided in Table 5.1. These membranes were chosen because each is a common membrane for its class (i.e., PSf and PES are common UF membranes, PTFE and PP are common MF membranes, etc.), so they illustrate the versatility of PDOPA membrane modification. PDOPA was

found to deposit uniformly on every membrane studied. The resistance of the modified membranes to fouling by emulsified oil droplets, a common foulant in wastewater streams such as produced water,[24, 30] was remarkably improved. This result is intriguing, and initially somewhat counterintuitive, because it suggests that modification of membranes with a polymer that mimics one of the most notorious biofoulants found in Nature can remarkably improve membrane resistance to fouling. Additionally, most PDOPA-modified membranes had higher flux recovery following simple water rinsing protocols following fouling, so PDOPA modification could potentially simplify and enhance membrane cleaning efficacy, thereby increasing membrane lifetime and reducing operating costs.

Table 5.1 Commercial membranes used in this study.

Classification	Membrane polymer	Manufacturer	Pore size	Flux [$Lm^{-2}h^{-1}$ bar^{-1}]	Study ID
RO	Polyamide	Dow (XLE	N/A	7.7*	XLE RO
NF	Polyamide	Dow (NF-90)	N/A	12.3*	NF-90
UF	Polysulfone	GE (A1 support)	~100 kDa MWCO	300	PSF A1 UF
UF	Polysulfone	Sepro (PS-20)	~20 kDa MWCO	1000*	PS-20 UF
UF	Polyethersulfone	Sepro (PES-30)	~20 kDa MWCO	300*	PES UF
MF	Polyvinylidene fluoride	Millipore	0.22 μm	5500	PVDF MF
MF	Polytetrafluoroethylene	GE	0.22 μm	6500	PTFE MF
MF	Polypropylene	GE	0.1 μm	2500	PP MF

NOTE: * indicates manufacturer's specification, otherwise any flux values reported here were measured in dead-end filtration cells using pure water.

Another advantage of PDOPA is its ability to covalently bind properly conjugated molecules under mild aqueous conditions and slightly elevated temperatures (~50° C).

That is, in addition to increasing fouling resistance on its own, such as in membranes to filter oily wastewater, dopamine treatment also acts as a "primer" for surfaces, such as PTFE, polyolefins, etc., that might otherwise be synthetically challenging to surface-modify, providing functional sites that permit facile attachment of other groups. For example, PDOPA-modified membranes contacted with an aqueous solution containing poly(ethylene glycol) amine (mPEG-NH_2, 5,000 MW, JenKem USA, Inc.) results in PEGylation of the PDOPA-modified surface which, in some cases, further enhances water flux, solute rejection, or both (c.f., Figure 5.1). This report describes the fouling resistance enhancement in many types of membranes by either PDOPA modification of membranes (termed PDOPA-modified membranes herein) or PDOPA-modified membranes that are subsequently treated with mPEG-NH_2 to form a PEG ad-layer on the PDOPA-modified surface (termed PDOPA-g-PEG-modified membranes herein).

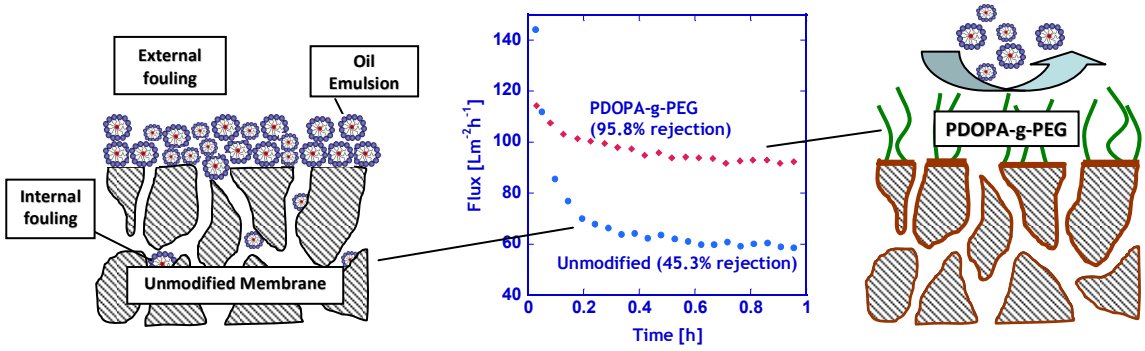

Figure 5.1: An illustration of emulsified oil membrane fouling and PDOPA-g-PEG membrane modification to improve fouling resistance of a porous membrane. PDOPA modification (indicated by the brown outlines) is uniform and ultra-thin (~5 nm), leading to a conformal coating of the membrane surface and pore structure. PEG grafting to the PDOPA layer is achieved using aqueous-based chemistry. Many PDOPA and PDOPA-g-PEG-modified membranes exhibit improved fouling resistance, including a poly(vinylidene fluoride) MF membrane (PVDF MF), whose unmodified and PDOPA-g-PEG modified oil emulsion filtration fluxes are presented here. Rejection values were measured at the end of the filtration (t=1h). Filtration conditions: 1350 ppm soybean oil, 150 ppm DC193 (Dow Corning) surfactant, 2 L/m crossflow (Re~2600), ΔP=0.3 atm.

5.3 Results and Discussion

5.3.1 Effect of PDOPA deposition on membrane flux and surface property characteristics

Figure 5.2 presents pure water permeance (i.e., pressure normalized flux) of a PSF A1 UF membrane as a function of exposure time to a PDOPA solution (i.e., PDOPA deposition time). At short deposition times, permeance decreases strongly as PDOPA deposition time increases. For example, permeance decreased from 297 $Lm^{-2}h^{-1}bar^{-1}$ to 2.2 $Lm^{-2}h^{-1}bar^{-1}$ after 16 hours of deposition. Figure 5.2 also presents the influence of deposition time on PDOPA deposition thickness, as measured using ellipsometry[87, 88], on thin, nonporous Udel PSF films. PDOPA deposition increased with increasing time, but appeared to approach a plateau of approximately 65 nm after about 8 hours. Similar results (i.e., significant deposition at early immersion times, followed by little further deposition at long immersion times) were observed on silicon substrates.[101, 102] 65 nm of PDOPA deposition corresponds to a very small fraction of the dopamine initially present in the solution (< 1%), so the plateau in deposition thickness (cf., Figure 5.2) is not a result of all of the dopamine depositing on the polysulfone film surface. Furthermore, the PDOPA solution remained dark brown, with visible formation of PDOPA particles after approximately one hour, indicating reaction of dopamine in the solution. The plateau in deposition thickness presumably reflects the competition between PDOPA deposition and PDOPA formation in solution to consume free dopamine. In support of this hypothesis, Lee et al. observed that immersing a substrate in a PDOPA solution that had been previously incubated for long periods of time (greater than three days) led to no deposition.[101]

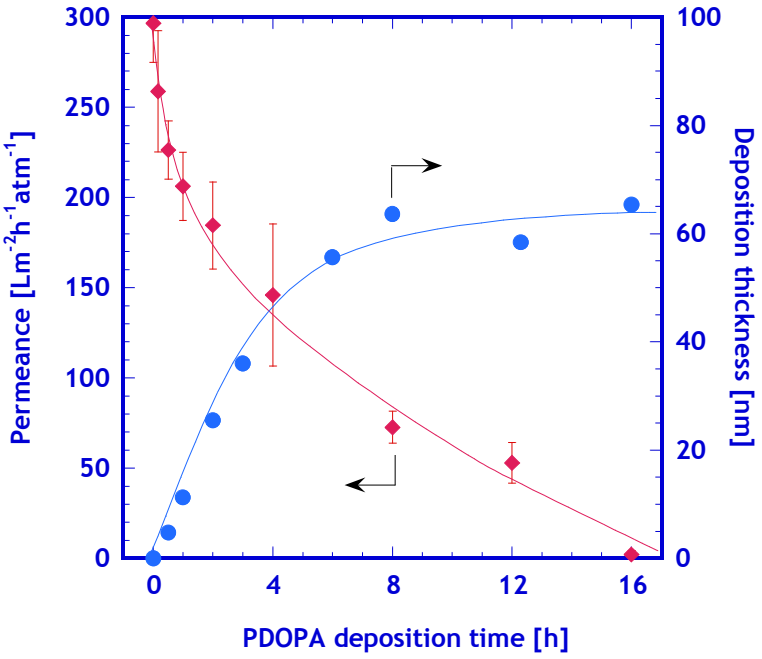

Figure 5.2: Pure water permeance as a function of PDOPA deposition time on a polysulfone ultrafiltration membrane (PSF A1 UF), and PDOPA deposition thickness as a function of PDOPA deposition time on Udel polysulfone thin films.[80]

The deposition thicknesses reported were in the same range as the pore size of the PSF A1 UF membrane, which was characterized using PEG molecular weight cutoff (MWCO) experiments (cf., Figure 5.3). Typically, the mean pore diameter of a membrane is assessed as the Stokes diameter of the PEG molecule having a rejection of 50%.[85] For the PSF A1 UF membrane, the rejection is 50% for a 17.5 kDa PEG molecule, which, using equation (8), yields a pore diameter of 7.7 nm. To provide some characterization of the pore size distribution, the PSF A1 UF molecular weight cutoff (i.e., the PEG molecular weight for which the rejection is 90%) is 92.5 kDa[55], corresponding to a pore diameter of 18 nm.[85]

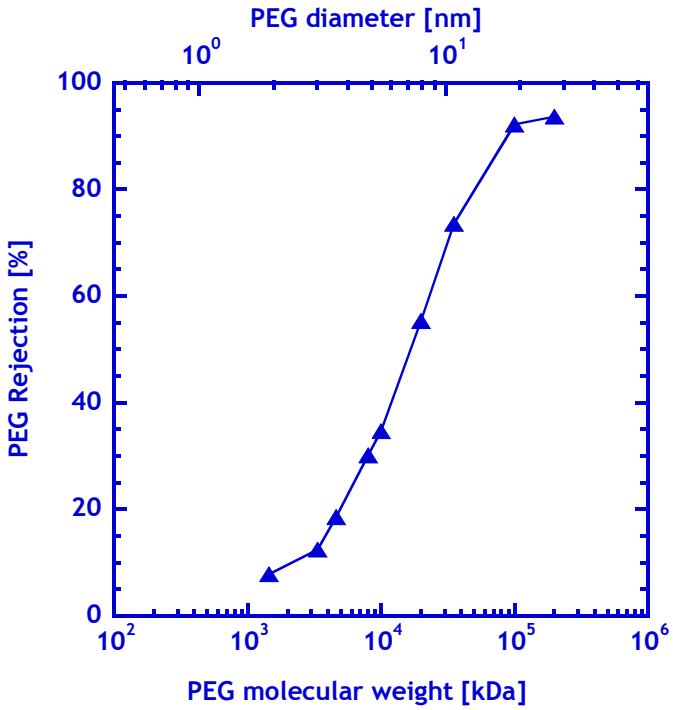

Figure 5.3: Effect of PEG molecular weight on rejection by an unmodified PSF A1 UF membrane. From these data, the molecular weight cutoff is approximately 92.5 kDa. Adapted from [55].

During the initial stages of deposition, PDOPA should be able to penetrate into the porous structure of the UF membrane because its molecular weight is still relatively small. Therefore, some PDOPA deposition probably occurs within the membrane pore structure, leading to pore constriction and a water permeance decrease. However, as deposition time increases, the effective PDOPA molecular weight has been reported to reach millions.[101] Eventually, the thickness of the PDOPA layer blocks the pores in the UF membrane, leading to the continuing decrease in membrane permeance observed in Figure 5.2 at long deposition times. Although the PDOPA deposition thickness appears to plateau around a deposition time of 8 h, the flux of the UF membrane continues to

decrease at longer deposition times (e.g., from 73 $Lm^{-2}h^{-1}bar^{-1}$ at a deposition time of 8 h to 2.2 $Lm^{-2}h^{-1}bar^{-1}$ at a deposition time of 16 h). At 8 h, many pores have been significantly constricted, as observed by the significant reduction in permeance compared to unmodified membranes. Therefore, even small amounts of further PDOPA deposition, as is likely to occur at deposition times greater than 8 h, may bridge and completely block the pores, leading substantial further decreases in membrane permeance. For water filtration applications, high water flux is desirable, so short PDOPA deposition times were the focus of this study, because they led to higher values of pure water flux.

Interestingly, even at low PDOPA deposition times, when the water flux of a PDOPA-modified membrane is only slightly less than that of an unmodified membrane, a significant increase in membrane surface hydrophilicity was observed. Table 5.2 presents captive *n*-decane bubble-in-water contact angles as a function of PDOPA deposition time on a PSF A1 UF membrane. At even the shortest deposition time considered, ten minutes, the contact angle decreased significantly, indicating an increase in membrane hydrophilicity. Membrane fouling resistance has been correlated with membrane surface hydrophilicity, with more hydrophilic surfaces being more resistant to, for example, fouling by emulsified oil droplets.[26]

Table 5.2: Influence of PDOPA deposition time on captive *n*-decane-in-water contact angles of PSF A1 UF membranes.

PDOPA deposition time [min]	Contact angle [°]
0	109 ± 5
10	49 ± 7
60	49 ± 4
120	58 ± 2
240	47 ± 5
480	47 ± 1
720	53 ± 4
960	55± 7

All membranes studied (except for the already very hydrophilic PVDF MF membranes) showed a marked increase in surface hydrophilicity following PDOPA treatment for even limited contact time, including the already hydrophilic PA NF and RO membranes (Table 5.3). The PVDF MF membranes were even more hydrophilic than the XLE RO membranes initially. Because PVDF is not expected to be hydrophilic based upon its chemical structure, it is likely that these membranes contained hydrophilic (or amphiphilic) surface-active additives (a common amphiphilic additive is poly(vinyl pyrrolidine)[103]) in the PVDF membrane casting mixture that rendered the surface of the PVDF membranes hydrophilic. Because the PVDF membranes had highly hydrophilic surfaces prior to PDOPA treatment, there was no observable increase in their hydrophilicity due to PDOPA treatment.

Table 5.3: Captive n-decane-in-water (XLE RO) or air-in-water (PVDF MF) bubble contact angles.

	Contact Angle [°]	
Sample	**Unmodified**	**PDOPA modified**
XLE RO	45 ± 3	36 ± 4
NF-90	49 ± 2	40 ± 3
PP MF*	81 ± 2	33 ± 5
PTFE MF*	120 ± 6	50 ± 3
PVDF MF*	31 ± 1	31 ± 4

NOTE: * indicates that air-in-water bubbles were used (decane would readily absorb into the porous membrane structure of the PVDF MF unmodified membranes). The PDOPA deposition time was 60 minutes.

For MF membranes, which have larger pores than UF membranes, modified via 60 min. immersion in PDOPA solution, the permeance (i.e., pressure-normalized flux) values of a modified and unmodified membrane are typically equal, probably because the addition of the dopamine conformal coating layer decreases the overall pore size by a negligible amount. Interestingly, highly hydrophobic membranes (e.g., PP and PTFE) actually exhibited somewhat higher (~5-30%) initial pure water permeance following PDOPA modification, likely due to the increased wettability of the PDOPA-modified membrane structure, which allowed additional pores to wet and contribute to membrane flux.

Figure 5.4 presents the streaming potential of unmodified, PDOPA-modified, and PDOPA-g-PEG-modified XLE RO membranes. Streaming potential allows us to quantitatively analyze the surface charge on membranes. XLE RO membranes were negatively-charged over a broad pH range, with an isoelectric point (neutral surface charge) around pH=3.5. This trend is common in polyamide membranes, as the interfacial polymerization used to produce the XLE RO membranes leads to an excess of

carboxylic acid on the membrane surface[13, 62, 104] Typical benzene polycarboxylic acids used to synthesize the polyamide structure can have a pK_a anywhere in between pH=2-5, which is consistent with the isoelectric point observed in the XLE RO membrane.[105] PDOPA reduced the magnitude of the membrane's surface charge slightly. This was also expected, as the pKa of the hydroxyl proton in the PDOPA catechol groups is 9.2, indicating that PDOPA is itself theoretically neautrally charged over all pH lower than 9.2.[106] However, the ultra-thin PDOPA coating layer (the coating layer is still expected to be much thinner than the characteristic surface roughness of the XLE RO membrane, discussed later) did not completely neutralize the surface charge associated with the native XLE RO polymer. The PEG grafting layer reduced the surface charge magnitude further. PEG-based hydrogels have been observed to neutralize surface charge on RO membranes in a previous study, and is expected due to PEG being non-ionizable and hydrophilic.[62]

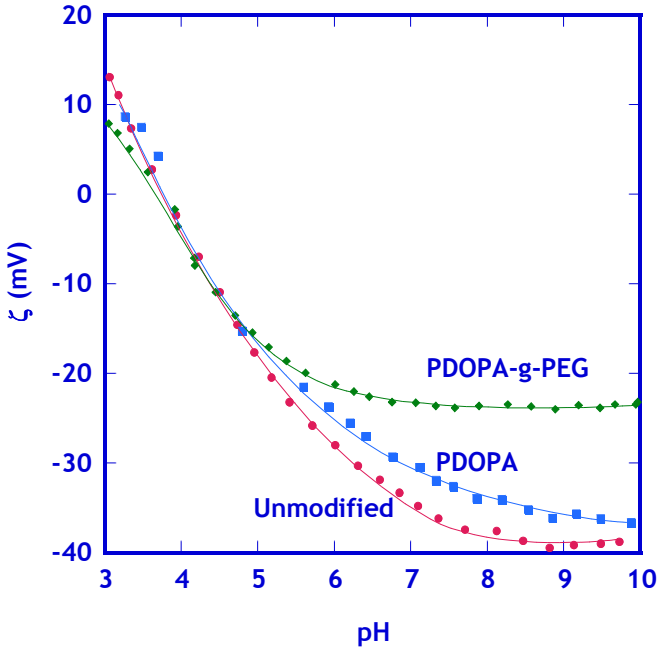

Figure 5.4: Streaming zeta potential, ζ, of an unmodified, PDOPA-modified, and PDOPA-g-PEG modified XLE RO membrane. A 60 min PDOPA deposition time and 60 min PEG (5 kDa) grafting time were used in the respective modifications. Lines were drawn to guide the eye.

Figure 5.5 presents atomic force microscopy (AFM) images of unmodified and PDOPA-modified PSf A1 UF, NF-90, and XLE RO membranes. The root-mean-square roughness, as calculated from the images, is also given below each image. PDOPA-modification, in each case, tended to reduce the surface roughness slightly. This reduction could lead to improved anti-fouling membrane properties, as surface roughness has been directly correlated with a membrane's fouling propensity.[107]

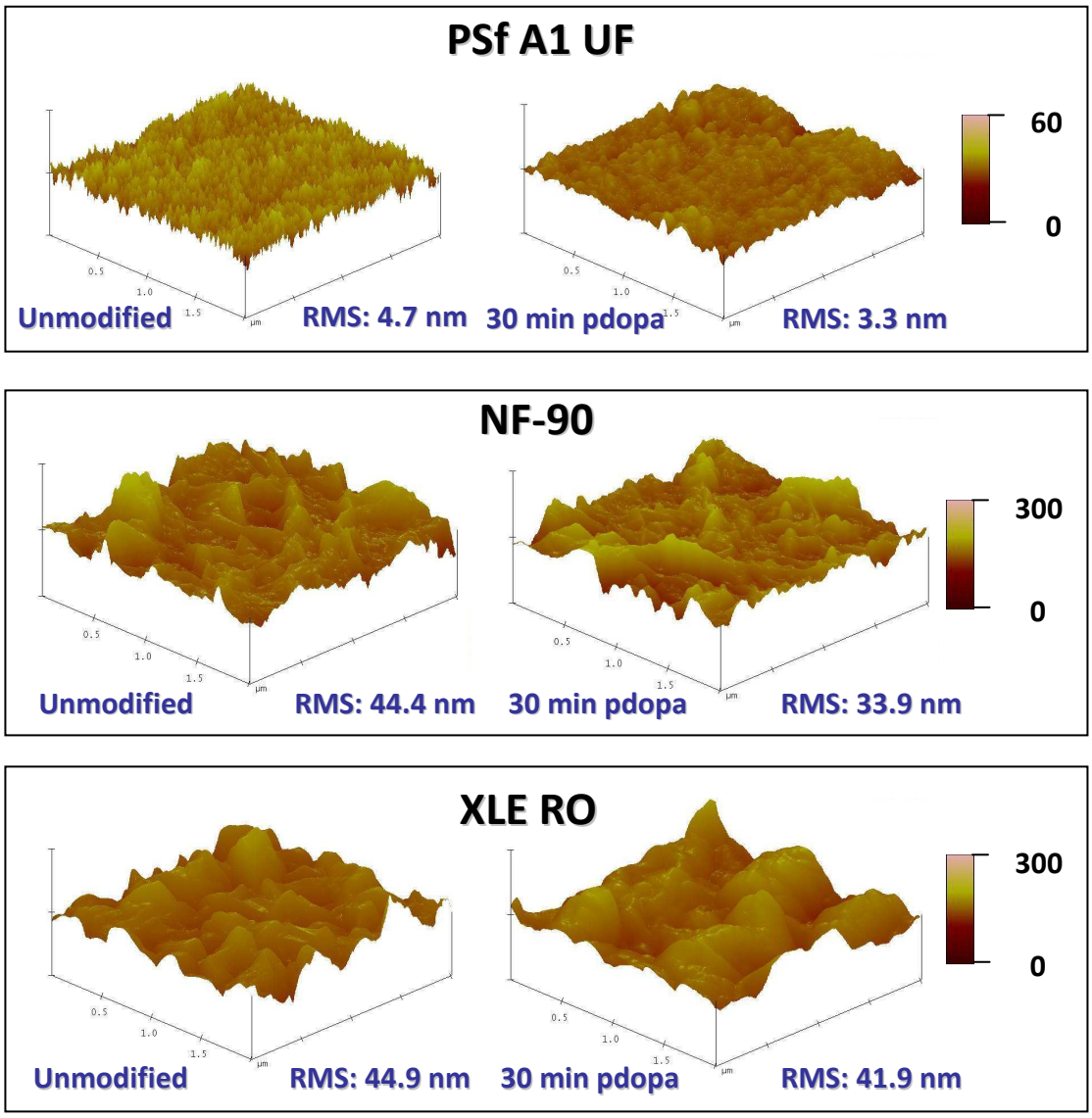

Figure 5.5: Atomic force microscopy images of unmodified and PDOPA-modified PSf A1 UF, NF-90, and XLE RO membranes. The root-mean-square roughness of each image is listed below each image.

5.3.2 PDOPA leaching from a TW30 Dow Filmtec RO membrane module

PDOPA modification of PSf membranes was robust over a wide pH range, because no significant surface discoloration or change in contact angle occurred even after sonicating a membrane for 5 minutes in 3M HCl solution. Moreover, no PDOPA

leaching was observed (as measured by UV spectroscopy) after approximately 4 days of rinsing a PDOPA-modified RO membrane module (TW30-1812-36, Dow Water Solutions) in water (PDOPA was still visibly present on wetted parts of the membrane module after 4 days). Figure 5.6 presents the PDOPA leaching from a TW30 membrane module. Approximately 0.3-0.5 ppm PDOPA is the detection limit of UV absorbance. This concentration corresponds to leaching rates of 0.9-1.2 mg/day using the procedure outlined in the experimental methods section. Both day 3 and day 4 leaching rates are below this threshold, with day 4 being significantly below this threshold. Therefore, after 4 days of membrane rinsing, leaching of PDOPA is undetectable. The initial leaching seen in the first two days is attributed to PDOPA that may have been, for example, entrained between the membrane spacer and membrane, or the module housing and the module. No PDOPA is expected to permeate through the membrane due to PDOPA's high molecular weight and therefore PDOPA leaching through the permeate during water filtration was not measured here. This negligible leaching has led to PDOPA-modified modules being certified for drinking water use by the National Sanitation Foundation (NSF standard 61). PDOPA's excellent adhesion may be attributed, at least in part, to the extraordinary strength of the catechol-substrate physical bond, which, for a titania substrate, has been shown to be on the order of half a typical covalent bond.[106] Some common bond rupture forces, including typical hydrogen bonds, covalent bonds, and a DOPA-Ti physical bond, are presented in Table 5.4.

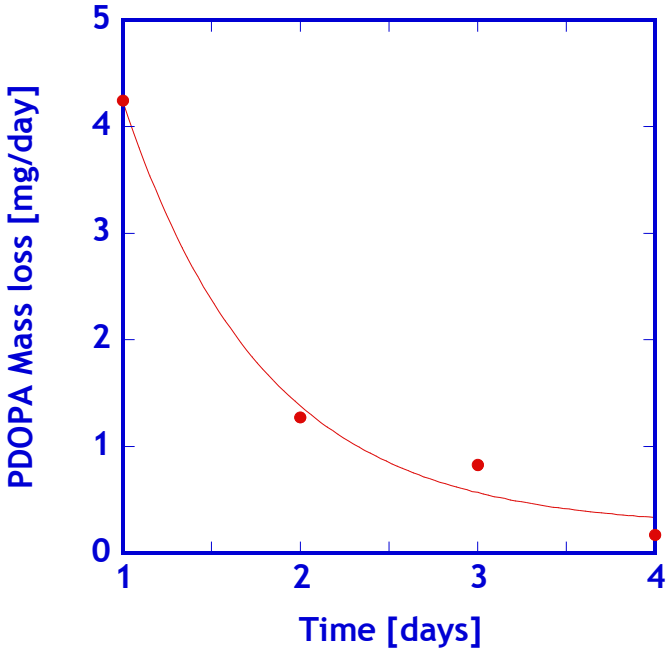

Figure 5.6: Total leaching of PDOPA from a TW30 membrane module while being rinsed with ultrapure water. PDOPA leaching was measured using UV absorbance. Line was drawn to guide the eye.

Table 5.4: Common bond rupture forces for selected bonds.

Bond type	Bond rupture force (pN)
C-H/π (H-bond)*	20-60
Water H-bond*	100-300
Dopa-Ti (physical)	800
Au-S (covalent)	1400
Si-C (covalent)	2000

NOTE: * indicates approximations based on F=D/L, where D is the bond dissociation energy, L is the bond length, and F is the approximate bond rupture force. References: [106, 108, 109, 110].

5.3.3 Oil emulsion fouling on unmodified, PDOPA modified and PDOPA-g-PEG modified membranes

Fouling experiments were performed in crossflow filtration using a synthetic vegetable oil/non-ionic surfactant emulsion described in the supporting information and elsewhere.[55] Regardless of membrane type, PDOPA-modified and PDOPA-g-PEG-

modified membranes generally outperformed their unmodified counterparts. For example, after one hour of filtering emulsified oil, the flux of a PDOPA-modified PSf UF (PS-20 UF) membrane is, surprisingly, 125% higher than that of an unmodified membrane and exhibited similar organic rejection (Figure 5.7a). A small additional improvement in membrane flux, relative to the PDOPA-modified membrane, is observed when a PEG ad-layer is bound to the polydopamine layer: the PDOPA-g-PEG-modified PSf UF flux is 145% higher than that of an unmodified membrane after one hour of filtration. As shown in Figure 5.7b, a PTFE MF membrane exhibited higher flux and rejection than an unmodified membrane following modification with PDOPA and PDOPA-g-PEG (85 Lm^{-2} h^{-1} for an unmodified membrane after 1 h of filtration, 103 and 133 Lm^{-2} h^{-1} for PDOPA and PDOPA-g-PEG-modified membranes, respectively). Generally, PDOPA and PDOPA-g-PEG modified MF and UF membranes had slightly higher organic rejection than their unmodified counterparts.

Other oil emulsion fouling studies on MF and UF membranes are presented in Figure 5.8. PDOPA-modified and PDOPA-g-PEG PES UF membranes improved oil emulsion filtration flux approximately 35% compared to their unmodified counterpart after 1 hour of filtration (Figure 5.8a). The PDOPA and PDOPA-g-PEG membranes show very similar fluxes, which is somewhat surprising given the flux improvement measured between PDOPA and PDOPA-g-PEG MF membranes. Behavior similar to this was also seen in the modified PS-20 UF membranes (Figure 5.7a). This result is likely due to the high added mass transfer resistance of the PEG ad-layer. The pure water flux

ratio of a non-fouled PDOPA-g-PEG modified to a PDOPA-modified PES UF membrane is 0.60, whereas the same ratio between a PDOPA-modified and an unmodified PES UF membrane is 0.93. Optimization of PEG attachment conditions to reduce its mass transfer resistance while maintaining good anti-fouling characteristics are currently underway.

The PDOPA-modified PVDF MF membrane exhibited a similar flux to the unmodified PVDF MF membrane (Figure 5.8). However, the PDOPA-modification dramatically increased the organic rejection. A 50% improvement in flux, coupled with a further increase in organic rejection, was measured in the PDOPA-g-PEG modified PVDF MF membrane. For MF membranes in general, unlike in the UF, RO, and NF membranes, the PEG ad-layer did not lead to a dramatic increase in mass transfer resistance, as the pure water flux of PDOPA-modified and PDOPA-g-PEG PVDF membranes are approximately the same and ~90% of the unmodified PVDF MF membrane's flux. The PEG did not increase the mass transfer resistance because its Stokes radius (~1.9 nm[85]) is still very small compared to the membrane's average pore size (220 nm). PP MF membranes yielded similar results to the PVDF MF membranes, with PDOPA-modified membranes having slightly higher organic rejection and flux than an unmodified PP MF membrane after 1 h of oil emulsion filtration and PDOPA-g-PEG having ~100% higher flux than the unmodified PP membranes. Higher organic rejection is also observed in the PDOPA-g-PEG membrane.

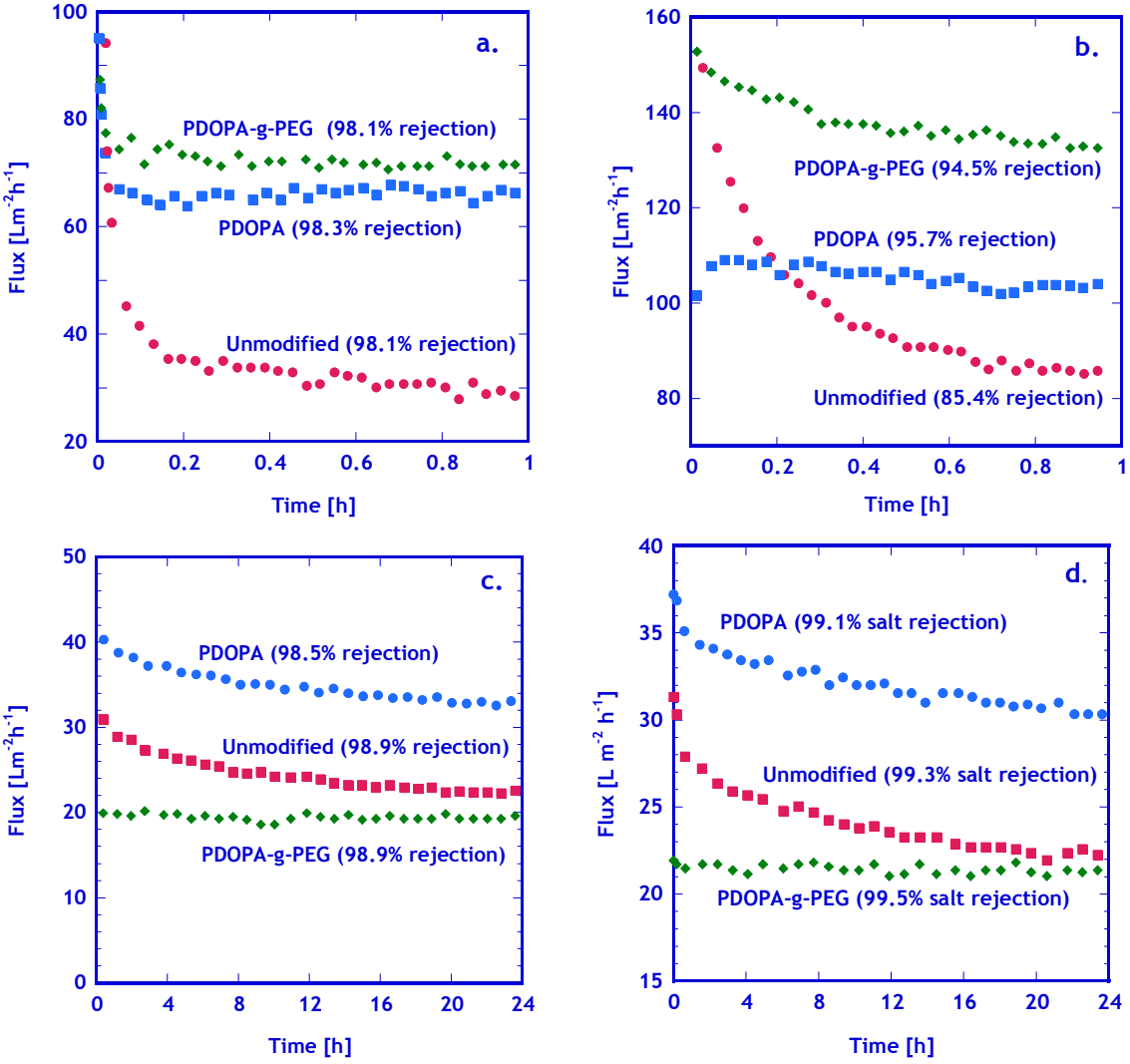

Figure 5.7: Effect of filtration time on membrane flux using unmodified, PDOPA-modified, and PDOPA-g-PEG-modified: a) polysulfone ultrafiltration (PS-20 UF) , b) PTFE MF, c) NF-90, and d) XLE RO membranes to filter an oil/water emulsion. Rejection values (organic rejection for MF and UF membranes, salt rejection for NF and RO membranes) were measured at the end of the filtration (t= 1 h for UF and MF membranes, t=24 h for NF and RO membranes). A 1350 ppm soybean oil, 150 ppm DC193 non-ionic surfactant emulsion was used as the organic foulant in this study.

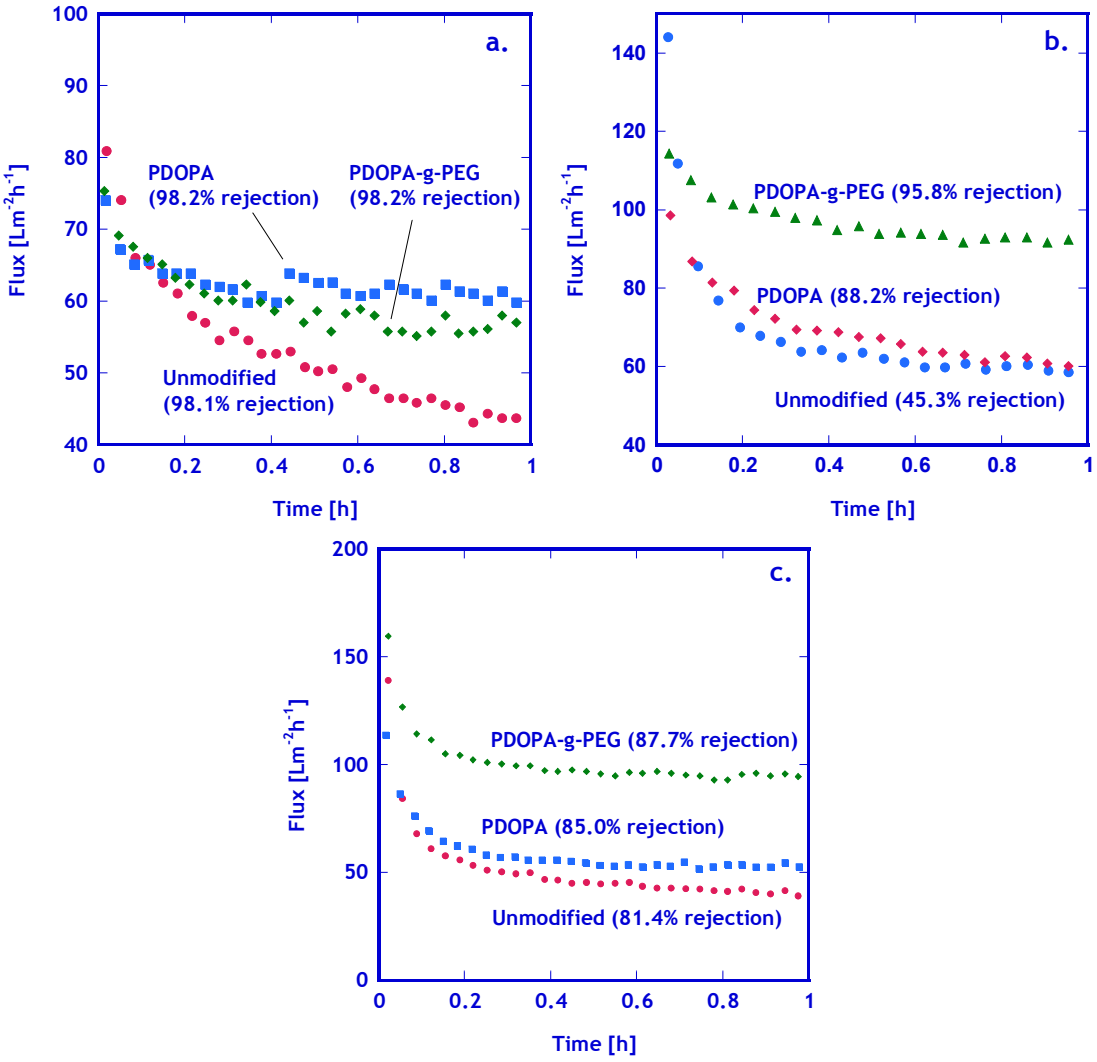

Figure 5.8: Effect of filtration time on membrane flux using unmodified, PDOPA-modified, and PDOPA-g-PEG-modified: a) PES UF, b) PVDF MF, and c) PP MF membranes to filter an oil/water emulsion. Organic rejection values were measured at the end of the filtration (t= 1h). A 1350 ppm soybean oil, 150 ppm DC193 non-ionic surfactant emulsion was used as the organic foulant in this study.

As mentioned previously, highly hydrophobic MF membranes (PP MF and PTFE MF) actually exhibited a non-fouled pure water flux increase when modified by PDOPA and PDOPA-g-PEG. Here, the pure water flux ratio of a non-fouled PDOPA-modified to an unmodified PP MF membrane was 1.13, with PDOPA-modified and PDOPA-g-PEG

PP MF membranes having similar fluxes. For PTFE MF membranes, the PDOPA-modified to unmodified flux ratio was 1.30 and the PDOPA-g-PEG to unmodified membrane flux ratio was 1.16. Because of its benign chemistry, PDOPA deposition would not be expected to lead to a flux increase through damage to the membrane or its porous structure. Therefore, the most likely explanation of increased hydrophobic MF flux is that PDOPA increased the wettability of the membrane porous structure which, when coupled with a negligible reduction in pore size associated with the deposition, allowed more pores to wet and contribute to the overall membrane flux.

As shown in Figure 5.7c and Figure 5.7d, both RO and NF polyamide membranes exhibited similar fouling trends, with PDOPA-modified membranes achieving approximately 30-50% higher flux than the unmodified membranes after one day of oil emulsion filtration, and the PDOPA-g-PEG-modified membrane showed no flux decline during the filtration, indicating no fouling occurred.

NF and RO membranes reject salt from feed streams, and as such, NaCl removal from oily waters was also tested for these membranes. The removal of salts and organics could be of interest to allow produced water (i.e., water generated in the course of oil and gas extraction operations) and other similar wastewaters to be beneficially used in industrial, agricultural, or even residential applications.[111] As expected, organic rejection was high (>99.9%; the permeate organic concentration was lower than the detection limit of our total organic carbon analyzer). Salt (NaCl) rejection data for NF and RO

membranes indicates that fouling by oily water of the unmodified PA membrane promotes slightly higher rejection for unmodified membranes compared to PDOPA-modified membranes (Figure 5.9). Oily water fouling was shown to increase NaCl rejection in RO membranes in a previous study.[62] Here, an unmodified NF-90 membrane had a NaCl rejection of 95.4% and a 30min PDOPA modified NF-90 membrane had a rejection of 96.7% (Figure 5.9a). A slight increase in rejection was also observed in the PDOPA-modified XLE RO membranes (Figure 5.9b). PEG-modified membranes had even higher initial rejections (98.7% for NF membranes, 98.9% for RO membranes). However, when an oil emulsion was added to the feed, the NaCl rejection of both modified and unmodified membranes increased, with the unmodified membranes exhibiting higher rejection than the PDOPA-modified membranes. This phenomenon is most likely caused by the higher amount of oil adsorbed to the polyamide layer of these membranes (i.e., more extensive fouling of the unmodified membranes). This adsorption leads to higher irreversible fouling and higher mass transfer resistance, which, in turn, leads to higher membrane rejection. However, PDOPA-g-PEG-modified membranes exhibit the highest salt rejection of all membranes. In previous studies, NF membranes exhibited similar increases in rejection when PEG molecules were grafted to their surface. [112, 113]

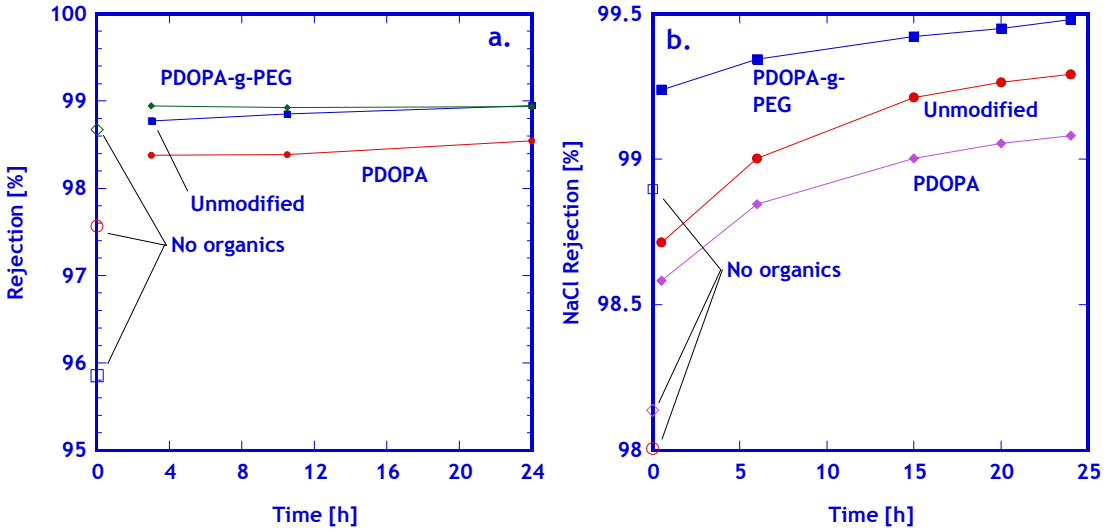

Figure 5.9: Dow Water Solutions a) NF-90 and b) XLE RO membrane NaCl rejection before oil emulsion filtration (hollow markers) and during an oil emulsion filtration (filled markers). 2000 ppm NaCl solution was used for all experiments. An oil emulsion (1350 ppm soybean oil and 150 ppm DC193 surfactant) was added to the membrane feed after "pure" salt water rejection was measured.

5.3.4 Irreversible oil emulsion fouling of unmodified and PDOPA-modified membranes

As shown in Figure 5.10, PDOPA and PDOPA-g-PEG-modified membranes exhibited an increase in irreversible emulsified oil fouling resistance, which could lead to more efficient cleaning cycles and lower overall operating costs in practical membrane applications. A higher percentage of initial membrane pure water permeance was recovered after oil fouling experiments using the modified membranes. Furthermore, PDOPA-g-PEG-modified RO and NF membranes recovered almost 100% of their original pure water flux after simply being rinsed in water following the fouling experiment.

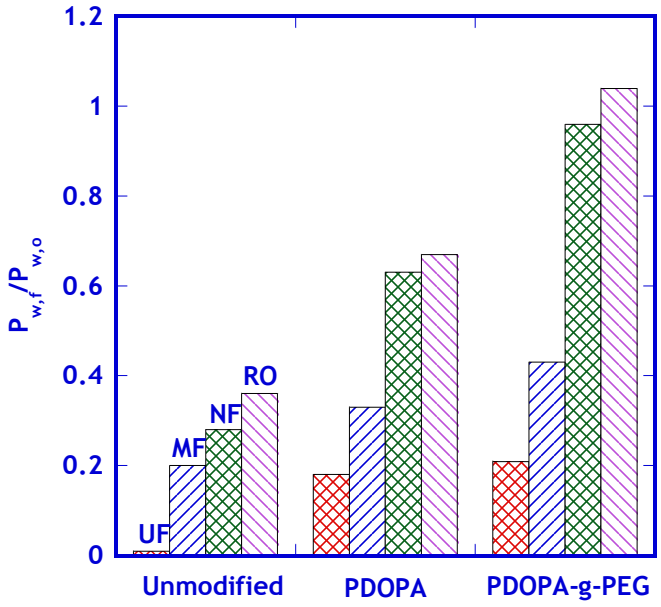

Figure 5.10: Irreversible fouling in PS-20 UF, PTFE MF, NF-90, and XLE RO membranes. $P_{w,f}$ is the pure water permeance following the filtration experiments in Figure 5.7a-d, and $P_{w,o}$ is pure water permeance before the filtration experiments. After the fouling experiments, all membranes were rinsed by circulating ultrapure water through the crossflow system before measuring $P_{w,f}$. Membrane characteristics (i.e., pore sizes, nominal fluxes, manufacturers, etc.) are listed in Table 5.1.

5.3.5 Positively-charged DTAB-decane emulsion fouling of XLE RO membranes

Figure 5.11 presents DTAB-decane emulsion fouling and irreversible fouling of unmodified and modified XLE RO membranes. A 1.5 h PDOPA deposition time was used in this experiment, and a 60 min PEG grafting time was used for the PDOPA-g-PEG-modification. DTAB is generally regarded as an extremely aggressive foulant for RO membranes because it is positively-charged (and therefore electrostatically attracted to the negatively-charged membrane), yet still retains significant hydrophobic character due to its 12-carbon aliphatic chain. This provides DTAB with two possible favorable

interactions (electrostatic and hydrophobic) that will allow it to adhere to the RO membrane surface. These interactions have been discussed previously.[62, 114]

As observed in Figure 5.11a, these favorable interactions between DTAB, and most likely an additional adsoption of decane to the DTAB hydrophobic ad-layer, led to a dramatic reduction in an unmodified XLE RO membrane's flux (the membrane's flux is only 2 $Lm^{-2}h^{-1}$ after a day of filtration). PDOPA modification slightly improves membrane hydrophilicity and slightly reduces the membrane surface charge. Therefore, a PDOPA-modified XLE RO membrane exhibited slightly higher flux than an unmodified membrane. However, the PDOPA-g-PEG membrane exhibited the best fouling resistance of all membranes. Through 10 h of filtration, the PDOPA-g-PEG membrane exhibited very little fouling, after which the flux started to decrease more rapidly. This improvement in fouling resistance was most likely a result of PEG graft brushes providing steric repulsion of DTAB from the membrane surface (and PEG imparting a more neutral surface charge, as was discussed earlier in this chapter). This phenomena (PEG brush steric repulsion) will be discussed more in Chapter 6 as it relates to BSA adhesion resistance. However, the steric repulsion would result in DTAB having a difficult time contacting the negatively-charged hydrophobic RO surface. Nevertheless, because DTAB is a relatively small molecule, it may be able to diffuse through the PEG ad-layer to the surface of the RO membrane. This diffusion process would take a long time due to the chemical dissimilarities between PEG and DTAB, and, therefore, the onset of severe fouling may be delayed by the slow diffusion process. To combat DTAB-decane fouling, membrane cleansing every few hours (i.e. before the onset of the rapid

flux decline) is suggested. As was the case with the non-ionic oil emulsion fouling, PDOPA-modified and PDOPA-g-PEG-modified XLE RO membranes both recovered a higher percentage of their initial, non-fouled pure water flux than the unmodified membrane after the DTAB-decane emulsion filtration (Figure 5.11b). Membrane cleaning was particularly effective for the PDOPA-g-PEG-modified membrane, as 100% of its initial flux was recovered. The unmodified membrane showed very poor flux recovery, indicating that DTAB and decane are strongly adhered to the membrane surface.

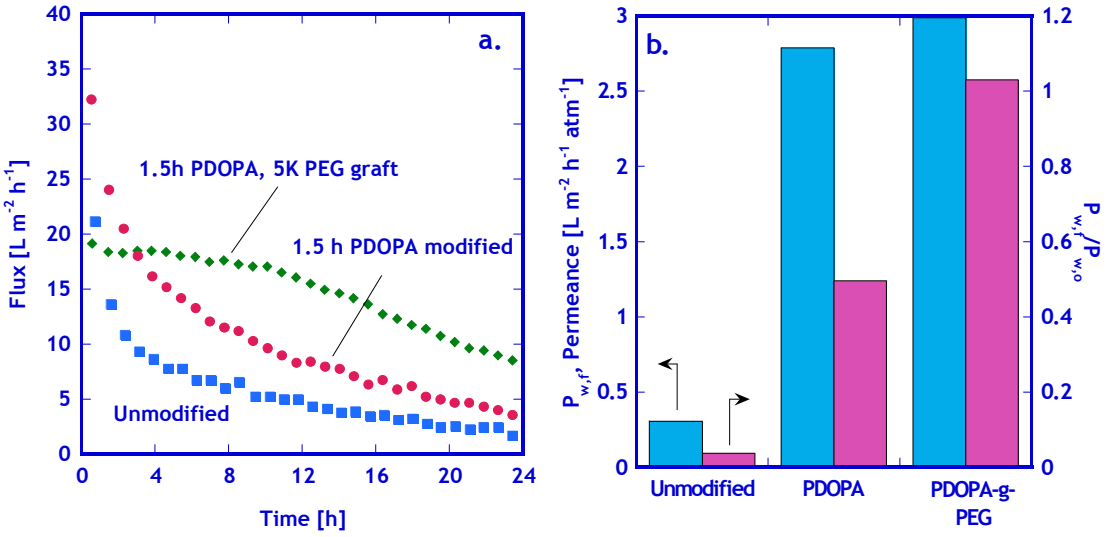

Figure 5.11: DTAB- decane positively-charged emulsion fouling experiments performed on unmodified, PDOPA-modified, and PDOPA-g-PEG-modified XLE RO membranes. a) Flux as a function of time, and b) post-fouling pure water permeance and the irreversible fouling seen in each membrane tested in Figure 5.11a. $P_{w,f}$ is the pure water permeance following the filtration experiments in Figure 5.11a, and $P_{w,o}$ is pure water permeance before the filtration experiments. After the fouling experiments, all membranes were rinsed by circulating hot (50 °C) ultrapure water through the crossflow system before measuring $P_{w,f}$. Filtration conditions: ΔP= 150 psi, 3.8 L/min crossflow (Re~4900), 15 ppm DTAB, 135 ppm decane, 2000 ppm NaCl.

5.3.6 Protein and bacterial adhesion to unmodified and PDOPA-modified membranes

Protein adhesion has been studied extensively due to the presence of proteins in many wastewaters and bioprocessing streams and the pernicious nature of protein fouling of membranes.[10, 12] Here, adhesion to membranes was explored using bovine serum albumin (BSA) as a model protein. Fluorescent BSA static adhesion studies were performed using rhodamine-N-hydroxyl succinimide-tagged BSA, which was synthesized and purified as described in the literature.[81] PA RO and NF membranes were found to have high fluorescent intensity at the same emission wavelength as fluorescein, so rhodamine tagging was used in this study. Figure 5.12 presents fluorescent microscopy images of unmodified, PDOPA-modified, and PDOPA-g-PEG-modified PES and PP membranes after contact with a rhodamine-tagged BSA solution (1 h contact time with 0.1 mg BSA/mL in water, pH=6.5). A dramatic decrease in BSA adhesion was observed following PDOPA-modification, and a further decrease was seen in PDOPA-g-PEG-modified membranes. Similar decreases were observed for all membranes except for XLE RO membranes, which fluoresced slightly at λ=575 nm (the emission wavelength of rhodamine). To quantitatively compare the amount of BSA adhered to each membrane, fluorescent intensities of each membrane were measured using a plate reader after the same protein contact protocol described above.[115]

Normalized fluorescent intensity (normalized to the membrane with the highest protein adhesion: unmodified PSf UF) for all membranes studied is presented in Table 5.5. Remarkably, 2-3 orders of magnitude decrease in protein adhesion is observed after

modification for the UF and MF membranes. Furthermore, PDOPA-g-PEG-modified membranes exhibit better resistance to protein adhesion than PDOPA-modified membranes. This protein adhesion decrease is consistent with the generally accepted link between membrane hydrophilicity and protein adhesion resistance.[12] Furthermore, PDOPA-g-PEG-modified surfaces have shown excellent protein adhesion resistance in other studies, which explains the PDOPA-g-PEG-modified membranes' low adhesion characteristics.[53, 54]

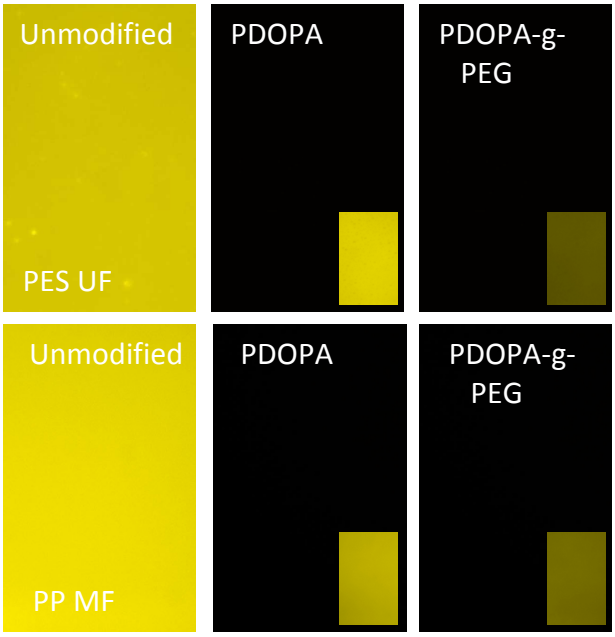

Figure 5.12: Rhodamine-tagged BSA adhesion on PES UF and PP MF membranes. Fluorescent microscopy images were recorded at 1 ms (exposure time insets are 80 ms) for PES membranes and 5 ms (insets are 500 ms) exposure time for PP membranes.

Table 5.5: Relative fluorescent intensity (λ_{em}=575 nm) of rhodamine-tagged BSA on a variety of membrane surfaces.

	Normalized fluorescent intensity [I_n/I_{PSF}]		
Membrane type	**Unmodified**	**PDOPA**	**PDOPA-g-PEG**
XLE RO	0.22	0.10	0.02
NF-90	1.5	0.79	0.05
PSF A1 UF	100	0.71	0.11
PES UF	56	1.79	0.01
PP MF	97	3.28	0.42
PTFE MF	4.3	0.003	0.05
PVDF MF	64	3.64	0.70

NOTE: These data provide a measure of static protein adhesion onto membrane surfaces. The fluorescent intensity recorded from BSA adhered to each membrane, I_n, were normalized by the fluorescent intensity of BSA adhered to a PSf UF membrane, I_{PSf}, which showed the highest protein adhesion of all membranes considered.

Biofouling, in the form of bacteria adhesion and proliferation, of membranes results not only in a reduction of flux, but also in a reduction of salt rejection in desalination processes due to biofilm-enhanced concentration polarization.[13, 66, 67] Therefore, *Pseudamonas aeruginosa* adhesion was explored as a model for bacterial fouling of unmodified and PDOPA-modified membranes. *P. aeruginosa* was chosen here because of its ubiquity in many water sources and its notorious ability to form robust biofilms.[82] These adhesion tests were performed in an LB media, which is rich in peptides and other yeast cell-based nutrients.[116] These bacteria nutrients can adhere to membranes in a fashion analogous to proteins. The deposition of these nutrients is an important first step in biofilm growth, as these foulants "prime" the membrane surface for bacterial attachment.[65] Therefore, because protein adhesion was dramatically reduced by the PDOPA and PDOPA-g-PEG modifications, we would expect bacteria adhesion to decrease, as well. Furthermore, many researchers have observed that an increase in surface hydrophilicity, a decrease in surface charge, and PEG grafting all lead to reduced

bacterial and cellular adhesion.[82, 117, 118] Figure 5.13 presents *P. aeruginosa* (which was genetically modified to luminesce) adhesion to unmodified, PDOPA-modified, and PODPA-g-PEG-modified membranes. Invariably, PDOPA deposition reduced *P. aeruginosa* adhesion, which most likely occurred as a result of the increased hydrophilicity and dramatically reduced protein adhesion imparted by the modification. PEG grafting to the PDOPA-modified membranes further reduced bacteria adhesion in some membranes (PVDF MF, XLE RO, and NF-90).

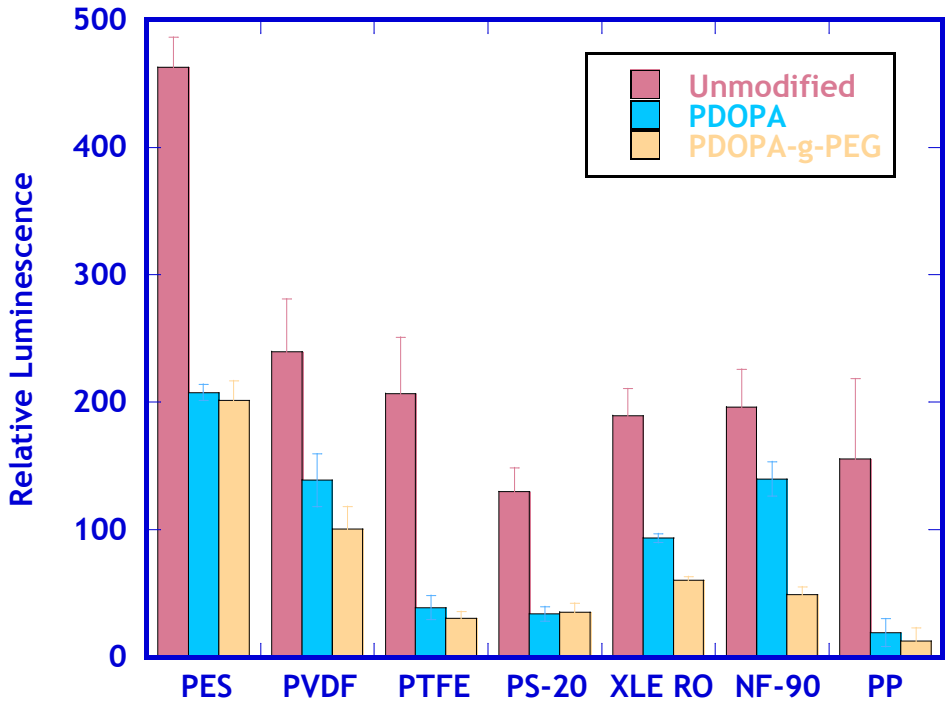

Figure 5.13: *P aeruginosa* adhesion (as measured by the bacteria's luminescence) to unmodified, PDOPA-modified and PDOPA-g-PEG-modified membranes. A 60 min PDOPA deposition time and a 60 min PEG grafting time was used for all modifications.

5.3.7 Oil emulsion fouling of TW30 Dow Filmtec RO membrane modules

A significant benefit of PDOPA deposition, relative to other membrane modification techniques, is its ease of application to entire membrane modules, not just

flat membrane sheets. Spiral wound RO membrane modules with housings (TW30-1812-36 modules from Dow Water Solutions) were modified by circulating a dopamine solution on the feed side of the module. The details of the modification procedure are given in the Supplementary Information. Further modification using Jeffamine M-1000 polyetheramine, an inexpensive, poly(propylene oxide)-poly(ethylene oxide) diblock copolymer terminated by a methyl group on the PEO block and an amine group on the PPO block) was also performed after the PDOPA modification to introduce PEG functionality to the membrane surface. Figure 5.14 presents emulsified oil fouling of unmodified, PDOPA-modified, and Jeffamine-modified TW30 membrane modules. In a similar fashion to flat sheet RO membranes, the throughput of the PDOPA-modified module is approximately 30% higher than that of an unmodified membrane after 1 day of operation. The Jeffamine-modified module had a lower starting flux than the other two membranes, but exhibited less irreversible fouling (Table 5.6). Jeffamine-modified modules also had higher NaCl rejection (without organics present in the feed) than the unmodified modules, but the unmodified modules had slightly higher rejection after one day of emulsified oil fouling due to the higher fouling by the emulsified oil of the unmodified PA module.

Table 5.6: Initial salt rejection and irreversible fouling data for TW30 unmodified and modified modules. The salt rejection was measured with no organics in the feed solution.

		Water throughput [L h^{-1} bar^{-1}]		
Module type (TW30)	**250 ppm NaCl rejection [%]**	**Before oil/water filtration, T_{BF}**	**After oil/water filtration, T_{AF}**	**T_{AF}/T_{BF}**
Unmodified	96.5	1.65	0.73	0.44
PDOPA	96.1	1.42	0.96	0.68
PDOPA-g-Jeffamine	96.9	0.78	0.77	0.99

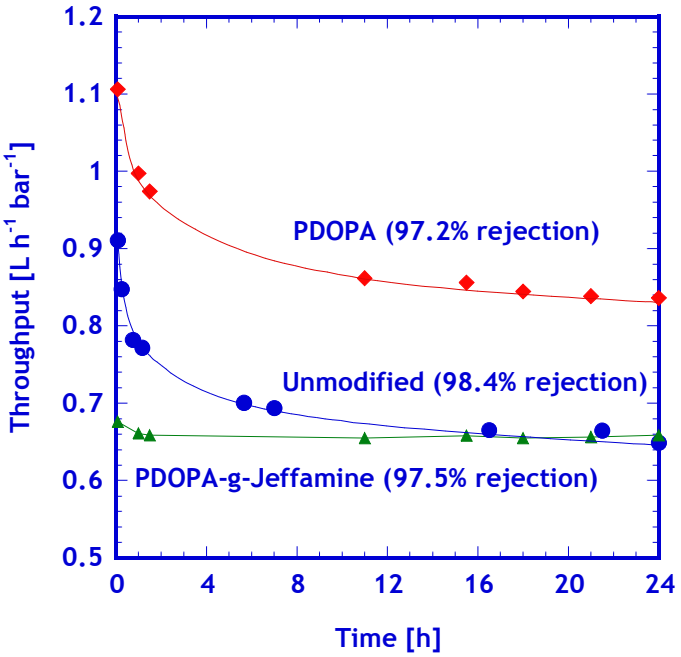

Figure 5.14: Effect of filtration time on permeate water flow rate, normalized by the transmembrane pressure difference, for an unmodified TW30 membrane module, a PDOPA-modified module, and a PDOPA-g-Jeffamine-modified module filtering an oil/water emulsion. Rejection values are for NaCl measured following 24 hours of filtration. Filtration conditions: 3.8 L/min feed flowrate, ΔP= 3.4 bar (50 psi), 25 °C. The feed was an aqueous solution containing 1350 ppm soybean oil, 150 ppm DC193 surfactant, 250 ppm NaCl and had a pH of 7.3.

5.4 Conclusions

A wide variety of membranes were modified using aqueous-based polydopamine deposition. The deposition layer could be controlled to be ultrathin (~5 nm in some cases). An increase in membrane surface hydrophilicity was observed in virtually all cases, and increased resistance to membrane fouling was observed when filtering an oil/water emulsion. Furthermore, irreversible fouling was reduced, sometimes dramatically, in all membranes tested. PEG was also covalently bound to the polydopamine layer using aqueous-based chemistry. The PEG ad-layer usually resulted in further increases in membrane fouling resistance and reduced irreversible fouling. Polydopamine modification significantly reduced protein adhesion to all membranes considered. Spiral-wound membrane modules were also modified by flowing a dopamine solution across the feed side of the membrane, which is an easily scalable process. Overall, polydopamine deposition was an effective membrane modification that has distinct advantages over other modifications due to its versatility and simplicity and, as a result, provides a promising surface modification strategy for effectively reducing fouling in many applications.

6. CHAPTER 6: INFLUENCE OF POLYDOPAMINE DEPOSITION CONDITIONS ON PURE WATER FLUX AND FOULANT ADHESION RESISTANCE OF REVERSE OSMOSIS, ULTRAFILTRATION, AND MICROFILTRATION MEMBRANES

6.1 Summary

The influence of polydopamine (PDOPA) deposition and poly(ethylene glycol) (PEG) grafting on pure water flux and bovine serum albumin (BSA) adhesion of two polysulfone ultrafiltration (UF) membranes, a poly(vinylidene fluoride) microfiltration (MF) membrane, and a polyamide reverse osmosis (RO) membrane is reported. When modified with PDOPA, all membranes exhibited a systematic reduction in protein adhesion. For example, 90 minutes of PDOPA deposition led to at least 96% reduction in BSA adhesion to these membranes at neutral pH. BSA adhesion was further reduced by subsequent PEG grafting to PDOPA (PDOPA-g-PEG). The membranes' pure water flux values (i.e., with no foulants present) were influenced to different extents by PDOPA and PDOPA-g-PEG modifications. In the porous membranes, the pure water flux reduction due to these modifications correlated with membrane pore size, with the smallest flux reductions being observed in the MF membrane (i.e., <1% flux reduction for all PDOPA modification times considered), which have the largest pores, and the largest flux reductions occurring in UF membranes (i.e., a 40% flux reduction after 90 minutes of PDOPA deposition), which have pore sizes on the order of the PDOPA deposition thickness. The RO membranes, which are nonporous, exhibited a flux reduction of 25% after 90 minutes of PDOPA deposition.

6.2 Introduction

Previously, deposition of polydopamine (PDOPA), which is a newly discovered, bio-inspired polymer[101], was observed to reduce oil/water emulsion-induced fouling in a wide variety of water purification membranes, including poly(tetrafluoroethylene), poly(vinylidene fluoride), and polypropylene microfiltration (MF) membranes, polysulfone ultrafiltration (UF) membranes, and polyamide desalination membranes.[80] Moreover, amine-terminated poly(ethylene glycol) (PEG-NH_2) was readily grafted to PDOPA-modified membranes (which are called PDOPA-g-PEG modified membranes) and, in many cases, further improved fouling resistance.[80]

In the previous chapter, poly(ethylene glycol) (PEG) grafting to PDOPA-modified membranes was accomplished using identical conditions for all membranes (1 mg/mL 5 kDa PEG-NH_2, 60 °C, 1 h grafting time for MF and UF membranes, 30 min for RO membranes).[80] Such PEG grafting had little influence on the pure water flux of PDOPA-modified MF membranes, but the PDOPA-g-PEG modified MF membranes exhibited a higher flux during emulsified oil filtration than either PDOPA-modified or unmodified membranes.[12, 80, 119-122] For example, PDOPA and PDOPA-g-PEG modified PTFE MF membranes exhibited a 20% and 56% higher flux, respectively, than their unmodified analog after one hour of emulsified oil in water filtration. In contrast, PEG grafting reduced pure water flux of UF and reverse osmosis (RO) membranes by more than 50% relative to the flux of their PDOPA-modified analogs. Consequently, PDOPA-g-PEG modified polysulfone ultrafiltration membranes (PS-20 UF) exhibited only slightly higher

flux than PDOPA-modified PS-20 UF membranes during emulsified oil filtration. Similarly, although no flux decrease was observed during emulsified oil filtration, PDOPA-g-PEG modified XLE RO membranes exhibited fluxes lower than those of unmodified membranes that had been fouled.

Based on these results, the current study was undertaken to explore the influence of PODPA deposition and PEG grafting conditions on pure water flux in MF, UF, and RO membranes. The membranes considered are listed in Table 6.1. The primary variables studied include PDOPA deposition time, PEG grafting temperature, PEG-NH_2 concentration in the grafting solution, and PEG-NH_2 molecular weight.

Table 6.1: Membranes used in this study.

Classification	Polymer	Manufacturer (Membrane Name)	Pore Size	Study ID
RO	Interfacially polymerized aromatic polyamide	Dow (XLE RO)	N/A	XLE RO
UF	Polysulfone	GE Water & Process Technologies (A1support)	~100 kDa MWCO	PSF A1 UF
UF	Polysulfone	Sepro (PS-20)	~20 kDa MWCO	PS-20 UF
MF	Poly(vinylidene fluoride)	Millipore (GVHP)	0.22 μm	PVDF MF

NOTE: MWCO = molecular weight cutoff

Protein adhesion has been explored in previous studies because of the presence of proteins in wastewater and bioprocessing streams and the aggressive nature of protein fouling of membranes.[10, 12, 119-122] To understand the ability of PDOPA and PDOPA-g-

PEG surface treatments to modify the interaction of proteins with membranes, a static bovine serum albumin (BSA) adhesion test was used to characterize the influence of surface modification conditions on BSA adhesion. Further studies are under way to determine the protein fouling properties of PDOPA and PDOPA-g-PEG modified membranes, and results from these studies will be reported separately.

PDOPA has been reported to form covalent bonds with certain molecules to form an ad-layer.[101] In this study, PEG-NH_2 was grafted to a deposited PDOPA layer on the membrane surface to take advantage of the well-known protein adhesion resistance and fouling resistance properties of PEG.[53] PEG reduces protein adsorption on a variety of inorganic and polymeric substrates, and it has been identified as one of the most effective fouling-resistant materials known.[53] A general trend of decreasing protein adsorption with increasing grafting density has been reported.[123] However, some studies observe this trend only for low molar mass PEG (i.e., <2 kDa), whereas protein adhesion is reported to go through a maximum as a function of grafting density for higher molar mass PEG grafts.[124, 125]

6.3 Background

6.3.1 Hydraulic resistance of PDOPA and PDOPA-g-PEG modified membranes

In porous membranes, such as UF and MF membranes, water flux and transmembrane pressure (TMP) difference are related as follows[72]:

$$J_i = \frac{\Delta p}{\mu R_i} \tag{1}$$

where J_i is the steady-state water flux, Δp is the transmembrane pressure difference (TMP), μ is the viscosity of the feed solution, and R_i is the membrane's hydraulic resistance. The solution-diffusion model is used to describe transport through nonporous membranes (e.g., RO membranes):[19]

$$J_i = A(\Delta p - \Delta \pi) \tag{2}$$

where A is the membrane's intrinsic water permeance, and $\Delta \pi$ is the osmotic pressure difference between the feed and permeate solutions.

When filtering pure water, equations (1) and (2), although derived from different transport models, have a common mathematical relationship between flux and TMP. By rearranging and combining equations (1) and (2) for pure water flux (i.e., $\Delta\pi=0$), one can formally define the hydraulic resistance of both porous and nonporous membranes as follows:

$$R_i = \frac{1}{\mu A} = \frac{\Delta p}{\mu J_i} = \frac{\Delta p \cdot t \cdot a}{\mu \cdot V} \tag{3}$$

where V is the volume of water collected during a time period t with a membrane of area a.

To quantify the effect of PDOPA modification and PEG grafting on membrane flux, an extension of equation (1) is employed for all membranes. PDOPA and PEG add resistances to the membrane's overall hydraulic resistance. A resistance in series model,

having contributions from both the membrane and a PDOPA/PDOPA-g-PEG surface layer, can be expressed as:[55]

$$J_{PDOPA} = \frac{\Delta p}{\mu(R_o + R_{PDOPA})} \tag{4}$$

and

$$J_{PEG} = \frac{\Delta p}{\mu(R_o + R_{PDOPA} + R_{PEG})}. \tag{5}$$

where J_{PDOPA} is the pure water flux of a PDOPA-modified membrane, J_{PEG} is the pure water flux of a PDOPA-g-PEG modified membrane, R_o is the unmodified membrane's hydraulic resistance, R_{PDOPA} is the hydraulic resistance of the PDOPA modification, and R_{PEG} is the hydraulic resistance of the PEG grafting layer. By combining equations (1), (4), and (5), R_{PDOPA} and R_{PEG} can be calculated as follows:

$$R_{PDOPA} = \frac{\Delta p}{\mu}\left(\frac{1}{J_{PDOPA}} - \frac{1}{J_o}\right) \tag{6}$$

and

$$R_{PEG} = \frac{\Delta p}{\mu}\left(\frac{1}{J_{PEG}} - \frac{1}{J_{PDOPA}}\right) \tag{7}$$

where J_o is the steady state pure water flux through an unmodified membrane.

6.4 Results and Discussion

6.4.1 Polydopamine modification of XLE RO, PS-20 and PSF A1 UF, and PVDF MF membranes: pure water flux

As was shown in Chapter 5, this study focuses on PDOPA modifications of 90 minutes or less because such shorter PDOPA modification times provide substantial

increases in hydrophilicity of the membranes considered without causing strong decreases in pure water permeance.

To provide an indication of the relative decrease in pure water flux resulting from PDOPA deposition, Figure 6.1 presents the influence of PDOPA deposition time on the fractional flux loss due to dopamine treatment, which is reported as the ratio of pure water flux of a PDOPA-modified membrane, J_{PDOPA}, to that of an unmodified analog, J_o. Each membrane responds differently to PDOPA modification. For example, PVDF MF membranes exhibited virtually no flux loss due to PDOPA modification. XLE RO membranes showed some flux loss, and the PS-20 UF membranes exhibited the largest decrease in flux with respect to deposition time. The PS-20 UF response is similar to the decrease observed for the PSF A1 UF membranes.

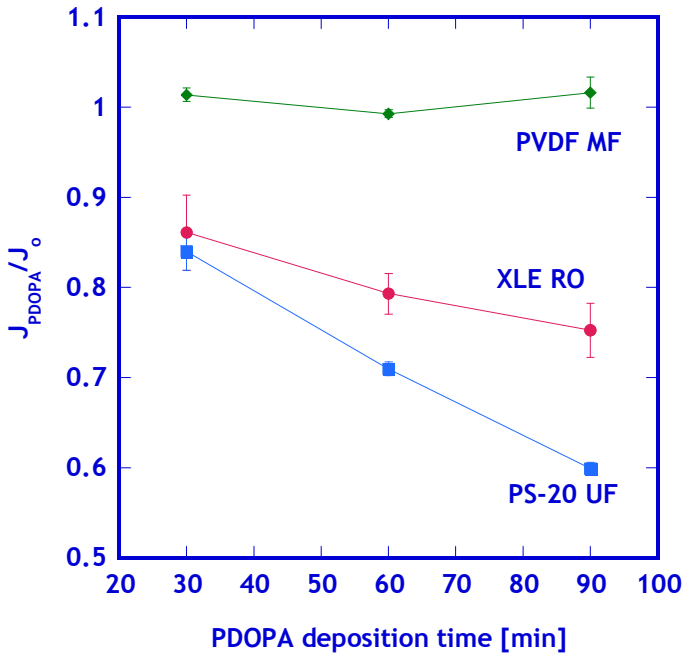

Figure 6.1: The influence of PDOPA deposition time on the ratio of PDOPA-modified membrane pure water flux (J_{PDOPA}) to unmodified membrane pure water flux (J_o). Error bars represent standard deviations from at least 3 separate experiments.

The differences shown in Figure 6.1 may be rationalized by considering each membrane's structure. The PVDF MF membranes have a nominal pore size of 0.22 μm, which is more than an order of magnitude larger than that of the PSF A1 UF membranes discussed earlier. Based on the deposition thickness results for polysulfone, the PDOPA thickness, even after 90 minutes of deposition, should be much smaller than the nominal pore size of the PVDF MF membranes. Therefore, any pore size decrease associated with PDOPA modification should be negligible, so the pure water flux was not influenced by modification.

During PDOPA deposition on PVDF MF membranes, PDOPA pore penetration was believed to be more pronounced than in the PSF A1 or PS-20 UF membranes,

because the PDOPA polymerization solution was observed to permeate through the MF membrane during the deposition process. Therefore, deposition likely occurred throughout the porous structure of the PVDF MF membrane. Consistent with this hypothesis, the pure water flux of other, more hydrophobic MF membranes (e.g., poly(tetrafluoroethylene) (PTFE) and polypropylene (PP)) actually increased following PDOPA modification.[80] For example, J_{PDOPA}/J_o values for PTFE and PP MF membranes were 1.30 and 1.10, respectively, after 60 minutes of PDOPA deposition. Because PDOPA modification occurs under aqueous conditions and is believed to occur via a mild oxidation mechanism similar to that involved in melanin formation,[101] PDOPA polymerization should not chemically degrade the membrane. Therefore, this flux increase should not be a result of membrane pore structure destruction. Therefore, we speculate that an increase in membrane wettability, due to PDOPA deposition on the pore walls, coupled with a negligible decrease in the membrane's effective pore diameter, led to an increase in pure water flux. Presumably, the PDOPA treatment permitted wetting of some pores in the highly hydrophobic PTFE and PP membranes that might not otherwise have been wetted without PDOPA treatment, thereby opening additional transport pathways in the membranes. This wetting effect was less pronounced in the already hydrophilic PVDF MF membranes where, as indicated in Figure 6.1, the J_{PDOPA}/J_o ratio is quite close to 1.

Visually, PDOPA treatment changes the color of membranes. For example, PVDF MF and PS-20 UF membranes turn dark brown during PDOPA deposition. The

XLE RO membranes had the least PDOPA deposition, since only a slight change in membrane color accompanied PDOPA deposition. Because of their essentially non-porous nature, PDOPA deposition on RO membranes presumably occurred essentially on the surface of the membrane, so any flux reduction (or mass transfer resistance increase) associated with the deposition resulted from water transport through a thin PDOPA surface layer and not pore constriction/blockage, as was the case in the porous UF and MF membranes. However, the polyamide RO layer was still the rate-controlling step in water transport through the modified membrane. Therefore, an increase in PDOPA deposition, due to increasing deposition time, resulted in only a small reduction in pure water flux. For example, the PDOPA hydraulic resistance (R_{PDOPA}, equation (6)) on an XLE membrane ranged from 700 x 10^{10} m^{-1} (30 minute deposition time) to 1,000 x 10^{10} m^{-1} (90 minute deposition time), which was significantly lower than the unmodified RO membrane's resistance, which was 3,400 x 10^{10} m^{-1} (cf., Table 6.2).

Table 6.2: Influence of PDOPA deposition on membrane hydraulic resistance.

	Hydraulic Resistance x 10^{10} (m^{-1})		
Membrane	**PVDF MF**	**PS-20 UF**	**XLE RO**
Unmodified, R_o	3.9	17.3	3400
PDOPA modified, R_{PDOPA}:			
30 min	3.8	20.5	4100
60 min	4.0	24.8	4250
90 min	3.8	29.3	4400

NOTE: All values were calculated using equation (3).

6.4.2 PEG grafting to PDOPA modified XLE RO, PS-20 UF, and PVDF MF membranes

a) Influence of grafting conditions on grafting density and pure water flux

Prior to PEG grafting, the PDOPA-modified membranes were prepared using a PDOPA deposition time of 60 minutes and the deposition conditions in the Materials and Experimental Methods section. Figure 6.2a presents the influence of PEG grafting temperature on the ratio of pure water flux of PDOPA-g-PEG-modified PS-20 UF membranes, J_{PEG}, to that of their PDOPA-modified analogs, J_{PDOPA}. 5 kDa PEG-NH_2 was used for these studies. The pure water flux was lower in all cases following PEG grafting (i.e., $J_{PEG}/J_{PDOPA}<1$). However, the extent of flux reduction due to PEG grafting was only weakly dependent on temperature because the flux reduction in PS-20 following PEG grafting changed by less than 10% (i.e., from $J_{PEG}/J_{PDOPA}=0.84$ to 0.77) as temperature changed from 20 to 60°C. This result suggests that the extent of PEG grafting did not change appreciably with temperature. The effect of temperature on PEG grafting was not explored for the other membranes considered in this study.

PDOPA deposition was necessary to achieve significant grafting of PEG-NH_2 to PS-20 UF membranes. For example, a PS-20 UF membrane not subjected to PDOPA deposition prior to being exposed to a 1 mg/mL 5kDa PEG-NH_2 solution (pH=8.8) for 60 minutes at 60°C exhibited a flux decline of only 5% relative to that of an unmodified membrane (i.e., $J_{PEG}/J_o=0.95$), indicating minimal PEG-NH_2 adhesion to an unmodified PS-20 UF membrane. In contrast, the observed flux loss due to PEG grafting, under similar conditions, to a PDOPA-modified membrane was 22% (i.e., $J_{PEG}/J_{PDOPA}=0.78$).

Thus, PEG-NH_2 does not readily react with or strongly adsorb to unmodified PS-20 UF membranes. Similarly, grafting or adsorption of PEG-NH_2 to unmodified PVDF MF membranes was not expected to occur and was not explored in this study. PEG-NH_2 grafting to unmodified XLE RO membranes is discussed in detail below.

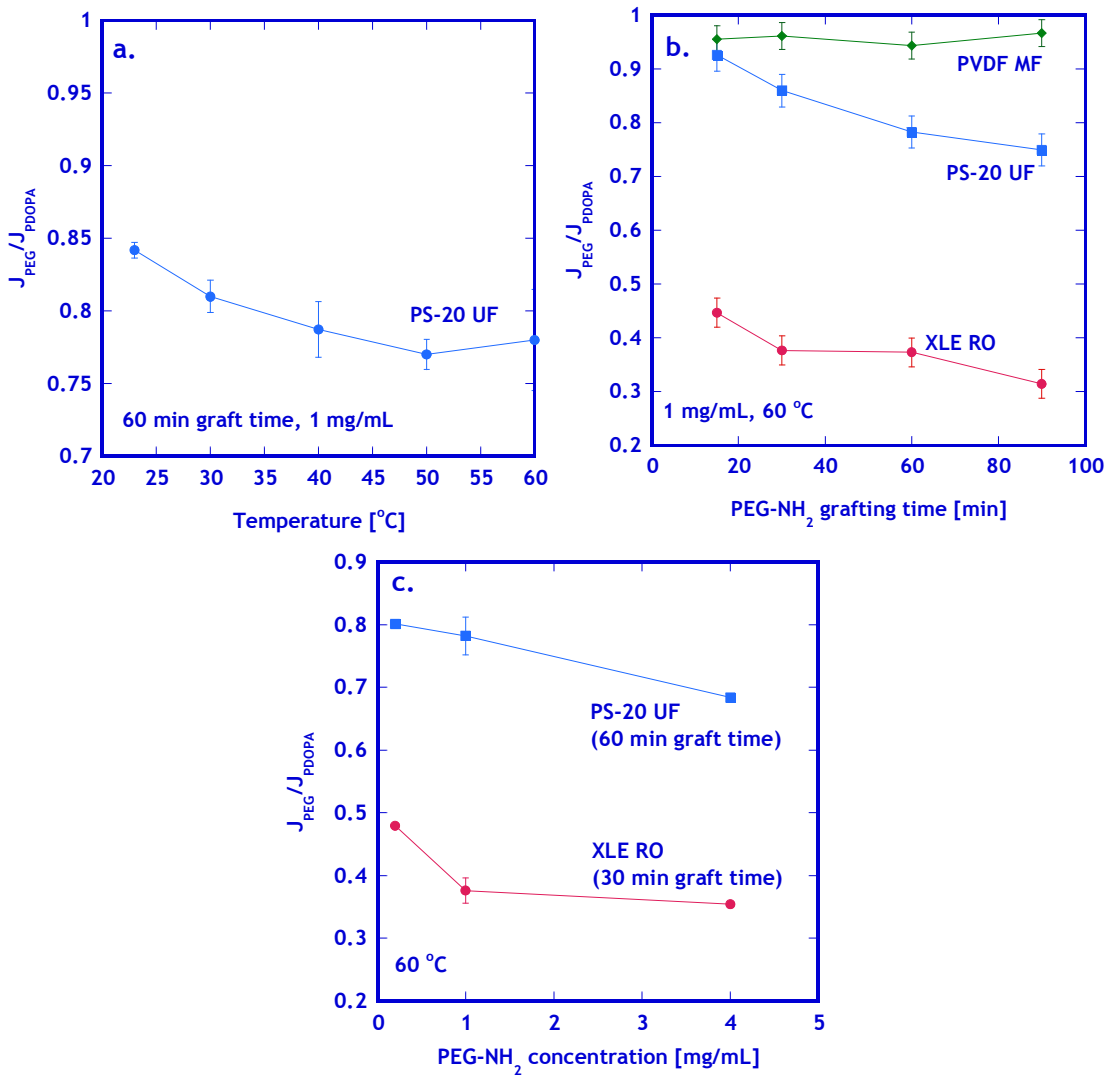

Figure 6.2: The ratio of pure water flux of PDOPA-g-PEG modified membranes, J_{PEG}, to the pure water flux of PDOPA-modified membranes, J_{PDOPA}, as a function of: a) PEG grafting temperature, b) PEG grafting time, and c) PEG-NH_2 concentration in the grafting solution. A 60 min PDOPA deposition (2 mg/mL dopamine, 15mM tris, pH=8.8, ambient conditions) was used for all membranes prior to PEG grafting. All PEG grafting was performed using 5 kDa PEG-NH_2 in 15 mM tris buffer at pH=8.8.

In the case of the PS-20 UF membranes, physical adsorption of PEG to PDOPA-modified membranes was not sufficient to cause a measurable flux decrease. For example, a PDOPA-modified PS-20 UF membrane was exposed to an aqueous solution containing 1 mg/mL of 3.35 kDa PEG-OH for one hour at a pH of 8.8 and 60°C. Unlike PEG-NH_2, PEG-OH cannot form covalent bonds with PDOPA. Such a membrane exhibited no flux decline (J_{PEG}/J_o=1.0), indicating that physical adsorption of PEG to PDOPA is negligible. Therefore, the flux loss observed in Figure 6.2 was ascribed to PEG that was covalently bound to PDOPA. This effect was not explored for PDOPA-modified PVDF MF and XLE RO membranes.

Figure 6.2b presents the influence of PEG grafting time on the ratio of the pure water flux of several PDOPA-g-PEG modified membranes to that of their PDOPA-modified analogs. PEG grafting did not significantly influence the PVDF MF membrane flux, because only a ~3% flux decrease was observed at any grafting time considered. The PS-20 UF membranes exhibited a decrease in flux with increasing PEG grafting time, suggesting that PEG grafting density increased with increasing grafting time. This hypothesis was confirmed by gravimetric analysis described in greater detail below.

The XLE RO membranes exhibited the most significant flux reduction as a result of PEG grafting. 15 minutes of PEG grafting to an XLE RO membrane led to a considerable decrease in flux (J_{PEG}/J_{PDOPA}=0.45). However, at grafting times ranging from 15 to 90 minutes, the flux decrease was only weakly influenced by grafting time,

since the flux decrease, J_{PEG}/J_{PDOPA}, only varied from 0.45 to 0.32. Presumably, most of the PEG grafting occurred at low grafting times (i.e., less than 15 minutes). PEG grafting to polyamide membranes is known to cause a decrease in membrane flux similar to, or even greater than that observed in this study. For example, Mickols[112] observed a flux decrease of 80% (i.e., J_{PEG}/J_o= 0.20) for an FT-30 Dow Filmtec RO membrane modified using an aqueous solution containing 1 wt% PEG diepoxide (3.4 kDa), and he observed a flux decrease of 68% (i.e., J_{PEG}/J_o=0.32) when an FT-30 membrane was modified by exposure to 0.2 wt% PEG diepoxide (0.2 kDa) solution. In both cases, the grafting time was 10 minutes, and the grafting temperature was 60°C.

The influence of PEG-NH_2 solution concentration on pure water flux for PS-20 UF and XLE RO membranes is presented in Figure 6.2c. Results for PVDF MF membranes are not presented because, based on the results presented in Figure 6.2b, there was no systematic decrease in flux following PEG-NH_2 grafting. A modest decrease in flux was observed at increasing PEG-NH_2 concentration for both PDOPA-modified PS-20 UF and XLE RO membranes, suggesting an increase in PEG grafting density with increasing PEG-NH_2 concentration. For the PS-20 UF membrane, the increase in PEG grafting density with increasing PEG-NH_2 concentration was consistent with gravimetric measurements of PEG grafting density.

Figure 6.3 presents gravimetric measurements of grafting density of 5 kDa PEG-NH_2 on a PDOPA-modified PS-20 UF membrane. In this figure, the effect of PEG

grafting time and PEG-NH_2 grafting solution concentration on grafting density is reported. In Figure 6.3a, the PEG-NH_2 solution concentration was 1 mg/mL, and the grafting experiments were conducted at 60 °C and a solution pH of 8.8. In Figure 6.3b, the influence of PEG-NH_2 solution concentration on grafting density was studied in membranes subjected to 60 minutes of PEG grafting at 60°C and a pH of 8.8. These experiments were conducted at conditions to match those of the PS-20 UF flux measurements reported in Figure 6.2b and c. Increasing grafting time and PEG-NH_2 solution concentration increases PEG grafting density. The effect of PEG grafting time and PEG-NH_2 grafting solution concentration on grafting density was not explored for PVDF MF or XLE RO membranes, although similar trends to those observed for PS-20 UF membranes would be anticipated. The observed increase in grafting density decreases the PS-20 UF membrane flux (as observed in Figure 6.2b and c), possibly due to pore constriction and pore blockage associated with the increase in grafting. As will be shown later, all PEG grafting densities led to similar reductions in BSA adhesion.

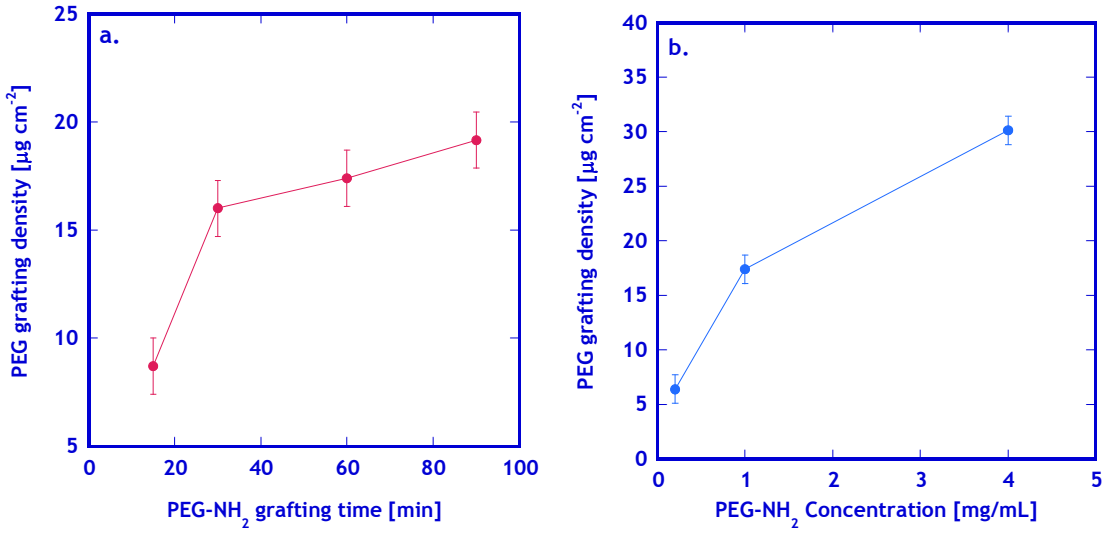

Figure 6.3: PEG grafting density on PDOPA-modified PS-20 UF membranes as a function of: a) PEG-NH_2 grafting time, and b) PEG-NH_2 concentration in the grafting solution. Grafting conditions for a): 1 mg/mL 5 kDa PEG-NH_2, 60 °C, 15 mM tris buffer (pH=8.8), and b): 60 min grafting time using 5 kDa PEG-NH_2, 60 °C, 15 mM tris buffer (pH=8.8). All values were obtained via gravimetric analysis. A 60 min PDOPA deposition (2 mg/mL dopamine, 15mM tris, pH=8.8, ambient conditions) was used for all membranes prior to PEG grafting.

Due to the rough surface and porous nature of membranes, apparent PEG grafting densities observed on membranes are significantly higher than grafting densities reported on smooth surfaces. For example, on a smooth, nonporous surface, grafting densities as low as 0.033 chains per nm^2 for 5 kDa PEG (which corresponds to 0.027 μg/cm^2) are sufficient to cause overlap between the areas occupied by adjacent PEG chains (assuming a radius of gyration of 3.1 nm for a 5 kDa PEG molecule).[126] At this grafting density, protein adhesion is greatly reduced due to steric repulsion. In our studies, much higher apparent grafting densities (for example, 30 μg/cm^2 for 5 kDa PEG-NH_2, 4 mg/mL, 60 °C, pH=8.8 on a 60 min PDOPA modified membrane) were observed on PS-20 UF membranes. However, this large graft density probably results from the membrane's surface roughness and internal porous structure, which substantially increases the total

effective surface area when compared to that of an analogous smooth, nonporous surface. For example, Ulbricht et al. reported a surface area, measured via BET nitrogen adsorption, of 23.1 m^2/g for a polypropylene MF membrane (0.4 μm pore diameter), which corresponds to an effective surface area of 760 m^2 per m^2 of membrane (165 μm thickness, membrane density of 0.2 g/cm^3).[127] Similar surface area values, ranging from approximately 15 to 23 m^2/g, have been reported for other UF and MF membranes.[128, 129] Therefore, assuming that PDOPA deposits on a significant portion of the PS-20 UF pore structure and that the PS-20 UF membranes have an effective surface area similar to other UF membranes, a 5 kDa PEG-NH_2 apparent grafting density of 30 $\mu g/cm^2$ would correspond to an actual grafting density of 0.04 $\mu g/cm^2$, which is slightly higher than the grafting density at the onset of PEG chain overlap. However, even larger polymer grafting densities on membranes have been observed in other studies. As an example, Ulbricht et al. observed PEG methacrylate grafting densities of up to 2000 $\mu g/cm^2$ on polyacrylonitrile (PAN) UF membranes using a UV-induced grafting method, and the presence of these PEG grafts on the PAN surface also correlated with significantly reduced protein adhesion. [130]

b) Influence of PEG-NH_2 molecular weight and PDOPA deposition time on PEG grafting

To more clearly isolate the influence of PEG grafting on pure water flux, it is useful to consider the hydraulic resistance of the PEG grafting rather than the ratio J_{PEG}/J_{PDOPA}, because, as shown in Figure 6.1, J_{PDOPA} increases with increasing PDOPA deposition time. Figure 6.4 presents the influence of PDOPA deposition time on R_{PEG}

(cf., equation (7)) for PDOPA-modified PVDF MF, PS-20 UF, and XLE RO membranes at three different PEG-NH_2 molecular weights. Grafting densities, measured via gravimetric analysis, are presented in Figure 6.5. R_{PEG} values for PDOPA-g-PEG modified PVDF MF membranes were much lower than the hydraulic resistances of unmodified and PDOPA-modified membranes (cf., Table 6.2). These low R_{PEG} values, coupled with the fact that there was no discernable trend between PDOPA deposition or PEG-NH_2 molecular weight and R_{PEG}, indicate that PEG grafting had little effect on the flux of PVDF MF membranes. However, as PDOPA deposition time increased, PEG grafting density did increase for PVDF MF membranes, as shown in Figure 6.5. Unfortunately, PDOPA deposition density was difficult to verify using a gravimetric analysis because PDOPA deposited in quantities below the detection limit of this gravimetric technique (i.e., <1 μm cm^{-2}). Furthermore, as expected, higher PEG-NH_2 molecular weights led to increased grafting densities. Nevertheless, probably because the PVDF MF pore size was large relative to the PDOPA layer thickness and the length of grafted PEG chains, an increase in PEG grafting density had little to no effect on flux.

PDOPA-modified PS-20 UF membranes exhibited similar trends and magnitudes in PEG grafting density as PDOPA-modified PVDF MF membranes: PEG grafting density increased as both PDOPA deposition time and PEG-NH_2 molecular weight increased. However, in contrast to the results from the PVDF MF membrane, the increase in PEG grafting density resulted in an increase in R_{PEG} for the PS-20 UF membrane. The pore size of the UF membrane is on the order of the size of the PEG

molecules used for grafting (e.g., the PS-20 rejection of 20 kDa PEG is 95%[44]). Therefore grafting most likely led to a combination of significant pore constriction and pore blockage (due to grafting on the membrane surface), which, in turn, increased the resistance to water transport.

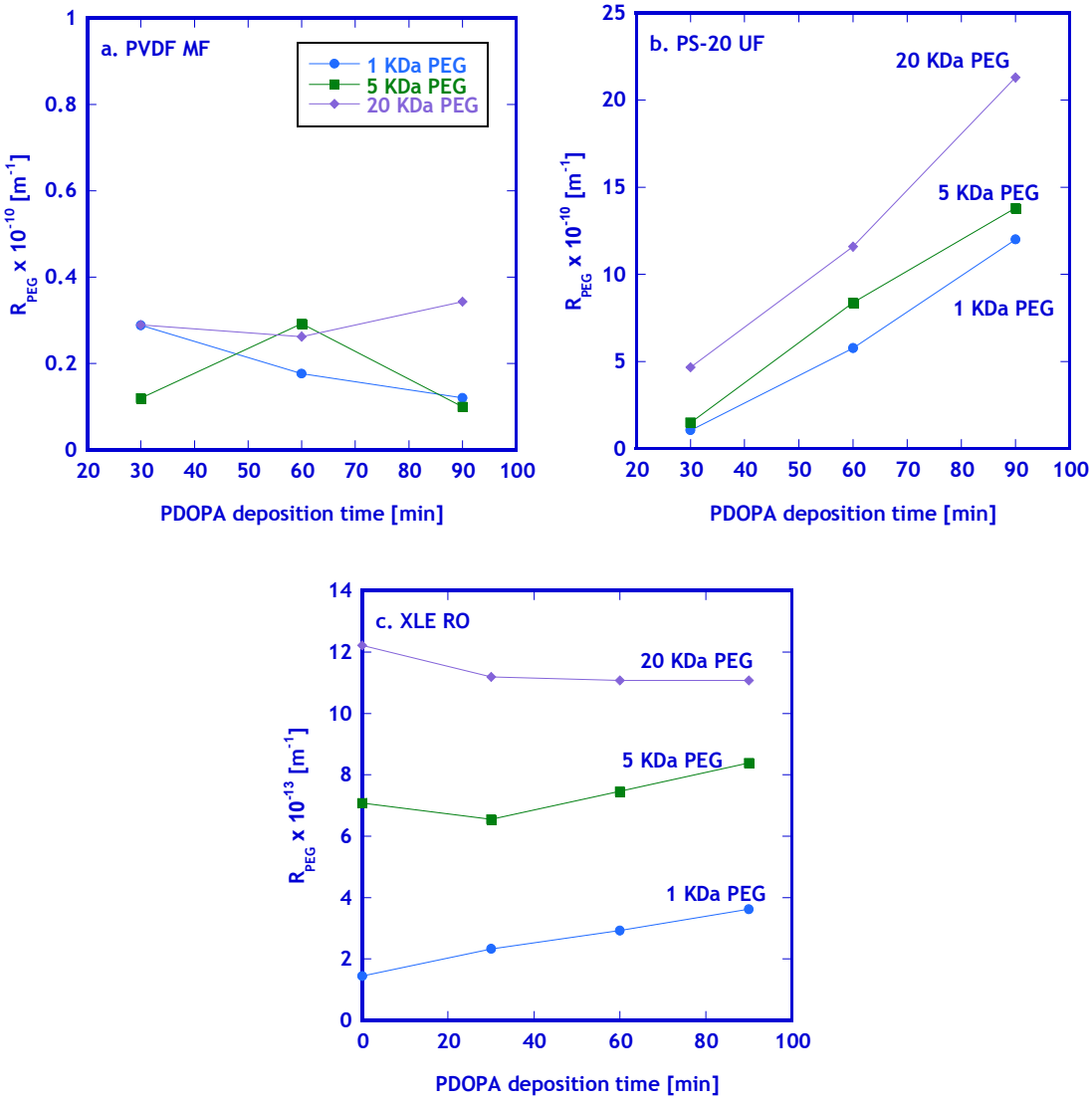

Figure 6.4: Hydraulic resistance of PEG grafted to PDOPA-modified: a) PVDF MF, b) PS-20 UF, and c) XLE RO membranes as a function of PDOPA deposition time and PEG-NH_2 molecular weight. PDOPA deposition conditions: 2 mg/mL dopamine in tris buffer (15 mM, pH=8.8) at ambient conditions. PEG grafting conditions: 60 min (PVDF MF and PS-20 UF) or 30 min (XLE RO) PEG grafting time using $2x10^{-4}$ mol/L PEG-NH_2, 60 °C, tris buffer (15 mM, pH=8.8). Standard errors were (in m^{-1}): $1.2x10^{9}$ (PVDF MF), $1.6x10^{10}$ (PS-20 UF), and $1.0x10^{13}$ (XLE RO). Standard errors were calculated from at least 2 replicate trials of 4 data points for each membrane.

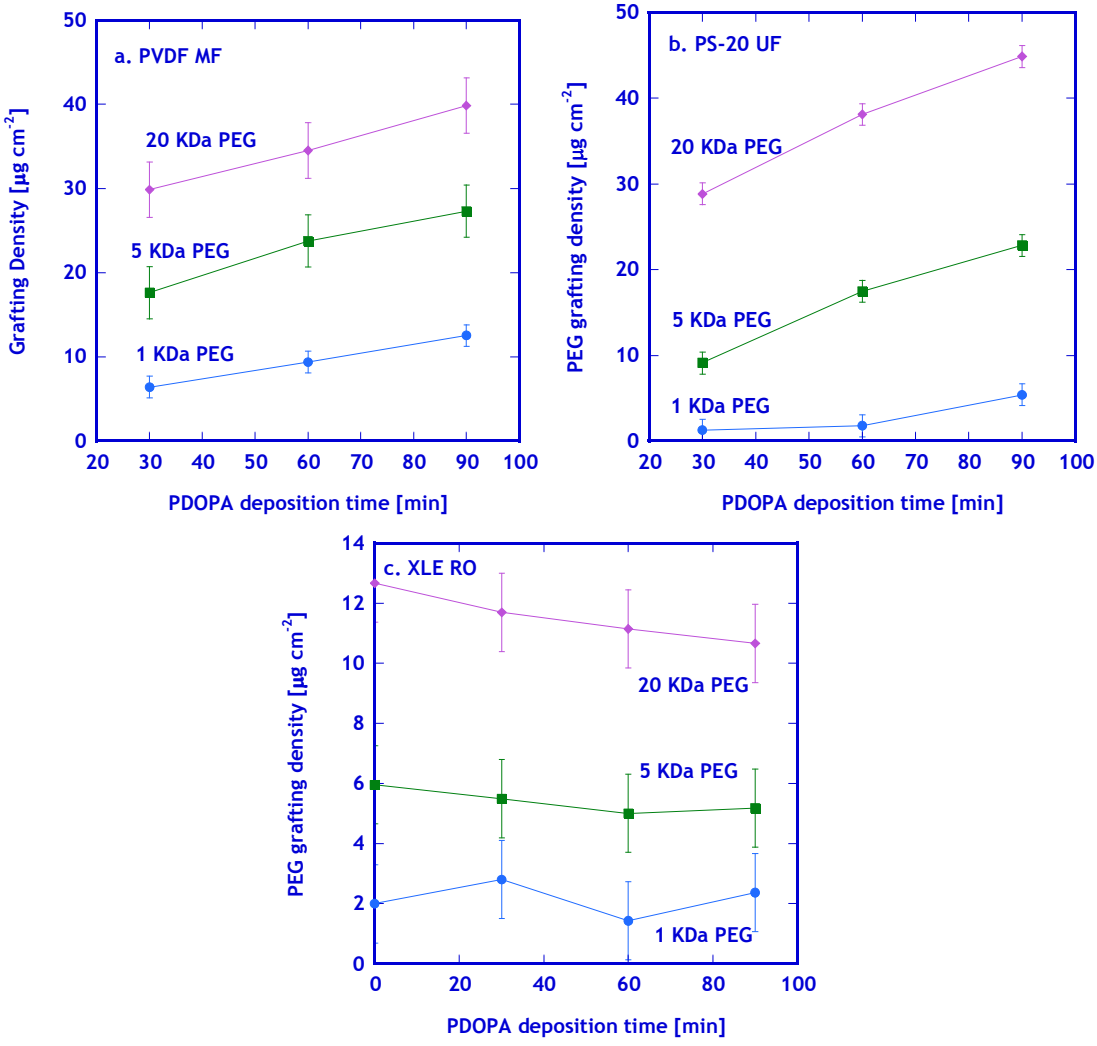

Figure 6.5: PEG grafting density as a function of PDOPA deposition and PEG-NH_2 molecular weight on: a) PVDF MF, b) PS-20 UF, and c) XLE RO membranes. All values were obtained via gravimetric analysis. PDOPA deposition conditions: 2 mg/mL dopamine in tris buffer (15 mM, pH=8.8) at ambient conditions. PEG grafting conditions: 60 min (PVDF MF and PS-20 UF) or 30 min (XLE RO) PEG grafting time using $2x10^{-4}$ mol/L PEG-NH_2, 60 °C, tris buffer (15 mM, pH=8.8). Error bars are the standard error of at least two replicate trials.

The XLE RO membranes have excess carboxylic acid functionality on their surfaces as a byproduct of the interfacial polymerization method used to synthesize the membrane.[62] The carboxylic acids moieties can react and form covalent linkages with PEG-NH_2.[131] PVDF MF and PS-20 UF membrane have no such reactive moieties

present in their structure. Therefore, PEG grafting was also characterized on unmodified XLE RO membranes. PEG grafting (without prior PDOPA deposition) to XLE RO membranes was performed by placing unmodified membranes in a $2x10^{-4}$ mol/L solution of 1, 5, or 20 kDa PEG-NH_2 (15 mM tris buffer, pH=8.8, 60 °C) for 30 minutes. Although PEG grafting densities on PDOPA-modified XLE RO were significantly lower than on PDOPA-modified PVDF MF or PS-20 UF membranes (cf., Figure 1.7), the decrease in flux (i.e., increase in resistance) associated with PEG grafting is more significant in the XLE RO membranes (as seen by the high R_{PEG} values, which are, in the case of 20 kDa PEG-NH_2, 3 times higher than the hydraulic resistance of an unmodified XLE RO membrane). No PEG grafting-associated flux loss was observed as PDOPA deposition time increased. Moreover, PEG grafting density remained essentially constant as PDOPA deposition time increased. Perhaps PDOPA deposition shields reactive carboxylic acid sites and makes reactive catechol/quinone sites available to the PEG-NH_2, with the net result being not much change in the number of reactive sites on the RO membrane surface for the PEG-NH_2. Thus, in contrast to the results obtained using the PVDF MF and PS-20 UF membranes, PDOPA deposition did not measurably increase PEG grafting to XLE RO membranes.

6.4.3 BSA adhesion resistance

As a first step towards assessing the ability of PDOPA and PDOPA-g-PEG surface treatment to alter protein adhesion to membranes, fluorescently tagged BSA adhesion experiments were performed on unmodified, PDOPA-modified, and PDOPA-g-PEG modified membranes. The method used in this study is a modified version of a

similar method reported in the literature.[115] Organic adhesion to membranes is a necessary step in any fouling process.[132, 133] Protein adhesion, in particular, to membranes is problematic because it primes the surface for and provides a nutrient source for biofilm-forming bacteria, which can lead to catastrophic flux reductions in membranes used for wastewater treatment or thrombosis in membranes used for applications in medical-related fields, such as hemodialysis.[65, 132, 133] Of course, the measurements reported here should be complemented by filtration experiments involving protein solutions to determine the fouling resistance, and those study are under way now in our laboratories.

Figure 6.6 presents the influence of PDOPA deposition time and PEG molecular weight on the relative amount of BSA adhered to the membranes. The amount of BSA on the membranes is characterized as the ratio of the fluorescent intensity of BSA adhered to modified membranes, I, to that of BSA adhered to their unmodified analogs, I_o. For the unmodified membranes, protein adhesion was in the following order:

PS-20 UF > PVDF MF > XLE RO.

This trend was also observed in previous studies that considered longer contact times between membranes and protein solutions.[80] PDOPA-only modified membranes are labeled "No PEG" in these plots. BSA adhesion to the PDOPA-modified membranes was significantly lower than that of the unmodified membranes. For example, a PVDF MF membrane, subjected to 30 minutes of PDOPA deposition, exhibited 83% lower BSA adhesion than its unmodified analog, and the reduction in BSA adhesion was even greater

after longer PDOPA deposition times. In the case of a PS-20 UF membrane subjected to 90 minutes of PDOPA deposition, the BSA adhesion was reduced by more than 99.9% compared to that of its unmodified analog. PDOPA modification also significantly reduced protein adhesion to XLE RO membranes, which already exhibited low protein adhesion[80] due to their high hydrophilicity and negative charge (BSA is also negatively charged at neutral to alkaline pH), and both of these factors have been linked to decreased BSA adhesion.[53] Furthermore, protein adhesion was reduced as PDOPA deposition time increased for all membranes.

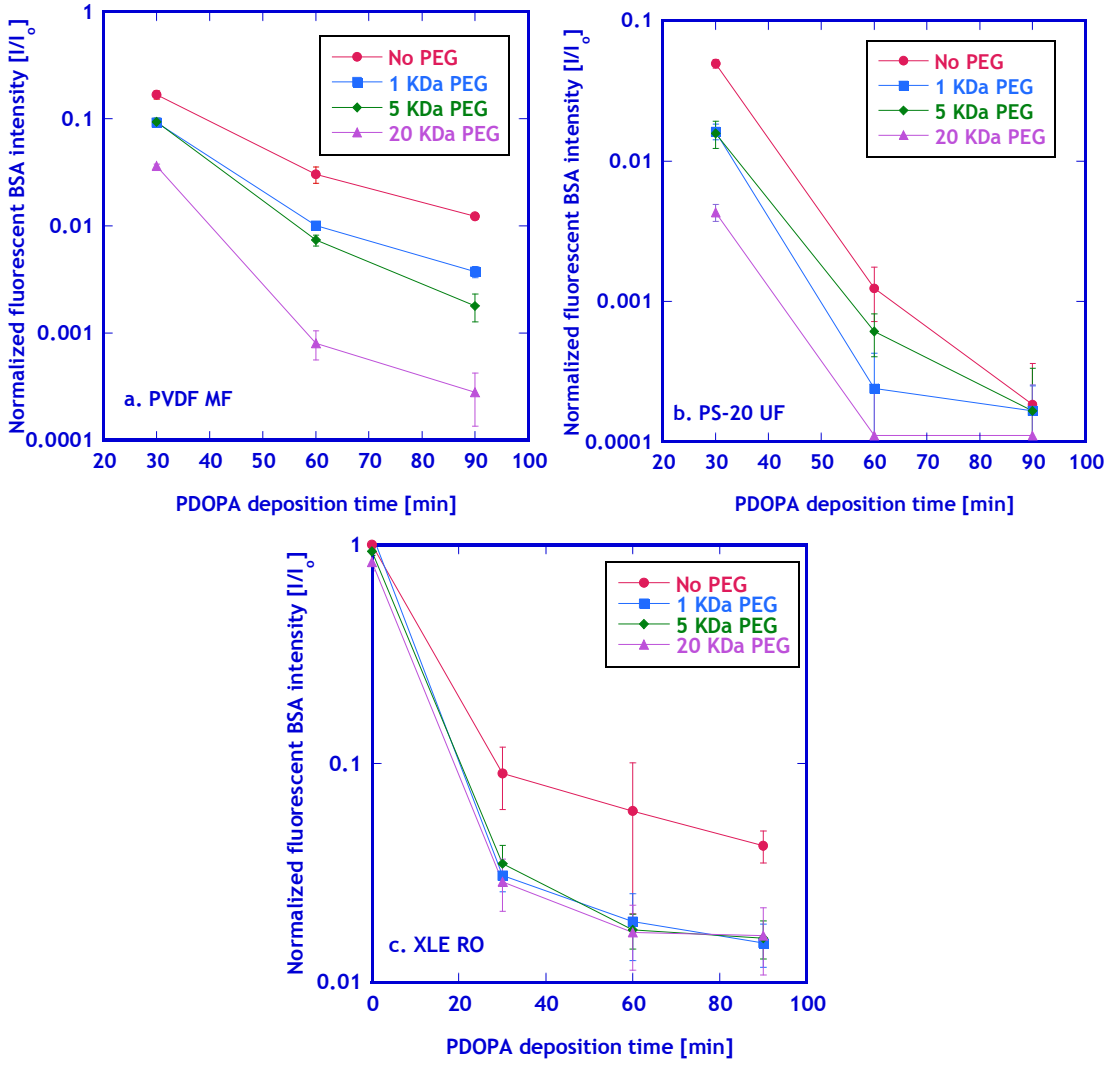

Figure 6.6: Influence of PDOPA deposition time on normalized fluorescent intensity of BSA adhered to: a. PVDF MF, b. PS-20 UF, and c. XLE RO membranes. Rhodamine-tagged BSA was used, and the intensity of the BSA adhered to the membrane was measured using $\lambda_{ex}/\lambda_{em}$=525 nm/575 nm and a plate reader. All intensities were normalized to the adhered BSA intensity measured on an unmodified membrane.

Protein adhesion reduction by PDOPA deposition is interesting given the chemical nature of PDOPA, which was designed to mimic an adhesive protein.[101] The reduction in protein adhesion could occur as a result of the formation of a small number

of PDOPA brushes, in a manner analogous to previously reported physisorbed polymers[134], that might be found throughout the PDOPA ad-layer, coupled with the fact that PDOPA is a highly hydrophilic substance. Hydrogen bonding between the hydrophilic catechol group in PDOPA and water molecules could lead to steric hinderance of proteins approaching the surface, which would render adhesion to the PDOPA surface difficult.[135-137] This mechanism of protein adhesion resistance is reminiscent of that observed with PEG brushes.[136, 137] However, PDOPA could probably react to form covalent bonds with protein amino acid residues, such as lysine, arginine, and cysteine, under alkaline conditions (our BSA adhesion tests were performed at neutral pH).[138] Therefore, PEG grafting may be needed to minimize protein adhesion over a broad pH range.

As indicated in Figure 6.6, PEG grafting to the PDOPA layer further decreased BSA adhesion relative to PDOPA-modified membranes. Overall, BSA adhesion decreased with increasing PDOPA deposition time in both PDOPA and PDOPA-g-PEG modified membranes. In PVDF MF membranes, a general trend of decreasing BSA adhesion with increasing PEG molecular weight was observed, with 20 kDa PDOPA-g-PEG-modified membranes exhibiting the lowest BSA adhesion for each PDOPA deposition time. All PDOPA-g-PEG modified PVDF MF membranes with a PDOPA modification time of 60 or 90 minutes exhibited more than 99% reduction in protein adhesion compared to that of unmodified PVDF MF membranes. For PS-20 membranes, 20 kDa PEG also provided the best resistance to BSA adhesion. PDOPA-modified PS-20

UF membranes subjected to 90 minutes of PDOPA modification exhibited essentially no measurable protein adhesion, so grafting PEG to this membrane resulted in no measurable reduction in BSA adhesion, at least according to the adhesion assay used in this study. PEGs of various molecular weights resulted in nearly identical reductions in BSA adhesion in PDOPA-g-PEG modified XLE RO membranes.

The synergistic protein adhesion resistance of combining PDOPA deposition and PEG grafting may be further elucidated by comparing protein adhesion to PEG-modified XLE RO membranes (i.e., membranes with no PDOPA deposition prior to PEG modification) and to PDOPA-g-PEG modified XLE RO membranes. Among the family of XLE RO membranes modified with only PEG (i.e., with no PDOPA), the membranes modified with 20 kDa PEG-NH_2 exhibited a 17% reduction in BSA adhesion compared to that of an unmodified analog. No reduction in BSA adhesion was observed upon modification with 1 kDa PEG-NH_2, and a 10% reduction was observed when the membrane was modified with 5 kDa PEG-NH_2. In contrast, the PDOPA-g-PEG treatment reduced BSA adhesion between 96 and 99% relative to that of unmodified XLE RO membranes.

At the high PEG grafting densities observed in our study, no definitive trend is observed between PEG grafting density and BSA adhesion reduction due solely to PEG adhesion (i.e., the difference in BSA adhesion between PDOPA-modified and PDOPA-g-PEG modified membranes). It is difficult to compare BSA adhesion reduction as a

function of PEG grafting density from the data in Figure 6.6 because the technique used to control grafting density (i.e., PDOPA deposition time) significantly influences BSA adhesion. Consequently, a series of experiments were performed where PEG grafting time and PEG-NH_2 concentration in the grafting solution were varied to control the PEG grafting density (as seen in Figure 6.3 for PS-20 UF membranes). Figure 6.7 presents BSA adhesion to PDOPA-modified and PDOPA-g-PEG modified membranes as a function of PEG grafting time and PEG-NH_2 concentration in the grafting solution. All membranes were initially subjected to a 60 minute PDOPA modification at the conditions set forth in the Materials and Experimental Methods section. The points at a PEG-NH_2 grafting time or concentration of zero correspond to BSA adhesion on membranes only subjected to PDOPA modification. Other than the initial decrease in BSA adhesion upon exposing the membranes to PEG, only a small reduction in BSA adhesion was observed for PVDF MF membranes as PEG grafting time and concentration increased. For PS-20 UF and XLE RO membranes, BSA adhesion showed no definitive trend with PEG grafting time and concentration. Therefore, PEG surface coverage, regardless of grafting time or concentration, is sufficiently high to give high levels of BSA adhesion resistance, at least within the limits of detection of BSA adhesion used in this work.

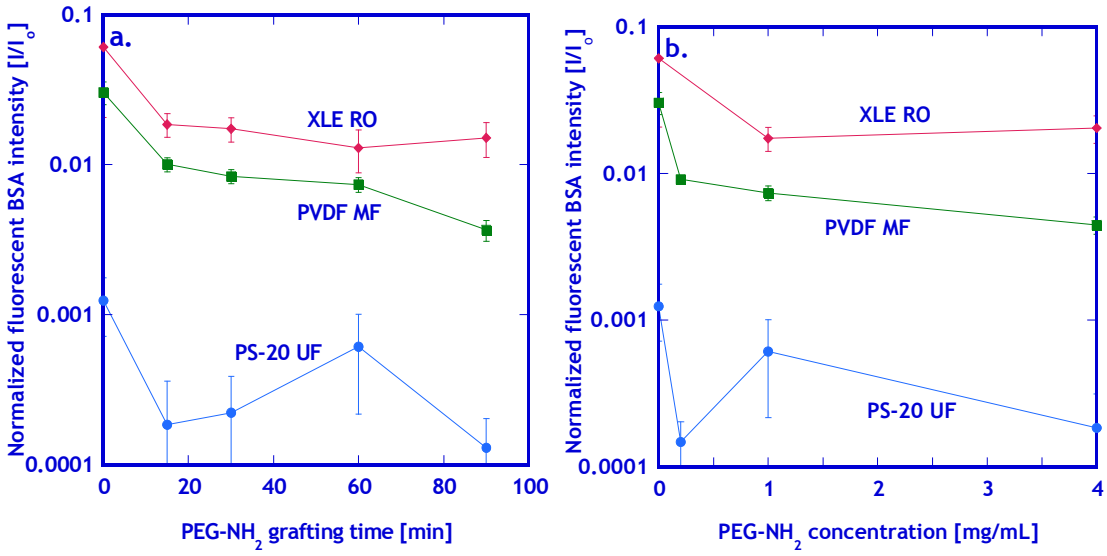

Figure 6.7: Influence of a. PEG grafting time and b. PEG-NH_2 conentration in the grafting solution on normalized fluorescent intensity of BSA adhered to PVDF MF, PS-20 UF, and XLE RO membranes. Prior to PEG grafting, these membranes were first PDOPA-modified using a 60 minute PDOPA deposition time at ambient conditions and the following dopamine solution: 2 mg/mL, 15mM tris, pH=8.8.

6.4.4 Correlation between BSA adhesion resistance and total flux loss due to PDOPA or PDOPA-g-PEG.

One objective of this study was to evaluate the tradeoff between improved BSA adhesion characteristics and the reduction in flux accompanying the membrane modifications considered in this study. Ideally, one would seek membrane modifications that yielded the maximum reduction in BSA adhesion and the minimum reduction in flux. Figure 6.8, a measure of the reduction in BSA adhesion, characterized as $1-I/I_o$, is plotted against the ratio of the modified membrane's pure water flux, J_T, relative to the flux of its unmodified analog, J_o. An ideal modification would result in membranes having a BSA adhesion reduction of 1 (corresponding to an I value of 0, indicating no BSA adhesion on the modified membrane) and the same flux as an unmodified membrane ($J_T/J_o=1$). As a result, values closest to the upper right corner of Figure 6.8 are desirable.

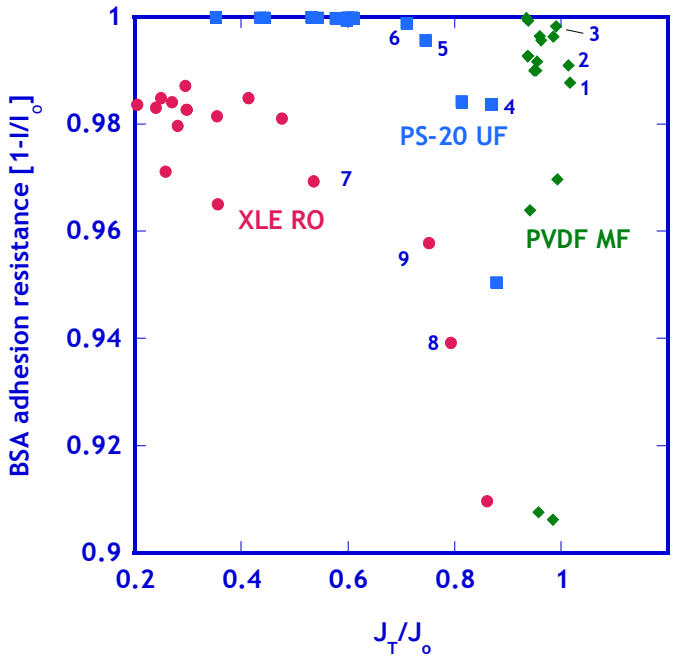

Figure 6.8: BSA adhesion reduction as a function of the ratio of modified membrane flux, J_T, to the unmodified membrane flux, J_o.

Table 6.3 provides some examples of the detailed modification conditions characterizing this tradeoff. In the PVDF MF membranes, which had the largest pores of the membranes considered in this study, all of the modification conditions considered gave relatively little change in flux, even those that provided a strong increase in resistance to BSA adhesion. Additionally, PDOPA deposition alone was sufficient to obtain high BSA resistance with little or no reduction in flux. In the PS-20 UF membranes, which have smaller pore size that the MF analogs, many of the most effective modification conditions, from a BSA adhesion standpoint (i.e., $1\text{-}I/I_o$ values closest to one), showed significant reductions in flux, and the most effective modification conditions (from a point of view of balancing BSA adhesion resistance and flux loss) had a combination of PDOPA deposition and PEG grafting. The XLE RO membranes

showed the clearest evidence of a distinct tradeoff between BSA adhesion resistance and flux, and modifications involving PEG grafting generally gave the most significant reductions in flux. In summary, PDOPA deposition, combined with PEG grafting, provides an effective tool for modifying membrane surfaces, and the balance of flux reduction and protein adhesion resistance must be determined experimentally for each membrane of interest.

Table 6.3: Modification parameters for membranes numbered in Figure 6.8.

Label from Figure 6.8	Membrane	PDOPA Deposition Time [min]	PEG-NH_2 Grafting Time [min]	PEG-NH_2 concentration [mg/ml]	PEG-NH_2 molecular weight [kDa]
1	PVDF MF	90	0	NA	NA
2	PVDF MF	30	60	4	20
3	PVDF MF	60	0	NA	NA
4	PS-20 UF	90	0	NA	NA
5	PS-20 UF	60	60	0.2	1
6	PS-20 UF	90	60	1	5
7	XLE RO	30	30	0.2	1
8	XLE RO	60	0	NA	NA
9	XLE RO	90	0	NA	NA

6.5 Conclusions

PVDF MF, PSF A1 and PS-20 UF and XLE RO membranes were modified using PDOPA. PEG-NH_2 could be grafted to PDOPA-modified membranes. PDOPA and PDOPA-g-PEG modifications influenced pure water flux differently in each membrane. For example, PDOPA and subsequent PEG grafting had little influence on PVDF MF membrane flux because the pore size of these membranes was likely to be much larger

than the thicknesses of the PDOPA deposition and the PEG graft layer. However, a decrease in PS-20 UF water flux was observed with increasing PDOPA deposition and PEG grafting density, probably because the pore size of these membranes was similar to the PDOPA deposition and PEG graft layer thicknesses. XLE RO membranes exhibited a small decrease in flux with increasing PDOPA deposition (most likely due to a low amount of PDOPA deposition compared to the other membranes considered), but PEG grafting significantly reduced XLE RO flux. PDOPA deposition substantially reduced BSA adhesion in all cases. Additional BSA adhesion reduction was observed when PEG was grafted to the membrane. A general trend of reduced BSA adhesion with increasing PEG graft molecular weight was observed for all membranes, except for the XLE RO, where all molecular weights of grafted PEG exhibited similar BSA adhesion. Finally, by plotting BSA adhesion resistance as a function of total unmodified membrane flux retained after a modification, a tradeoff between protein adhesion resistance and pure water flux was observed for several membranes.

7. CHAPTER 7: PROBING ION PARTITIONING VIA CHARGE EXCLUSION IN SULFONATED POLYSULFONE MATERIALS

7.1 Summary

The effect of electrostatic properties on solute partitioning via charge exclusion in sulfonated poly(arylene ether sulfone) (BPS) membranes is discussed. BPS materials exhibit different electrostatic properties, and, therefore, different ion partitioning capabilities in thin-film composite and freestanding thick-film form. Interestingly, freestanding thick films exhibit nearly neutral electrostatic charge, as measured by streaming zeta potential analysis. Therefore, thick BPS films do not exhibit certain drawbacks, such as reduced salt rejection of mixed-valence feeds and reduced rejection of solutes that undergo speciation at various pH, associated with charge exclusion ion partitioning, which is an important partitioning mechanism in conventional NF membranes. However, composite membranes prepared from a selective BPS coating layer and a porous Udel polysulfone support exhibit a negatively charged surface and, therefore, are prone to the same ion partitioning drawbacks of other negatively charged membranes. For example, in a BPS-32K thin film composite membrane, sodium ion passage increases from 3.7% to 68.8% as the calcium ion concentration increases from 0 ppm to 100 ppm, whereas a BPS-35N dense film exhibits a constant sodium ion passage of approximately 7% at calcium ion concentrations up to 350 ppm.

7.2 Introduction

7.2.1 Sulfonated polysulfone as a chlorine-tolerant desalination membrane candidate

Interfacially polymerized polyamide membrane, whose typical polyamide structure is shown in Figure 3.3, have gained favor over traditional cellulose acetate reverse osmosis membranes due to their superior water and ion transport characteristics and stable operation over a wide range of pH.[13] However, polyamide membranes are susceptible to chlorine degradation even at low chlorine concentrations (i.e., a few ppm).[139] Chlorine degradation occurs as a result of the amide nitrogen vulnerability, which is enhanced by the electron withdrawing capability of the adjacent carbonyl group.[139] Other undesirable aromatic polyamide reactions with chlorine also occur, which leads to polymer chain scission and, consequentially, severe reduction in membrane ion rejection.[140] Chlorine degradation of state-of-the-art RO membranes is important because chlorine, in the form of hypochlorite, is extensively used as a biocide in water treatment applications due to its effectiveness, availability, and low cost.[22, 139] Chlorine treatment is necessary to control biofilm growth on membrane system surfaces, which, if left unchecked, leads to a decrease in flux and, in some cases, ion rejection, and eventually to membrane replacement.[67] Therefore, chlorine is removed from RO feed waters by adding sodium bisulfite, which reduces the hypochlorite ion to a non-oxidizing chloride ion.[141] This additional processing step leads to increased costs and, consequently, higher product water costs. If chlorinated raw water could be purified using membranes, the chemical dechlorination steps could be eliminated. To purify

chlorinated water using reverse osmosis, new chlorine-tolerant membranes must be developed with transport characteristics similar to state-of-the-art polyamide membranes.

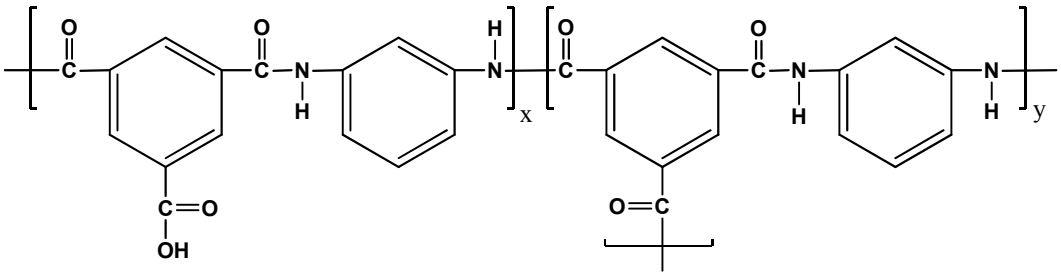

Typical polyamide structure

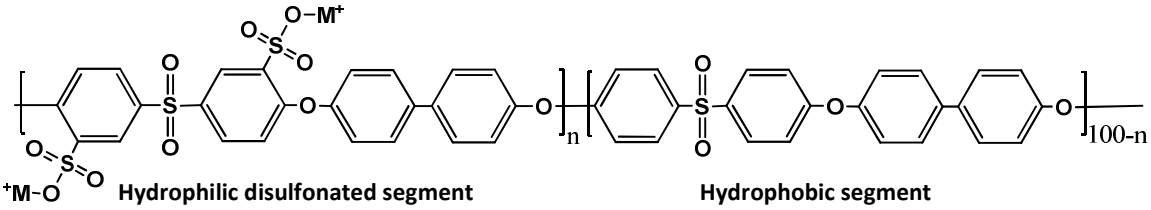

Disulfonated poly(arylene ether sulfone) copolymer, BPS

Figure 7.1: A typical polyamide crosslinked structure and the sulfonated polysulfone copolymers (BPS series) used in this study (n=20-50%). M+ can be either a K+ or Na+ counterion or a free acid (H+).

Park et al. recently explored hydrophilic sulfonated polysulfones as candidates for desalination membranes.[22] Polysulfone is a tough, high-strength thermoplastic that is highly resistant to oxidating agents (such as hypochlorite) over a broad pH range (2-13).[142] Sulfonation of polysulfone is useful for achieving reasonable water permeability, because polysulfone is an inherently hydrophobic polymer. Other researchers have explored sulfonated polysulfones for desalination membranes in the past, because the polysulfone backbone is robust and not readily prone to chemical or biological degradation.[143-145] Previous attempts to produce a chlorine-tolerant RO membrane focused on post-polymerization sulfonated polysulfone (PSPSf).[145] To produce PSPSf,

polysulfone is treated with strong acids, such as chlorosulfuric and sulfuric acid, which results in poor mechanical integrity, difficult transport reproducibility due to various unwanted side-reactions, and low sulfonation degrees, which, consequently, lead to low membrane water permeation.[22] However, Park et al. studied polymers (named 'BPS' by Park et al. and others[22, 75]) synthesized using directly sulfonated monomers that, when polymerized with analogous hydrophobic co-monomers for mechanical strength (Figure 3.3), led to highly reproducible and tunable membrane transport properties with good membrane mechanical integrity.

Park et al. focused on two general BPS polymer properties. First, water and salt transport were characterized through thick (~30-50 μm), dense, sulfonated polysulfone films with various hydrophilic (sulfonated monomer) content. A general tradeoff relationship between salt rejection and water permeability was observed as the hydrophilic content in the sulfonated polymers increased. Second, the BPS chlorine resistance was characterized in dense freestanding films and thin-film composite (with a polysulfone UF support membrane) membranes. As expected, the sulfonated polysulfones exhibited excellent chlorine stability, especially compared to conventional polyamide RO membranes.

7.2.2 BPS dense film and thin film composite salt rejection

Park et al. observed an interesting phenomenon when comparing BPS dense film and thin-film composite (TFC) sodium chloride salt rejection. Sodium chloride rejection using BPS-35H and 40H freestanding dense films and thin-film composites (TFCs) are

reported in Table 7.1.[22] For each BPS material, the TFC membranes have higher rejection than the freestanding films, and, as a result, Park et al. suggest that the coating layer is defect-free. However, this result is surprising, because even if the coating layer were defect-free, similar rejection would be expected from both dense films and TFCs if no salt concentration polarization was present. However, the higher water flux through the thin film composites could lead to higher ion concentration polarization, which, theoretically, would slightly reduce the observed salt rejection in these membranes.[13] In other words, defect-free thin film composites should exhibit a lower salt rejection than their dense film analogs as a result of increased concentration polarization. The higher BPS material salt rejection in TFC form indicates that fundamental BPS material properties may be different in dense film and TFC form. As a result, this study focuses on surface charge differences, and their influence on charge exclusion, between BPS dense films and thin film composite membranes.

Table 7.1: Comparison of NaCl rejection of BPS materials in freestanding dense film form and thin-film composite (TFC) form.

		NaCl Rejection [%]	
Polymer coating solution	**Water permeance [L m^{-2} h^{-1}]**	**Dense film**	**TFC**
0.5 w% BPS-35H	2.7	88.2	91.3
0.5 w% BPS-40H	3.8	85.9	89.5

NOTE: Measurement conditions: 3.8 L/min crossflow, ΔP=400 psi, T=25 °C, 2000 ppm NaCl.

7.2.3 Ion partitioning mechanisms in membranes with fixed charges

Sulfonation introduces fixed negative charges into the polymer matrix and increases the polymer's hydrophilic domain size.[75] The incorporated charge and effective

ion channels play distinct roles in the ion partitioning mechanisms found in the BPS materials. Three ion partitioning mechanisms can be present in desalination membranes containing fixed ionic charges: charge exclusion, dielectric exclusion, and steric exclusion.[146] Membranes that have smaller effective pore sizes are able to reject more solutes due to higher steric exclusion, and, likewise, membranes with a higher effective membrane charge are able to reject higher amounts of like-charged ionic species due to higher charge exclusion via Donnan equilibrium.[43] Dielectric exclusion occurs due to differences between the dielectric constants of the membrane polymer and feed solution.[146, 147] This dielectric difference contributes to a difference in the electrochemical potential between the solution inside a membrane and in the bulk feed, and therefore contributes to a membrane's ion partitioning capability.[147] This chapter will focus on charge exclusion because the ion partitioning phenomena discussed herein are mainly believed to be related to this mechanism.

7.3 Results and Discussion

7.3.1 Support membrane pretreatment to prevent pore collapse

Pore collapse during the composite membrane drying procedure is possible without proper support membrane pretreatment.[148] Support pretreatment was performed by immersing the membrane in a pretreatment solution for 2 hours. Pure water, pure isopropanol (IPA), 15% v/v glycerin in IPA (IPA-Gly) and Di(EG) were used as pretreatment solutions. Figure 7.2 presents the support membrane pure water flux as a function of pretreatment solution concentration. Figure 7.2a presents water flux of IPA and water treated membranes immediately after being removed from the pretreatment

solution and the water flux of IPA-Gly and Di(EG) treated membranes after being dried at ambient conditions for 2 hours. The water and IPA-treated membranes showed no appreciable flux (i.e., 0 $Lm^{-2}h^{-1}$) after being dried at ambient conditions for 2 hours, indicating that significant pore collapse occurred. Furthermore, water was not entirely effective in wetting the membrane pores, because the water-treated membrane only exhibited ~40% of an IPA-treated membrane's flux. The pore collapse in these two membranes most likely occurred due to the large forces (due to water and IPA having relatively high surface tensions) exerted on the pore wall from the evaporating liquid. However, fluxes similar to those of an undried IPA-treated membrane were observed in the IPA-Gly and Di(EG)-treated membranes, even after drying. This indicates that at ambient conditions, glycerin and Di(EG) do not evaporate from the membrane and, therefore, preserve the porous structure. If glycerin and Di(EG) were to evaporate from the membrane, the pore structure would almost assuredly collapse, because these liquids have higher surface tensions and boiling points (Table 7.2) than IPA, which was shown to completely collapse the membrane pores during drying. Both high liquid surface tension and boiling points have been correlated to increased pore collapse upon liquid evaporation.[148]

Table 7.2: Surface tensions and boiling points of liquids used in the pretreatment of Udel polysulfone supports during composite membrane preparation. Surface tension values from[149]. Boiling point values from Sigma Aldrich.

Liquid	Surface tension @ 20 °C [mN/m]	Boiling point [°C]
Water	72.8	100
Isopropanol	23.0	82.3
Glycerin	64.0	290
Diethylene glycol	44.8	244

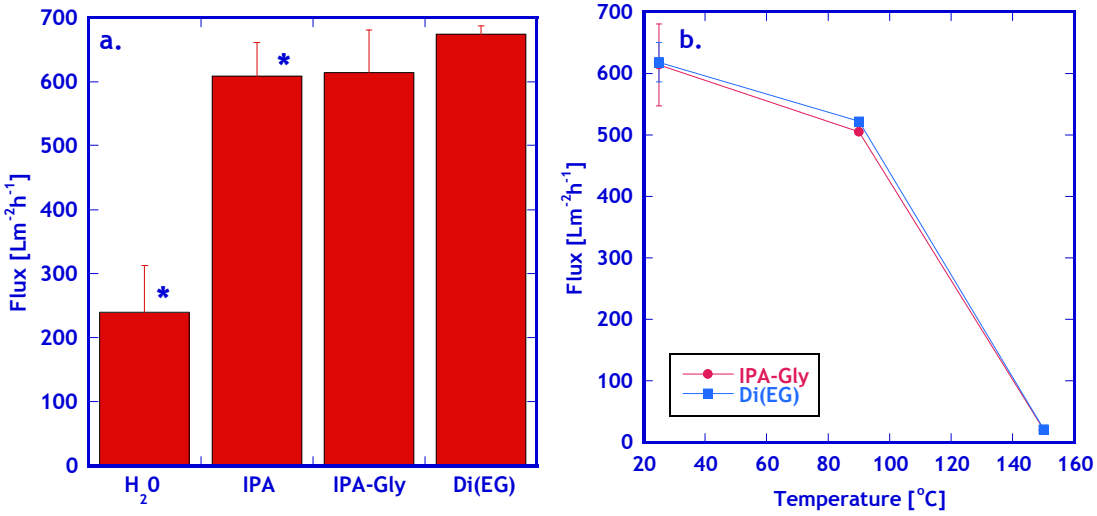

Figure 7.2: a. Influence of pretreatment solution content on ultrapure water flux (ΔP=1.4 atm) of porous Dow Water Solutions polysulfone support membranes. * indicates that the membranes were not dried before water flux measurements; essentially no water flux was observed in these two membranes following drying. The drying process was to maintain the membrane at ambient conditions for 2 hours. b. Water flux after drying under vacuum for 2 hours at various temperatures.

Drying IPA-Gly and Di(EG)-treated membranes under vacuum for 2 hours at elevated temperatures more effectively removed Gly and Di(EG) from the membrane pores, resulting in decreased membrane water flux due to increased pore collapse (Figure 7.2b). Drying these membranes at 150 °C reduced their water fluxes to ~10 $Lm^{-2}h^{-1}$. However, drying at 90 °C resulted in only a slight decrease in membrane water flux relative to similar drying conditions at room temperature. Therefore, 90 °C was selected as the drying temperature for the composite membrane studies described herein. The IPA-Gly mixture was used to pretreat support membranes because Gly has a higher boiling point than Di(EG). Therefore, Gly will remain in the pore structure, and consequentially preserve it, while evaporating Di(EG) from the selective BPS thin film.

7.3.2 Solvent selection for BPS TFC membrane preparation

To achieve high membrane flux, composite membranes were prepared using a thin selective BPS layer and a porous non-sulfonated Udel polysulfone support.[22] The composite membranes synthesized by Park et al. used a highly sulfonated polysulfone (BPS-40H) that easily dissolved in formic acid. Formic acid is not a solvent for non-sulfonated polysulfone, so it would not dissolve the porous support membrane. As a result, preparation of highly sulfonated thin-film composite membranes was straightforward.

However, to prepare membranes with ion rejection capabilities similar to conventional RO membranes, a selective layer of low-sulfonation degree BPS (i.e., BPS-20) is required. Unfortunately, as the BPS sulfonation degree decreases, two critical issues arise: first, the BPS polymers become partially insoluble in formic acid, even at relatively high sulfonation degrees (e.g., BPS-32). Second, low-sulfonation BPS polymers become increasingly chemically similar to the polysulfone support, thereby making potential sulfonated polymer-selective solvents difficult to find. A solution to the latter issue may be to use other polymer porous support membranes. However, the polysulfone support is an industry standard for RO membranes, and, therefore, it is the support of choice for this study.

These issues, coupled with the highly corrosive and generally toxic nature of formic acid, led researchers at Virginia Polytechnic University to develop other potential

sulfonated polymer-selective solvents. Their search led to the discovery of a class of compounds, polyhydric alcohols, that could act as selective solvents for the BPS materials.[150] Among the polyhydric alcohols, di(ethylene glycol) (Di(EG)) was used in this study.

7.3.3 BPS thin film composite characterization: Water flux and NaCl rejection

Using a 1% w/v BPS-20K in Di(EG) solution as the coating solution, a completely defect-free coating layer was nearly impossible to achieve using just a single coating step, because sodium chloride rejection (<90%) of these membranes was always well below the nominal rejection value expected for a BPS-20K film (99.2%) and highly irreproducible. Therefore, when using Di(EG) as a solvent, a second coating step was necessary to reduce defects in the thin BPS layer. This extra coating step, however, increased the overall thickness of the BPS layer, effectively reducing the membrane's water permeance. Nevertheless, using two coating steps with a 1% w/v BPS-20K solution results in a membrane with NaCl rejection of 96% and a permeance of 0.38 L m^{-2} h^{-1} bar^{-1} while filtering a 2000 ppm NaCl feed solution (ΔP=225 psig). A similar coating procedure using an initial 0.2% w/v BPS-20K solution followed by 3 brush coatings of a 0.1% BPS-20K solution led to a composite membrane with similar, although slightly improved, transport properties (salt rejection=95.5%, water permeance= 0.45 L m^{-2} h^{-1} bar^{-1}). SEM images (Figure 7.3a) of this membrane showed a BPS layer thickness of approximately 100 nm, which is approximately the thickness expected to achieve the observed water permeance based on equation (12) in chapter 2.

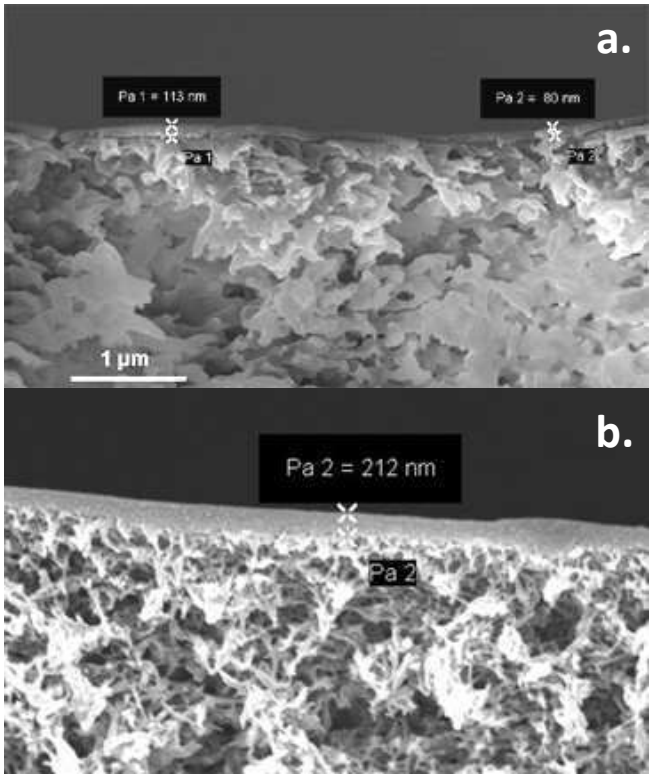

Figure 7.3: SEM images of BPS-20K (a) and BPS-20H (b) thin film composite membranes on a polysulfone support. The BPS layer is clearly seen on the surface of the support membrane. Both membranes were prepared using a 0.2% BPS coating, followed by three 0.1% BPS coatings. Adapted from[150].

However, this extraordinarily thin coating layer is unexpected, as Park et al. observed that a 0.5% w/v BPS in formic acid solution gave coating layer thicknesses around 1 μm with only one coating step.[22] Theoretically, the coating procedure used in this study should have produced coating layer thicknesses of around 2 μm (100 μm x 1% BPS solution x 2 coatings, assuming the brush coating produced a conservatively thin 100 μm coating solution thickness) or 0.5 μm, depending on the coating procedure outlined above. Furthermore, the composite membranes (~96% rejection) never reached the 99.2% rejection expected for a defect-free BPS-20K coating layer. Therefore, a

combination of pore penetration coupled with coating layer defects probably led to the observed trends of ultra-thin coating layers and lower-than-expected rejection.

Pore penetration could explain the observed BPS coating layer thickness: the coating solution wicked into the pores (as visually witnessed by the wetting of the support's pore structure during the membrane drying process) and could have reduced the total amount of solution left on the membrane surface to form the BPS layer. Although SEM images showed that the support membrane remained porous, the porous structure in Figure 7.3a appeared to be slightly constricted compared to the fibrous porous structure observed in Figure 7.3b. Although these membranes were prepared in the same manner (4 BPS coatings), pore penetration, and therefore BPS polymer deposition, could be more pronounced in certain areas of the membrane as a result of the first BPS coating having defects. This process would lead to patchy pore penetration of the subsequent coating solutions, which would result in the pore structure difference observed in the two images in Figure 7.3. The pore penetration and resulting conformal porous BPS coating would lead to minimal pore constriction and, therefore, only slightly reduced support membrane water permeance. However, the decrease in coating solution thickness on the membrane surface would lead to an ultra-thin coating layer. Small defects are also likely present in the coating layer, as indicated by the lower-than-expected rejection. Complete solvent removal from the BPS layer was difficult due to Di(EG)'s high boiling point, and, consequentially, defects in the BPS layer were formed as water removed the Di(EG) from

the membrane. These defects would also contribute to appreciable membrane water permeance. Further evidence of coating layer defects will be discussed later.

7.3.4 Surface charge and salt passage of post-polymerization sulfonated polysulfone and BPS dense films

Post-polymerization sulfonated polysulfone (PSPSf) membranes have been explored as possible chlorine-tolerant RO membranes in the past, with Millipore marketing such a membrane under the trade name Hi-Flux CP.[145, 151] One issue that arose with these membranes was a decrease of monovalent cation rejection in the presence of divalent cations. For example, Figure 7.4 presents ion passage through a PSPSf (supported by porous non-sulfonated polysulfone[145]) composite membrane and two BPS material dense films (thickness ~27 μm). The PSPSf shows a precipitous drop in ion rejection (percent rejection, R, is related to percent salt passage, SP, by the following equation: R=100-SP) as the calcium ion concentration increases, whereas the 2 BPS dense films exhibit essentially constant ion rejection regardless of Ca^{2+} concentration. Parise et al. suggested that this phenomenon was observed because Donnan charge equilibrium led to charge exclusion being an important mechanism of ion rejection in PSPSf composites.[151] Charge exclusion occurs due to fixed membrane charges acting as a barrier to ions with like charges.[151]

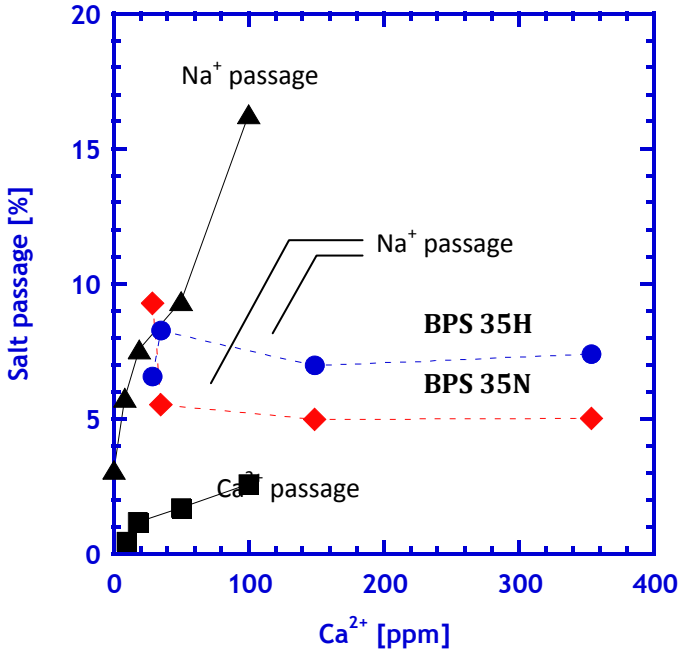

Figure 7.4: Salt passage through a post-polymerization sulfonated polysulfone membrane (Hi-Flux CP, ▲ and ■) and two BPS dense films in the presence of Ca^{2+} ions. Hi-Flux CP data from[151].

The extent of charge exclusion as a mechanism for ion partitioning is highly dependent on the polymer electrokinetic properties. Streaming zeta potential analysis is a suitable method to analyze the electrokinetic properties of a polymer film surface, which, in turn, can be used to estimate the polymer's bulk charge properties.[114, 147] The zeta potential, ζ, of Radel and Udel polysulfone indicates that unsulfonated polysulfones appear highly negatively charged over a broad range of pH, including neutral pH (Figure 7.5). Radel polysulfone is the non-sulfonated analog of the BPS materials studied here (i.e., Radel is BPS-00), and a Udel polysulfone ultrafiltration membrane is used as the support membrane to make TFCs. For reference, the zeta potential of a common polyamide RO membrane is included in Figure 7.5 and is more neutral than the non-

sulfonated polysulfones. The polysulfones' streaming potentials were similar to other hydrophobic polymers that do not contain fixed charged groups (e.g., polyethylene[152] and polypropylene[153]). Other researchers ascribe the negative charge observed in hydrophobic polymers to a preferential adsorption of hydroxide ions over hydronium ions.[154, 155] Due to an uneven molecular charge distribution, both hydroxide and hydronium ions have a strong hydrophobic end and a strong hydrophilic end. However, the effect of the uneven charge distribution is more pronounced in hydroxide ions, leading to a stronger hydrophobic end and, therefore, stronger adsorption to hydrophobic materials.[155]

Interestingly, a post-polymerization sulfonated Radel sample (which was acid-form and had an estimated 35 mol% sulfonation based on the polymer's ion-exchange capacity) had a slightly less negative zeta potential than unsulfonated Radel at high pH, even though the sulfonation introduced fixed negative charge into the polymer backbone. This phenomenon (i.e., that a negatively charged polymer exhibits a less negative surface charge than an uncharged polymer) has been ascribed to sulfonation increasing the polymer's hydrophilicity, which, in turn, reduces the preferential adsorption of hydroxide ions at the polymer surface, thereby reducing the negative zeta potential.[152, 153] Additionally, because the zeta potential is related to the electric potential a short distance away from the polymer surface, it is also conceivable that a negatively charged polymer would have it's surface charge somewhat screened due to the attraction of positively charged cations from the electrolyte solution. A neutral polymer, on the other hand,

would not attract positive cations to its surface and, consequently, could not benefit from this effect. For Radel PSPSf, these phenomena provide a plausible explanation of the results. Furthermore, Radel's isoelectric point shifted from a pH of approximately 3.6 in its unsulfonated form to a pH below 3 when sulfonated, which is expected given the strong acidic nature of the sulfonic groups.[152] The PSPSf remained negatively charged at all pH values.

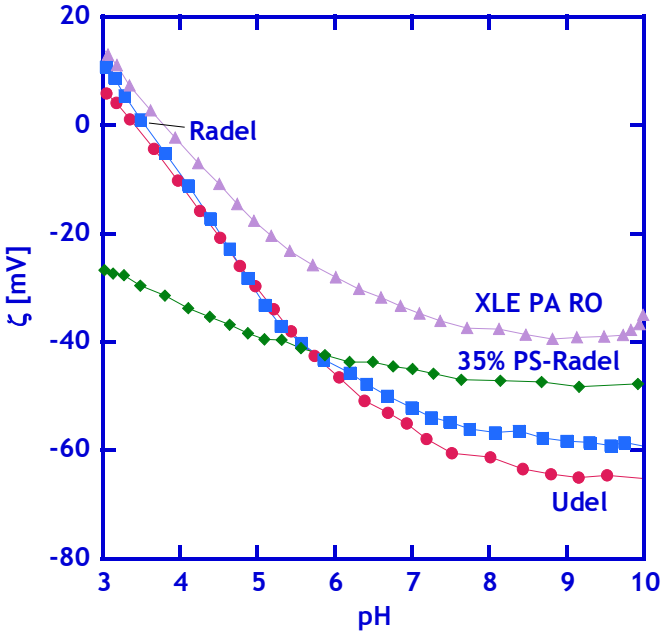

Figure 7.5: Streaming zeta potential of XLE polyamide RO membrane and Udel, Radel, and post-polymerization sulfonated Radel polysulfone. 10 mM NaCl in water was used as the reference solution and a pressure ramp of 300 mbar was used for each measurement.

The high effective negative charge of the PSPSf membrane, when compared to the charge of conventional polyamide RO membranes (i.e., XLE RO), suggests that charge exclusion in PSPSf could be important for ion partitioning in this material; because the polymer is negatively charged, anions will be preferentially excluded over

cations. Therefore, anion type and charge could have a substantial effect on overall salt passage through PSPSf membranes.[151] Negatively-charged PSPSf will bind cations, with higher valence cations being preferred over monovalent cations.[151] This phenomenon would be particularly important when filtering solutions containing cations of mixed valances (e.g., calcium and sodium ions). The higher valence cations (such as calcium) would be expected to selectively bind to and partially neutralize the membrane charge. This phenomenon would be expected to reduce the membrane's charge exclusion ability, thereby allowing the passage of more anions. To insure electroneutrality, cations would also permeate through the membrane, with monovalent (i.e., Na^+) ions presumably permeating more readily than larger, potentially more tightly bound multivalent ions (although the passage of both ions increased with increasing divalent ion concentration, as shown in Figure 7.4).

Interestingly, dense film BPS-35N and H exhibited constant sodium ion rejection with increasing Ca^{2+} concentration (Figure 7.4), which is surprising given the chemical similarities between the BPS materials and PSPSf. The zeta potential analysis of dense BPS films in both the acid and potassium salt forms is shown in Figure 7.6. All BPS materials, aside from BPS-20K, were only slightly negatively charged. BPS-20H had a high standard deviation (±~5 mV), while all other samples usually had a standard deviation of ±1 mV or less. Presumably, the small zeta potential of these samples might suggest that ion exclusion due to surface charge effects could be small in these materials.

If so, then it would be reasonable to assume that increasing the Ca^{2+} concentration would have little effect on Na^{+} passage in mixed-valence feeds.

Although the chemical and physical origins of the apparent neutral charge exhibited by the BPS dense films are not entirely understood, presumably a combination of counterion shielding of the sulfonic groups and an increase in film hydrophilicity (which occurs as sulfonation degree increases) may contribute to neutralizing the film surface charge as sulfonation degree increases. Furthermore, the streaming potential difference of PSPSf and BPS materials may be related to the difference in the spatial distribution of the sulfonic acid groups in each material. The sulfonic acid groups are randomly placed in the PSPSF chain, while in the BPS materials, the sulfonic acid placement always occurs in pairs of 2. However, further studies are needed to fully understand the effect of the sulfonic spatial distribution on material surface charge.

The effect of BPS hydrophilicity on the film's zeta potential is clearly observed when comparing BPS-20H and BPS-20K, whose ion exchange capacities and, therefore, fixed charge densities are identical (Table 7.3). However, the water uptake of these films is significantly different, with the acid form (18.1%) exhibiting a much higher uptake than the salt form (4.5%). As expected, the increase in water uptake led to a more neutrally charged film. On the other hand, increasing fixed charge density in the polymer seems to also neutralize the film's surface charge. Although BPS-32K has a lower water

uptake than BPS-20H, its ion exchange capacity is higher (1.41 for BPS-32K, 0.92 for BPS-20H), which produced a more neutral film.

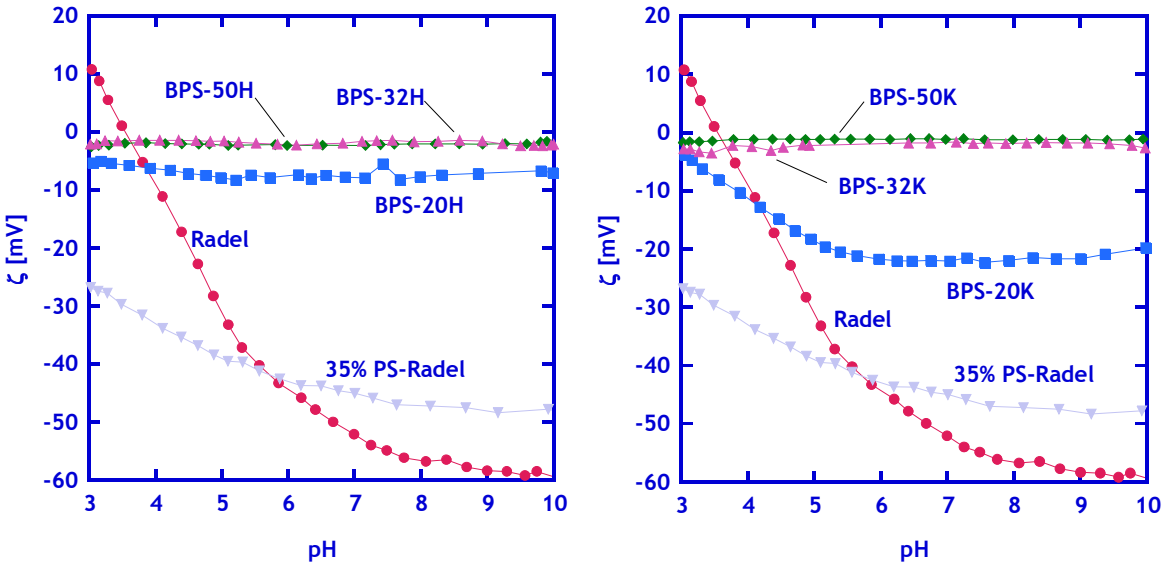

Figure 7.6: Streaming zeta potential of acid (left) and potassium (right)-form BPS materials compared to Radel and post-polymerization sulfonated Radel. 10 mM NaCl in water was used as the reference solution and a pressure ramp of 300 mbar was used for each measurement.

Table 7.3: Water uptake, ion exchange capacity (IEC), and zeta potential (pH=7) for BPS-20H, 20K, and 32K freestanding films. Water uptake and ion exchange capacity data are from [22].

Film	Water uptake [%]	IEC [meq g^{-1}]	ζ, pH=7
BPS-20H	18.1	0.92	-7.8
BPS-20K	4.5	0.92	-22.0
BPS-32K	10.4	1.41	-1.8

7.3.5 Arsenic speciation and rejection in polyamide RO and BPS dense films

A membrane's surface charge plays an important role in rejecting solutes which speciate as a result of ion dissociation at various pH.[156] For example, arsenic is a common groundwater contaminant that will be present in various ionic (or non-ionic)

species depending on solution pH.[43] Arsenic can be present in two valences, As(V) and As(III), each of which can speciate as shown below:

$$H_2AsO_4^- \leftrightarrow HAsO_4^{2-} \quad pKa\sim6.8, As(V)^{43}$$

$$H_3AsO_3 \leftrightarrow H_2AsO_3^- \quad pKa\sim9.1, As(III)^{156}$$

The As(V) species (arsenate) is negatively charged at practical pH values and is, therefore, usually more readily rejected by negatively charged membranes than the As(III) species (arsenite). Arsenite is neutrally charged at pH values less than 9.1 and, therefore, charge exclusion is not a dominant partitioning mechanism for As(III).[157] The effect of arsenic speciation and charge exclusion on arsenic rejection using a low-pressure RO membrane is presented in Figure 7.7.[156] This membrane's arsenate rejection was high and similar between pH values of 5 and 10; over this range, the charges of the arsenate ion and membrane were negative, which contributes to rejection via charge exclusion. Similar to other aromatic polyamide desalination membranes, at a pH of about 3, the membrane was near its isoelectric point and, therefore, a slight decrease in the arsenate rejection was observed. In contrast, this membrane exhibited much lower rejection of arsenite at pH values below the pKa of aresenite (~9.1). At these pH values, since the arsenite is neutral, charge exclusion plays no role in the rejection properties of the membrane. The decrease in rejection, from ~87% at a pH of 10 to 50% at a pH of 3, clearly illustrates the importance of charge exclusion in arsenic species partitioning.

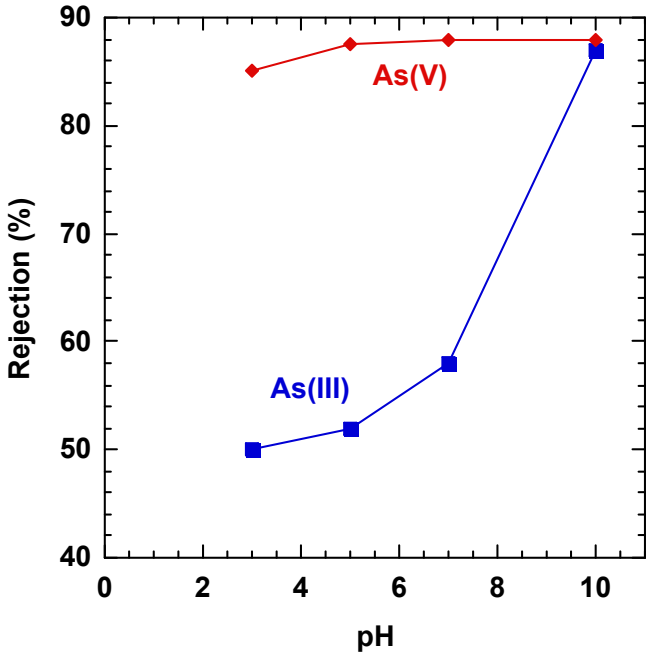

Figure 7.7: As(V) and As(III) rejection by an RO membrane (ES-10, Nitto Denko). Adapted from [156].

However, as shown in Figure 7.8, arsenic speciation has little effect on rejection in highly-sulfonated (>30 mol%) BPS dense films. At both high and low pH values, high rejection is observed for both As(V) and As(III) species. This high rejection is qualitatively consistent with the zeta potential results presented in Figure 7.6. The essentially neutral surface charge of these films suggests that charge exclusion might not be a controlling mechanism in arsenic rejection. The protonated arsenite and arsenic species have similar molecular weight (141 and 126 g/mol, respectively) and, therefore, may be of similar size, so the similar rejection values observed for both of these compounds is a reasonable result considering that the membrane surface appears neutrally charged from the zeta potential results.

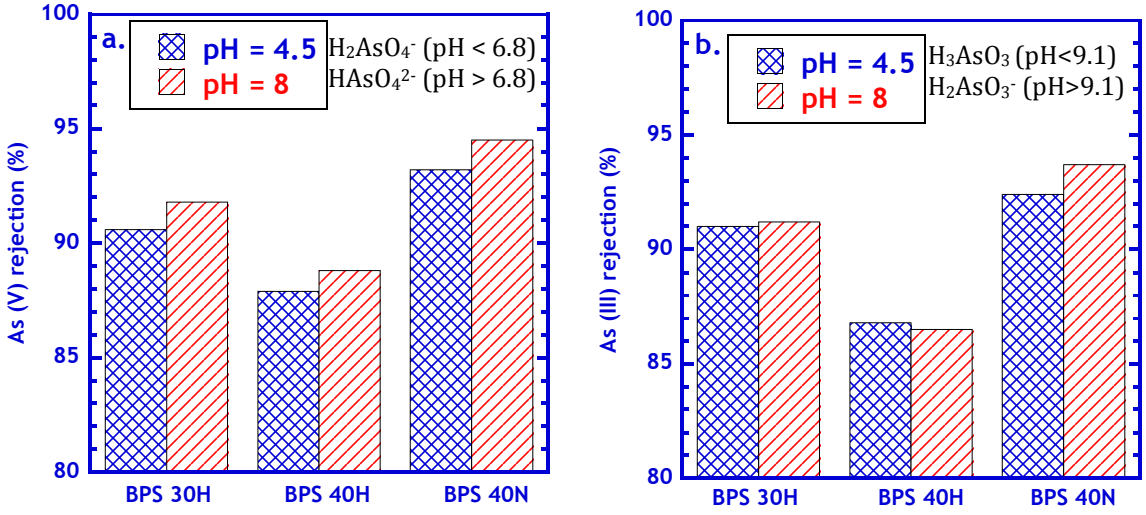

Figure 7.8: a. As(V) and b. As(III) rejection of BPS dense films.

7.3.6 Surface charge and salt passage of BPS thin-film composite membranes

As shown in Figure 7.9, the streaming zeta potential of BPS TFCs was more negative than their dense film analogs. The TFCs were prepared using three coatings of a solution containing 1 wt % polymer to insure that no defects were present in the coating layer. The increased negative surface charge in the TFCs (relative to the dense film results) is surprising, but could explain why the TFC membranes have a higher NaCl rejection than BPS dense films (cf., Table 7.1). If the surface is more negatively charged in the TFC membranes than in the dense films, then charge exclusion would be enhanced and, consequently, chloride ion rejection, and, therefore, overall sodium chloride rejection would be increased. The chemical and physical origins of the increased negative zeta potential of the TFCs can only be postulated. Very thin coating layers could possibly interact with the underlying Udel polysulfone support and affect certain

BPS polymer properties (i.e., increase negative charge, decrease the dielectric constant), which would enhance both charge and dielectric exclusion. A more extensive study into polymer support-polymer thin-film interactions would be needed to further understand the unique transport effects observed in this study.

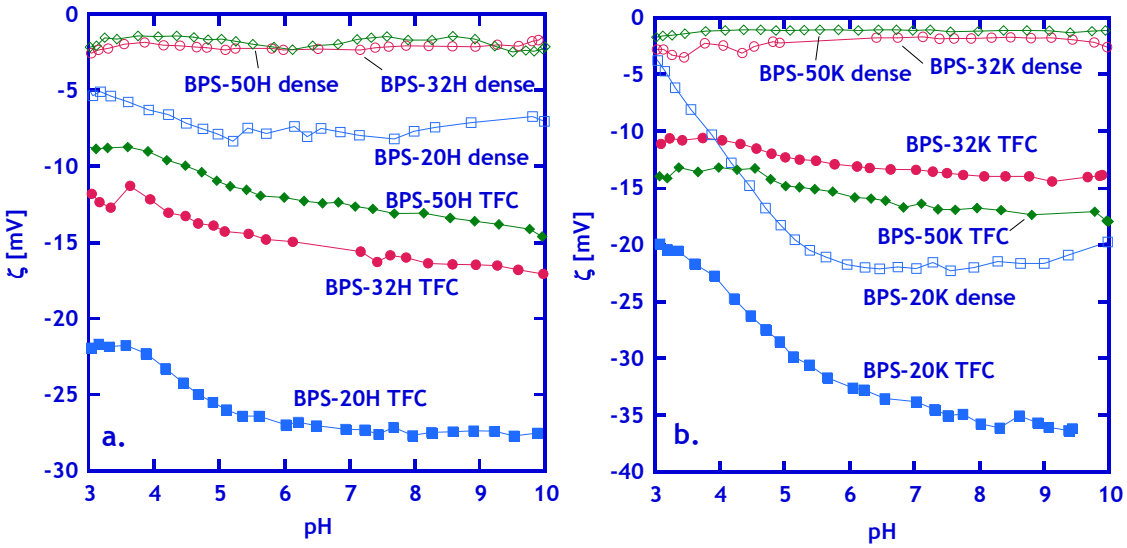

Figure 7.9: Streaming zeta potential of selected BPS dense films and TFCs in (a.) acid and (b.) potassium salt form. 10 mM NaCl in water was used as the reference solution and a pressure ramp of 300 mbar was used for each measurement.

Figure 7.10 presents sodium ion passage of a mixed-valence electrolyte feed solution (380 ppm NaCl and various $CaCl_2$ concentrations) as a function of feed solution calcium ion concentration for BPS dense films (these values are those reported in Figure 7.4 and are given here for comparison) and BPS TFCs. The rejection of the dense films and TFCs are strikingly different, with the TFCs salt partitioning ability greatly diminishing as the calcium ion concentration increases. Here, the BPS TFCs behave qualitatively similarly to the PSPSf membranes characterized in Figure 7.4, indicating

that calcium shields the fixed negative charges in the TFCs and therefore permits higher anion and overall salt passage.

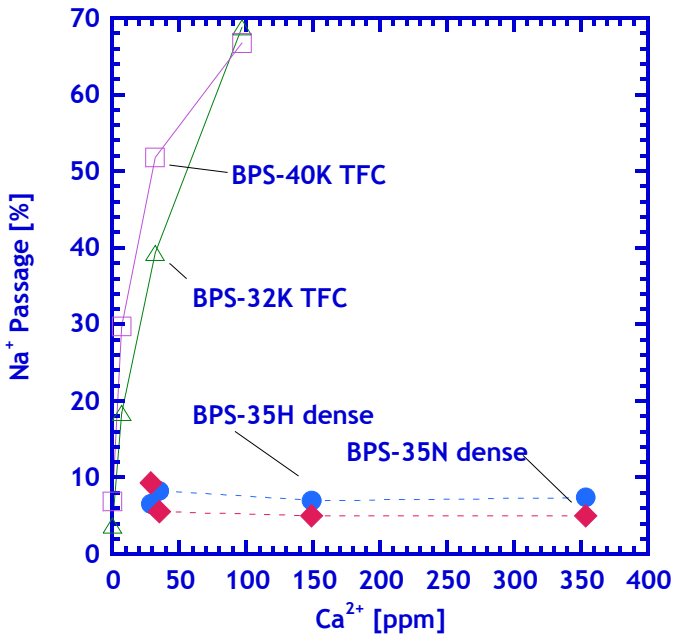

Figure 7.10: Sodium ion passage in BPS dense films and BPS thin-film composites. Testing conditions for the TFCs: 3.8 L/min crossflow, ΔP=400 psi, T=25 °C, pH= 6.7, 380 ppm NaCl (150 ppm Na^+).

Furthermore, single-salt rejection values for BPS-32K and 40K TFCs are relatively high for NaCl, but low for $CaCl_2$ (cf., Table 7.4). In contrast, a BPS-40H TFC characterized by Park et al. had a NaCl rejection of 89.5% and a $CaCl_2$ rejection of 69.5%.[22] BPS-32K and BPS-40K dense films have higher NaCl rejection (95.1% and 92.5%, respectively) than BPS-40H dense films (85.9%); therefore, BPS-32K and 40K TFCs are expected to have higher rejection of NaCl and $CaCl_2$ than BPS-40H TFCs. However, only NaCl, and not $CaCl_2$, rejection is higher in the BPS-32K and 40K TFCs than BPS-40H TFCs.

Table 7.4: Salt rejection values for BPS TFC membranes.

	Rejection [%]	
Membrane	**NaCl**	**$CaCl_2$**
BPS-32K TFC	96.3	60.0
BPS-40K TFC	93.1	47.5
BPS-40H TFC	89.5*	69.5*

NOTE: 3.8 L/min crossflow, ΔP=400 psi, T=25 °C, pH=6.7. 380 ppm NaCl (150 ppm Na^+) and 416 ppm $CaCl_2$ (150 ppm Ca^{2+}) were used for NaCl and $CaCl_2$ rejection, respectively. *Values from [22].

Tiny defects, whose size are similar to chloride ion diameters, in the BPS-32K and 40K TFC coating layers could explain this observation. $CaCl_2$ rejection would be low in negatively charged membranes with defects, because the calcium ions shield and reduce the effective charge in the TFCs. Chloride ions would, therefore, pass more freely through the defects as a result of reduced charge exclusion, consequently increasing overall $CaCl_2$ passage. However, charge shielding would not occur for a NaCl (monovalent) solution, and, therefore, chloride ions could be rejected to a higher degree as a result of increased charge exclusion. The increased charge exclusion could outweigh any ion partitioning losses due to defects, particularly if there were only a small number of ion-sized defects. Therefore, NaCl rejection of TFCs could be higher, even in TFCs with defects, than what would be expected based on analogous dense film NaCl rejection. Defect-free TFCs could potentially have significantly higher salt rejection values than those measured using dense films, which is what Park et al. observed for BPS-35H and 40H TFCs (Table 7.1). Future research should focus on techniques to prepare low sulfonation degree (i.e., < 35 mol%) TFC membranes that are defect-free and sufficiently thin to allow high water flux. Further studies are also needed to verify the extent and size of the defects in these membranes.

BPS-32K TFC arsenic rejection as a function of pH is presented in Figure 7.11. As in the mixed-valence salt passage experiments, the arsenic rejection of the BPS TFC was significantly different from that of the BPS dense film arsenic rejection (Figure 7.8) and was more reminiscent of negatively-charged RO membranes such as that shown in Figure 7.7. Arsenate rejection remained high over the entire range of pH considered, presumably because the arsenate ion and the membrane were always negatively charged. However, the arsenite rejection was lower than that of the arsenate species and decreased with decreasing pH, as is common for charged NF and loose RO membranes.[43, 156]

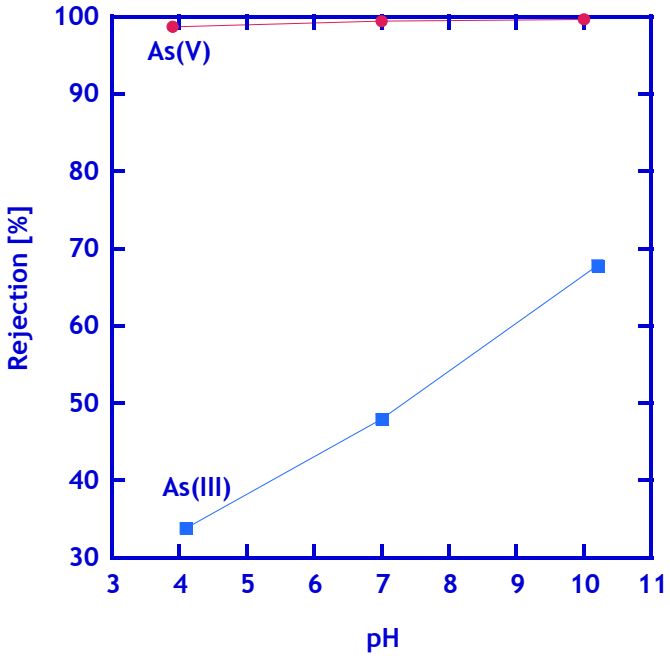

Figure 7.11: Arsenate (As(V)) and arsenite (As(III)) rejection at various pH using a BPS-32K TFC membrane. 3.8 L/min crossflow, ΔP=400 psi, T=25 °C, 10 mM NaCl.

7.4 Conclusions

Thin film composite membranes were prepared from BPS coatings on a porous Udel polysulfone support. Pore penetration of the coating solution, which was composed

of < 1w/v% of BPS in Di(EG), led to very thin BPS coating layers and TFCs with appreciable ion rejection and water flux. Water and ion transport characteristics were different in BPS composite membranes and dense films. These differences were presumably connected to an observed difference in zeta potential characteristics of the dense films and thin-film composite membranes. Interestingly, thick, dense moderately-sulfonated (>30 mol%) BPS films had essentially neutral charge (~-1- -3 mV) at pH values from 3 to 10 as measured by streaming zeta potential analysis. These same dense films exhibited high sodium ion rejection in the presence of calcium ions and high arsenic rejection regardless of solution pH. However, BPS thin-film composite membranes exhibited an increased negative surface charge (e.g., ~-10- -17 mV for BPS-32), and charge exclusion appeared to exert a stronger effect on rejection properties in the TFCs. Defects were most likely present in the BPS coating layer (as evidenced by the low single-salt $CaCl_2$ rejection) and, as a result, these membrane's steric exclusion capability was probably reduced. The increased importance of charge exclusion, coupled with the decreased ability of steric exclusion, led to low salt rejection in mixed-valence feeds and low arsenite rejection. Both of these trends are seen in post-polymerization sulfonated polysulfones and other negatively charged NF and loose RO membranes.

8. CHAPTER 8: CONCLUSIONS AND RECOMMENDATIONS

8.1 Conclusions

Membrane technology has gained significant traction in water purification applications, such as wastewater reclamation and desalination, in recent years because advances in the field have made membranes competitive with other, more traditional purification technologies, such as distillation. However, fouling of water purification membranes remains a concern. This thesis focused on tuning membrane materials' properties and, more specifically, membrane surface characteristics, to mitigate fouling for a variety of membranes. Two different membrane surface modifications (chitosan-PEG hybrid coating layer on UF membranes and PDOPA/PDOPA-g-PEG deposition on many membranes) were used to reduce fouling by emulsified oil solutions as well as reduce protein and bacteria adhesion to membranes. Furthermore, unique material properties were also explored in sulfonated polysulfones, which were previously identified as chlorine-tolerant desalination membranes.

Polydopamine and polydopamine-g-PEG surface modification: Polydopamine (PDOPA) deposition was found to be a simple, yet effective, modification technique for numerous membranes of varying structure and chemical composition. Furthermore, poly(ethylene glycol) (PEG), a common non-fouling material, could be easily conjugated to a deposited PDOPA layer. PDOPA deposition led to an increase in membrane surface hydrophilicity in nearly all membranes studied. The enhanced hydrophilicity was coupled with slightly reduced surface roughness and surface charge,

as probed by zeta potential. Grafting PEG to the PDOPA layer usually further enhanced the membrane's fouling resistance, consistent with PEG's well-known anti-fouling characteristics. Due to the non-selective nature of PDOPA deposition (i.e., PDOPA would polymerize under benign aqueous conditions and deposit from solution onto any surface it contacted), PDOPA was easily applied to membrane modules. Fouling (especially irreversible fouling) of membranes in module form was also reduced by PDOPA and PDOPA-g-PEG.

Three membranes, XLE RO, PVDF MF, and PS-20 UF, were considered in more detail, and the influence of PDOPA deposition and PEG grafting conditions on protein and bacteria adhesion was studied for these membranes. PDOPA and subsequent PEG grafting had little effect on PVDF MF membrane flux, presumably because the pore size of these membranes was much larger than the thickness of the PDOPA deposition and PEG graft layers. A decrease in PS-20 UF water flux was observed with increasing PDOPA deposition and PEG grafting density, presumably because the pore size of these membranes was similar to the PDOPA deposition and PEG graft layer thicknesses. XLE RO membranes exhibited a small decrease in flux with increasing PDOPA deposition (most likely due to a low amount of PDOPA deposition compared to the other membranes considered), but PEG grafting significantly reduced XLE RO flux.

BSA adhesion was reduced by PDOPA deposition on all membranes considered. Higher amounts of PDOPA deposition were correlated with decreases in BSA adhesion.

PEG grafting further reduced BSA adhesion. A general trend of reduced BSA adhesion with increasing PEG graft molecular weight was observed for the PVDF MF and PS-20 UF membranes. However, all PEG molecular weights exhibited similar BSA adhesion resistance on XLE RO membranes.

Overall, polydopamine deposition was an effective modification technique that is versatile and simple and, as a result, provides a promising surface modification strategy for effectively reducing fouling in many applications.

Chitosan-PEG hybrid UF coating layer: Hydrogels based on chitosan crosslinked with a bifunctional PEG epoxide (PEGDGE) were synthesized. These hydrogels were characterized using SEM, water flux measurements, and molecular weight cutoff experiments. Based on the results of the hydrogel characterization, a 1.4 PEGDGE/chitosan ratio solution was selected as a candidate for coating onto UF membranes for fouling studies.

PSf UF/PEG-chi hybrid composite membranes were prepared using a "draw-down" method. The PEG-chi hybrid coating thickness could be controlled by varying the chitosan concentration in the coating solution (keeping the chitosan/PEGDGE ratio constant). However, thin coating layers led to more defects, as indicated by variability in the pure water permeance of the resulting composite membranes. Relative to an unmodified PSf UF membrane, the PEG-chi hybrid coating layer significantly reduced

fouling when filtering an emulsified oil/water mixture. Furthermore, the PEG-chi hybrid coatings significantly reduced irreversible internal fouling, which could make membrane cleaning cycles more efficient. When comparing the fouling performance of composite membranes with varying PEG-chi layer thickness, the flux through thin-layer membranes is always high compared to thick-layer membranes. However, thin layers led to higher amounts of irreversible fouling when compared to thick layers. This is presumably due to a higher number of defects in the thin layers, which leads to more irreversible internal membrane fouling.

BPS dense film and thin film composite characterization: Thin film composite membranes were prepared from BPS material coating layers and a Udel polysulfone (PSf) ultrafiltration support. Diethylene glycol (Di(EG)) was used as the BPS solvent in this study. The BPS coating solution would penetrate the porous structure of the PSf support, which led to an ultrathin (~100 nm) coating layer. The pore penetration was not found to markedly affect the porous support structure (*i.e.,* no pore blockage and minimal pore constriction was observed using SEM) as probed by SEM. Differences in BPS dense films and BPS thin-film composites surface properties (*i.e.,* surface charge) led to differences in ion transport properties through each. Using freestanding dense BPS films, Na^+ rejection in the presence of Ca^{2+} was high (>90%) regardless of Ca^{2+} concentration. Furthermore, As(III) rejection was high over a broad pH range, including low pH. These high rejection values were a result of the moderately-sulfonated (>30 mol%) BPS films being nearly neutrally charged (~-1- to -3 mV) over

pH=3-10, as measured by streaming zeta potential analysis. However, BPS thin-film composites were more negatively charged (~-10 to -17 mV for BPS-32) and, therefore, charge exclusion was presumed to be a dominant ion partitioning mechanism in these membranes. Defects were most likely present in the BPS coating layer (as a result of residual Di(EG) being washed out of the BPS layer) and, as a result, these membranes' steric exclusion capability was reduced. The increased importance of charge exclusion, coupled with the decreased capability of steric exclusion, led to low salt rejection in mixed-valence feeds and low arsenite rejection. Both of these trends are consistent with literature reports in post-sulfonated polysulfones and other negatively charged NF and RO membranes.

8.2 Recommendations

Chitosan-PEG hybrid UF coating layer: Although chitosan-PEG hybrid coatings have been studied to reduce oil emulsion fouling in polysulfone UF membranes, chitosan is a positively-charged polysaccharide that may provide attachment sites for other polysaccharides and negatively-charged organics (*i.e.*, proteins). It is, therefore, not recommended to study chitosan-based hydrogels for fouling resistance in real-life water purification applications. However, chitosan-based membranes have been studied extensively for pervaporation[158-163] and gas separation[164, 165] applications where a polar vapor/gas needs to be removed from a gas mixture. Furthermore, PEG-based materials have been studied for similar separation applications[166, 167], although PEG is usually grafted or copolymerized to another more mechanically robust polymer (such as polyimides) when employed in pervaporation applications[168, 169]. To this end, defect-free

chi-PEG hybrid composite membranes could be used in pervaporation and gas separation applications, such as natural gas sweetening, hydrogen purification, or ethanol dehydration.

PDOPA and PDOPA-g-PEG modifications: Currently, the mechanism of PDOPA formation and deposition is poorly understood. Fundamental research to discover the molecular structure of PDOPA is challenging, because PDOPA is insoluble and seems to exhibit paramagnetic-like properties when analyzed using NMR. Knowing the exact PDOPA structure could provide clues as to how the polymerization and deposition occurs, which could suggest strategies to increase the polymerization kinetics, make the deposition more rapid, and perhaps generally improve the fouling efficiency of PDOPA coatings.

One issue to be addressed with PDOPA is its chlorine tolerance. Based on preliminary studies, PDOPA is attacked by hypochlorite at concentrations higher than approximately 10 ppm. Insight into the PDOPA structure may help develop new chemistries that could render PDOPA more resistant to chlorine attack. Also, the exploration of other cleaning agents (such as citric acid and sodium bisulfite) may be important for applications employing PDOPA-modified membranes.

PDOPA-modification was extremely successful at reducing fouling in laboratory-scale filtrations. However, it is still unproven in real-life applications, such as seawater

filtration, membrane bioreactor applications, and produced water filtration. Fortunately, due to the versatility of the PDOPA modification, membrane module modification and pilot plant testing could potentially be arranged to test the viability of PDOPA as a practical membrane modification strategy. In the laboratory, the adhesion properties of other common foulants, such as alginates (polysacharrides), natural organic matter, algae, and other proteins should be explored on unmodified and PDOPA-modified membranes.

To reduce the cost of PEG grafting to the PDOPA layer (and to produce lower molecular weight PEG), a simple chemistry can be used to produce amine-terminated PEG. This chemistry is outlined in Figure 8.1.[170] A 3:1 molar ratio of thionyl chloride to hydroxyl-terminated PEG (PEG-OH) is refluxed with a few drops of dimethyl formamide (DMF) at 60 °C. The resulting chloride-terminated PEG (PEG-Cl) can be purified by first evaporating the unreacted $SOCl_2$ and DMF from the reaction mixture and then passing the PEG through a silica gel column. The PEG-Cl can also be purified by dissolving it in excess warm ethanol (2 L of ethanol for 50 g of PEG-Cl), and then recrystallizing it by cooling the ethanol to 4 °C (the PEG-Cl will precipitate from the ethanol solution at this temperature). Once the PEG-Cl is purified, it is mixed with 25% ammonium hydroxide (NH_4OH) in water and allowed to react for at least 2 days at 50 °C in a sealed vessel. The excess NH_4OH and water can be removed using a rotary evaporator, leaving pure PEG-NH_2 in high yield.

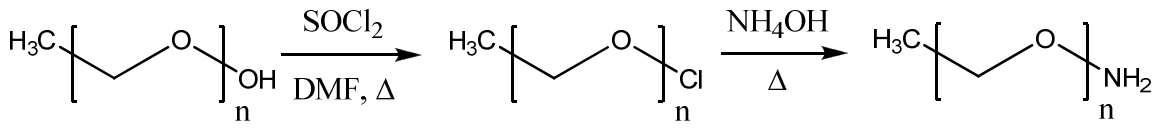

Figure 8.1: Synthesis of PEG-NH_2 from low cost PEG-OH.

PDOPA could also be explored for gas separation and pervaporation applications (one group has already performed initial experiments using PDOPA modified membranes in pervaporation applications).[102] A long (>16h) PDOPA deposition on polysulfone ultrafiltration membranes is recommended in these types of separations to create a thin, but dense, defect-free coating layer on the membrane surface.

BPS desalination membranes: The pore penetration and defect hypotheses, as well as the fundamental differences in thick film and TFC membranes, put forth in this study should be tested. Measuring gas permeability selectivity using composite membranes will verify the existence (or lack thereof) of defects in the coating layer. Thick-film BPS-20K selectivity for oxygen over nitrogen could be measured, and thin film composite membrane selectivity could be compared to these values to assess the integrity of the coating layer. A more complete, yet potentially more difficult, experiment to probe transport property differences in thick and thin film membranes would involve spin coating thin BPS films (~500-1000 nm) and, using a procedure similar to that outlined previously,[171, 172] placing these films on the surface of a polysulfone support membrane. This technique insures that no pore penetration is present in the composite membranes. By characterizing transport through the thin BPS layer in this configuration, ideal transport properties (*i.e.*, those of a defect-free coating

layer with no BPS pore penetration) of BPS thin-film composites could be better understood and compared to the properties of both the thin-film composites and dense thick-films considered in these studies.

9. REFERENCES

1. Oki, T. & Kanae, S. Global hydrological cycles and world water resources. Science 313, 1068-1072 (2006).

2. Fenwick, A. Waterborne infectious diseases - Could they be consigned to history? Science 313, 1077-1081 (2006).

3. Water for life: making it happen, World Health Organization. http://www.who.int/water_sanitation_health/monitoring/jmp2005/en/index.html (2005).

4. Service, R. F. Desalination freshens up. Science 313, 1088-1090 (2006).

5. US Bureau of Reclamation. Water 2025: preventing crises and conflict in the West. (2003).

6. US Environmental Protection Agency. 2006-2011 EPA strategic plan: charting our course, 29-54 (2006).

7. Arthur, D., Langhus, B. & Rawn-Schatzinger, V. Coalbed natural gas resources: water rights and treatment technologies. GasTIPS 9, 20-24 (2003).

8. http://aqua-sol.com/water_technology.html.

9. Mallevialle, J., Odendaal, P. E. & Wiesner, M. R. The Emergence of Membranes in Water and Wastewater Treatment, in Water Treatment: Membrane Processes, McGraw Hill Co., New York, NY. 1.1-1.10 (1996).

10. Cheryan, M. Microfiltration and Ultrafiltration Handbook. Technomic Publishing, Lancaster, Pa. (1998).

11. Pollen picture courtesy of Dr. Howard Berg, Donald Danforth Plant Science Center, http://www.danforthcenter.org/Cells/images/pollen.jpg.

12. Belfort, G., Davis, R. H. & Zydney, A. L. The behavior of suspensions and macromolecular solutions in crossflow microfiltration. Journal of Membrane Science 96, 1-58 (1994).

13. Baker, R. W. Membrane Technology and Applications, John Wiley and Sons, West Sussex, England. (2004).

14. Brehant, A., Bonnelye, V. & Perez, M. Comparison of MF/UF pretreatment with conventional filtration prior to RO membranes for surface seawater desalination. Desalination 144, 353-360 (2002).

15. Wolf, P. H., Siverns, S. & Monti, S. UF membranes for RO desalination pretreatment. Desalination 182, 293-300 (2005).

16. Durham, B. & Walton, A. Membrane pretreatment of reverse osmosis: long-term experience on difficult waters. Desalination 122, 157-170 (1999).

17. Freeman, B. D. & Pinnau, I. Gas and liquid separations using membranes: an overview. ACS Symposium Series 876 (Advanced Materials for Membrane Separations), American Chemical Society, Washington, DC, 1-23 (2004).

18. Petersen, R. J. Composite reverse osmosis and nanofiltration membranes. Journal of Membrane Science 83, 81-150 (1993).

19. Wijmans, J. G. & Baker, R. W. The solution-diffusion model: a review. Journal of Membrane Science 107, 1-21 (1995).

20. Hilal, N., Al-Zoubi, H., Darwish, N. A., Mohamma, A. W. & Abu Arabi, M. A comprehensive review of nanofiltration membranes:Treatment, pretreatment, modelling, and atomic force microscopy. Desalination 170, 281-308 (2004).

21. Bowen, W. R. & Mukhtar, H. Characterisation and prediction of separation performance of nanofiltration membranes. Journal of Membrane Science 112, 263-274 (1996).

22. Park, H. B., Freeman, B. D., Zhang, Z.-B., Sankir, M. & McGrath, J. E. Highly chlorine-tolerant polymers for desalination. Angewandte Chemie International Edition 47, 6019-6024 (2008).

23. Greenlee, L. F., Lawler, D. F., Freeman, B. D., Marrot, B. & Moulin, P. Reverse osmosis desalination: Water sources, technology, and today's challenges. Water Research 43, 2317-2348 (2009).

24. Santos, S. M. & Wiesner, M. R. Ultrafiltration of water generated in oil and gas production. Water Environment Research 69, 1120-1127 (1997).

25. Judd, S. The status of membrane bioreactor technology. Trends in Biotechnology 26, 109-116 (2008).

26. Le-Clech, P., Chen, V. & Fane, T. A. G. Fouling in membrane bioreactors used in wastewater treatment. Journal of Membrane Science 284, 17-53 (2006).

27. Yang, W., Cicek, N. & Ilg, J. State-of-the-art of membrane bioreactors: Worldwide research and commercial applications in North America. Journal of Membrane Science 270, 201-211 (2006).

28. Tal, A. Seeking sustainability: Israel's evolving water management strategy. Science 313, 1081-1084 (2006).

29. Van der Bruggen, B. & Vandecasteele, C. Distillation vs. membrane filtration: overview of process evolutions in seawater desalination. Desalination 143, 207-218 (2002).

30. Cheryan, M. & Rajagopalan, N. Membrane processing of oily streams: Wastewater treatment and waste reduction. Journal of Membrane Science 151, 13-28 (1998).

31. Mairal, A. P., Ng, A., Wijmans, J. G., Pinnau, I. & Ly, J. H. Treatment of shipboard-generated oily wastewaters, US Patent Application #2004079706. (2004).

32. Nestle, H. Oily waste treatment systems, presented at: Office of Naval Research EQ (6.2) program review, environmental quality information exchange, Annapolis, MD. June 26, 2002.

33. Johnston, S. T., Smith, K. A. & Deen, W. M. Concentration polarization in stirred ultrafiltration cells. AIChE Journal 47, 1115-1125 (2001).

34. Song, L. F. & Elimelech, M. Theory of concentration polarization in cross-flow filtration. Journal of the Chemical Society-Faraday Transactions 91, 3389-3398 (1995).

35. Buckley, C. A. & Hurt, Q. E. Membrane Applications: A Contaminant-Based Perspective, in Water Treatment: Membrane Processes, McGraw Hill Co., New York, NY. 3.1-3.24 (1996).

36. Al-Bastaki, N. & Abbas, A. Use of fluid instabilities to enhance membrane performance: a review. Desalination 136, 255-262 (2001).

37. Psoch, C. & Schiewer, S. Critical flux aspect of air sparging and backflushing on membrane bioreactors. Desalination 175, 61-71 (2005).

38. Mallubhotla, H., Nunes, E. & Belfort, G. Microfiltration of yeast suspensions with self-cleaning spiral vortices - possibilities for a new membrane module design. Biotechnology and Bioengineering 48, 375-385 (1995).

39. Redkar, S., Kuberkar, V. & Davis, R. H. Modeling of concentration polarization and depolarization with high-frequency backpulsing. Journal of Membrane Science 121, 229-242 (1996).

40. Judd, S. Submerged membrane bioreactors: flat plate or hollow fibre? Filtration & Separation 39, 30-31 (2002).

41. Psoch, C. & Schiewer, S. Anti-fouling application of air sparging and backflushing for MBR. Journal of Membrane Science 273, 273-280 (2006).

42. Ma, H., Bowman, C. N. & Davis, R. H. Membrane fouling reduction by backpulsing and surface modification. Journal of Membrane Science 173, 191-200 (2000).

43. Vrijenhoek, E. M., Hong, S. & Elimelech, M. Influence of membrane surface properties on initial rate of colloidal fouling of reverse osmosis and nanofiltration membranes. Journal of Membrane Science 188, 115-128 (2001).

44. Taniguchi, M. & Belfort, G. Low protein fouling synthetic membranes by UV-assisted surface grafting modification: varying monomer type. Journal of Membrane Science 231, 147-157 (2004).

45. Taniguchi, M., Kilduff, J. E. & Belfort, G. Low fouling synthetic membranes by UV-assisted graft polymerization: monomer selection to mitigate fouling by natural organic matter. Journal of Membrane Science 222, 59-70 (2003).

46. Nabe, A., Staude, E. & Belfort, G. Surface modification of polysulfone ultrafiltration membranes and fouling by BSA solutions. Journal of Membrane Science 133, 57-72 (1997).

47. Ulbricht, M. & Belfort, G. Surface modification of ultrafiltration membranes by low temperature plasma II. Graft polymerization onto polyacrylonitrile and polysulfone. Journal of Membrane Science 111, 193-215 (1996).

48. Wang, P., Tan, K. L., Kang, E. T. & Neoh, K. G. Plasma-induced immobilization of poly(ethylene glycol) onto poly(vinylidene fluoride) microporous membrane. Journal of Membrane Science 195, 103-114 (2002).

49. Yu, H.-Y., Xie, Y.-J., Hu, M.-X., Wang, J.-L., Wang, S.-Y. & Xu, Z.-K. Surface modification of polypropylene microporous membrane to improve its antifouling property in MBR: CO2 plasma treatment. Journal of Membrane Science 254, 219-227 (2005).

50. Belfer, S., Purinson, Y., Fainshtein, R., Radchenko, Y. & Kedem, O. Surface modification of commercial composite polyamide reverse osmosis membranes. Journal of Membrane Science 139, 175-181 (1998).

51. Belfer, S., Gilron, J., Purinson, Y., Fainshtain, R., Daltrophe, N., Priel, M., Tenzer, B. & Toma, A. Effect of surface modification in preventing fouling of commercial SWRO membranes at the Eilat seawater desalination pilot plant. Desalination 139, 169-176 (2001).

52. Asatekin, A., Menniti, A., Kang, S., Elimelech, M., Morgenroth, E. & Mayes, A. M. Antifouling nanofiltration membranes for membrane bioreactors from self-assembling graft copolymers. Journal of Membrane Science 285, 81-89 (2006).

53. Ostuni, E., Chapman, R. G., Holmlin, R. E., Takayama, S. & Whitesides, G. M. A survey of structure-property relationships of surfaces that resist the adsorption of protein. Langmuir 17, 5605-5620 (2001).

54. Chapman, R. G., Ostuni, E., Liang, M. N., Meluleni, G., Kim, E., Yan, L., Pier, G., Warren, H. S. & Whitesides, G. M. Polymeric thin films that resist the adsorption of proteins and the adhesion of bacteria. Langmuir 17, 1225-1233 (2001).

55. Ju, H., McCloskey, B. D., Sagle, A. C., Wu, Y.-H., Kusuma, V. A. & Freeman, B. D. Crosslinked poly(ethylene oxide) fouling resistant coating materials for oil/water separation. Journal of Membrane Science 307, 260-267 (2008).

56. Li, R. H. & Barbari, T. A. Performance of poly(vinyl alcohol) thin-gel composite ultrafiltration membranes. Journal of Membrane Science 105, 71-78 (1995).

57. Wang, X., Fang, D., Yoon, K., Hsiao, B. S. & Chu, B. High performance ultrafiltration composite membranes based on poly(vinyl alcohol) hydrogel coating on crosslinked nanofibrous poly(vinyl alcohol) scaffold. Journal of Membrane Science 278, 261-268 (2006).

58. Myung, S. W., Choi, I. H., Lee, S. H., Kim, I. C. & Lee, K. H. Use of fouling resistant nanofiltration and reverse osmosis membranes for dyeing wastewater effluent treatment. Water Science and Technology 51, 159-164 (2005).

59. Kim, I. C., Ka, Y. H., Park, J. Y. & Lee, K. H. Preparation of fouling resistant nanofiltration and reverse osmosis membranes and their use for dyeing wastewater effluent. Journal of Industrial and Engineering Chemistry 10, 115-121 (2004).

60. Hyun, J., Jang, H., Kim, K., Na, K. & Tak, T. Restriction of biofouling in membrane filtration using a brush-like polymer containing oligoethylene glycol side chains. Journal of Membrane Science 282, 52-59 (2006).

61. Yoon, K., Kim, K., Wang, X. F., Fang, D. F., Hsiao, B. S. & Chu, B. High flux ultrafiltration membranes based on electrospun nanofibrous PAN scaffolds and chitosan coating. Polymer 47, 2434-2441 (2006).

62. Sagle, A. C., Van Wagner, E. M., Ju, H., McCloskey, B. D., Freeman, B. D. & Sharma, M. M. PEG-coated reverse osmosis membranes: Desalination properties and fouling resistance. Journal of Membrane Science 340, 92-108 (2009).

63. Nunes, S. P., Sforca, M. L. & Peinemann, K. V. Dense Hydrophilic Composite Membranes For Ultrafiltration. Journal Of Membrane Science 106, 49-56 (1995).

64. Louie, J. S., Pinnau, I., Ciobanu, I., Ishida, K. P., Ng, A. & Reinhard, M. Effects of polyether-polyamide block copolymer coating on performance and fouling of reverse osmosis membranes. Journal of Membrane Science 280, 762-770 (2006).

65. Percival, S. L., Walker, J. T. & Hunter, P. R. Microbiological aspects of biofilms and drinking water. CRC Press, New York, NY, USA (2000).

66. Chong, T. H., Wong, F. S. & Fane, A. G. The effect of imposed flux on biofouling in reverse osmosis: Role of concentration polarisation and biofilm enhanced osmotic pressure phenomena. Journal of Membrane Science 325, 840-850 (2008).

67. Herzberg, M. & Elimelech, M. Biofouling of reverse osmosis membranes: Role of biofilm-enhanced osmotic pressure. Journal of Membrane Science 295, 11-20 (2007).

68. Ang, W. S., Lee, S. & Elimelech, M. Chemical and physical aspects of cleaning of organic-fouled reverse osmosis membranes. Journal of Membrane Science 272, 198-210 (2006).

69. Madaeni, S. S. & Mansourpanah, Y. Chemical cleaning of reverse osmosis membranes fouled by whey. Desalination 161, 13-24 (2004).

70. Shintani, T., Matsuyama, H. & Kurata, N. Development of a chlorine-resistant polyamide reverse osmosis membrane. Desalination 207, 340-348 (2007).

71. Alley, E. R. Water quality control handbook, McGraw Hill, New York, NY, 2006. (2006).

72. Wiesner, M. R. & Aptel, P. Mass transport and permeate flux and fouling in pressure-driven processes, in: Water Treatment: Membrane Processes, McGraw Hill Co., New York, NY. 4.1-30 (1996).

73. Pedroni, V. I., Gschaider, M. E. & Schulz, P. C. UV spectrophotometry: Improvements in the study of the degree of acetylation of chitosan. Macromolecular Bioscience 3, 531-534 (2003).

74. Rinaudo, M., Milas, M. & Le Dung, P. Characterization of chitosan. Influence of ionic strength and degree of acetylation on chain expansion. International Journal of Biological Macromolecules 15, 281-5 (1993).

75. Wang, F., Hickner, M., Kim, Y. S., Zawodzinski, T. A. & McGrath, J. E. Direct polymerization of sulfonated poly(arylene ether sulfone) random (statistical) copolymers: candidates for new proton exchange membranes. Journal of Membrane Science 197, 231-242 (2002).

76. Sumner, M. J., Harrison, W. L., Weyers, R. M., Kim, Y. S., McGrath, J. E., Riffle, J. S., Brink, A. & Brink, M. H. Novel proton conducting sulfonated poly(arylene ether) copolymers containing aromatic nitriles. Journal of Membrane Science 239, 199-211 (2004).

77. Lee, H.-S., Badami, A. S., Roy, A. & McGrath, J. E. Segmented sulfonated poly(arylene ether sulfone)-b-polyimide copolymers for proton exchange

membrane fuel cells. I. Copolymer synthesis and fundamental properties. Journal of Polymer Science Part A: Polymer Chemistry 45, 4879-4890 (2007).

78. From Sigma-Aldrich, St. Louis, MO. www.sigmaaldrich.com.

79. Van Wagner, E. M., Sagle, A. C., Sharma, M. M. & Freeman, B. D. Effect of crossflow testing conditions, including feed pH and continuous feed filtration, on commercial reverse osmosis membrane performance. Journal of Membrane Science 345, 97-109 (2009).

80. McCloskey, B. D., Park, H. B., Miller, D. J., Rowe, B. W., Ju, H. & Freeman, B. D. A universal, biofouling-inspired surface modification to increase membrane fouling resistance. Nature, submitted (2009).

81. Amine Reactive Probes. Molecular Probes, Inc. http://probes.invitrogen.com/media/pis/mp00143.pdf (2009).

82. Pasmore, M., Todd, P., Smith, S., Baker, D., Silverstein, J., Coons, D. & Bowman, C. N. Effects of ultrafiltration membrane surface properties on Pseudomonas aeruginosa biofilm initiation for the purpose of reducing biofouling. Journal of Membrane Science 194, 15-32 (2001).

83. For reference, a TW30-1812-36 membrane module is approximately 5 cm diameter x 30 cm length.

84. Dow Water and Process Solutions. http://www.dow.com/liquidseps/prod/tw30_181236.htm.

85. Singh, S., Khulbe, K. C., Matsuura, T. & Ramamurthy, P. Membrane characterization by solute transport and atomic force microscopy. Journal of Membrane Science 142, 111-127 (1998).

86. Schaep, J. & Vandecasteele, C. Evaluating the charge of nanofiltration membranes. Journal of Membrane Science 188, 129-136 (2001).

87. Papanu, J. S., Hess, D. W., Bell, A. T. & Soane, D. S. In situ ellipsometry to monitor swelling and dissolution of thin polymer films. Journal of the Electrochemical Society 136, 1195-1200 (1989).

88. Huang, Y. & Paul, D. R. Experimental methods for tracking physical aging of thin glassy polymer films by gas permeation. Journal of Membrane Science 244, 167-178 (2004).

89. Singla, A. K. & Chawla, M. Chitosan: some pharmaceutical and biological aspects-an update. Journal of Pharmacy and Pharmacology 53, 1047-1067 (2001).

90. Krajewska, B. Membrane-based processes performed with use of chitin/chitosan materials. Separation and Purification Technology 41, 305-312 (2005).

91. Kumar, M. & Ravi, N. V. A review of chitin and chitosan applications. Reactive & Functional Polymers 46, 1-27 (2000).

92. Uragami, T., Kato, T., Nagayasu, H. & Yura, I. Transport of nucleic-acid bases against their concentration gradients through quaternized chitosan membrane. Carbohydrate Polymers 21, 289-293 (1993).

93. Dusek, K. Phase separation during the formation of three-dimensional polymers. Journal of Polymer Science: Part C 16, 1289-99 (1967).

94. Schauer, C. L., Chen, M.-S., Chatterley, M., Eisemann, K., Welsh, E. R., Price, R. R., Schoen, P. E. & Ligler, F. S. Color changes in chitosan and poly(allyl amine) films upon metal binding. Thin Solid Films 434, 250-257 (2003).

95. Tatsumi, D. & Yamauchi, T. Application of ATR-FTIR spectroscopy combined with sputter etching for depth profiling of a chemical additive within a pulp fiber. Journal of Applied Polymer Science 69, 461-468 (1998).

96. Ham, J. S., Bolen, M. C. & Hughes, J. K. Use of high pressure to study polymer-solvent interaction. Journal of Polymer Science 57, 23-38 (1962).

97. Reddy, S., Arzt, E. & del Campo, A. Bioinspired surfaces with switchable adhesion. Advanced Materials 19, 3833-3837 (2007).

98. Liu, Y., Tang, J., Wang, R., Lu, H., Li, L., Kong, Y., Qi, K. & Xin, J. H. Artificial lotus leaf structures from assembling carbon nanotubes and their applications in hydrophobic textiles. Journal of Materials Chemistry 17, 1071-1078 (2007).

99. Feng, L., Li, S., Li, Y., Li, H., Zhang, L., Zhai, J., Song, Y., Liu, B., Jiang, L. & Zhu, D. Super-hydrophobic surfaces: from natural to artificial. Advanced Materials 14, 1857-1860 (2002).

100. Xia, F. & Jiang, L. Bio-inspired, smart, multiscale interfacial materials. Advanced Materials 20, 2842-2858 (2008).

101. Lee, H., Dellatore, S. M., Miller, W. M. & Messersmith, P. B. Mussel-inspired surface chemistry for multifunctional coatings. Science 318, 426-430 (2007).

102. Li, B., Liu, W., Jiang, Z., Dong, X., Wang, B. & Zhong, Y. Ultrathin and stable active layer of dense composite membrane enabled by poly(dopamine). Langmuir 25, 7368-7374 (2009).

103. Deshmukh, S. P. & Li, K. Effect of ethanol composition in water coagulation bath on morphology of PVDF hollow fibre membranes. Journal of Membrane Science 150, 75-85 (1998).

104. Cadotte, J. E., Petersen, R. J., Larson, R. E. & Erickson, E. E. A new thin-film composite seawater reverse osmosis membrane. Desalination 32, 25-31 (1980).

105. Khaled, M. Y. & McNair, H. M. Capillary zone electrophoretic separation of isomeric benzoic acids using cyclodextrin. Journal of High Resolution Chromatography 19, 143-150 (1996).

106. Lee, H., Scherer, N. F. & Messersmith, P. B. Single-molecule mechanics of mussel adhesion. Proceedings of the National Academy of Sciences 103, 12999-13003 (2006).

107. Elimelech, M., Zhu, X. H., Childress, A. E. & Hong, S. K. Role of membrane surface morphology in colloidal fouling of cellulose acetate and composite aromatic polyamide reverse osmosis membranes. Journal of Membrane Science 127, 101-109 (1997).

108. Meyer, E. A., Castellano, R. K. & Diederich, F. Interactions with aromatic rings in chemical and biological recognition. Angewandte Chemie International Edition 42, 1210-1250 (2003).

109. Suresh, S. J. & Naik, V. M. Hydrogen bond thermodynamic properties of water from dielectric constant data. The Journal of Chemical Physics 113, 9727-9732 (2000).

110. Grandbois, M., Beyer, M., Rief, M., Clausen-Schaumann, H. & Gaub, H. E. How strong is a covalent bond? Science 283, 1727-1730 (1999).

111. Produced Water Management Information System, US DOE: NETL. http://www.netl.doe.gov/technologies/pwmis/index.html.

112. Mickols, W. E. Composite membrane with polyalkylene oxide modified polyamide surface. United States Patent #6,280,853 (2001).

113. Niu, Q. J. Reverse osmosis membrane with branched poly(alkylene) oxide modified antifouling surface. United States Patent Application #11/380,776 (2007).

114. Childress, A. E. & Elimelech, M. Effect of solution chemistry on the surface charge of polymeric reverse osmosis and nanofiltration membranes. Journal of Membrane Science 119, 253-268 (1996).

115. Taylor, M., Urquhart, A. J., Anderson, D. G., Williams, P. M., Langer, R., Alexander, M. R. & Davies, M. C. A methodology for investigating protein adhesion and adsorption to microarrayed combinatorial polymers. Macromolecular Rapid Communications 29, 1298-1302 (2008).

116. Luria, S. E. & Burrous, J. W. Hybridization between Escherichia coli and Shigella. Journal of Bacteriology 74, 461-476 (1957).

117. Du, H., Chandaroy, P. & Hui, S. W. Grafted poly-(ethylene glycol) on lipid surfaces inhibits protein adsorption and cell adhesion. Biochimica et Biophysica Acta (BBA) - Biomembranes 1326, 236-248 (1997).

118. Jenney, C. R. & Anderson, J. M. Effects of surface-coupled polyethylene oxide on human macrophage adhesion and foreign body giant cell formation in vitro. Journal of Biomedical Materials Research 44, 206-216 (1999).

119. Kelly, S. T. & Zydney, A. L. Mechanisms for BSA fouling during microfiltration. Journal of Membrane Science 107, 115-27 (1995).

120. Ho, C.-C. & Zydney, A. L. Effect of membrane morphology on the initial rate of protein fouling during microfiltration. Journal of Membrane Science 155, 261-275 (1999).

121. Bowen, W. R. & Quan, G. Properties of microfiltration membranes: Flux loss during constant pressure permeation of bovine serum albumin. Biotechnology and Bioengineering 38, 688-696 (1991).

122. Mueller, J. & Davis, R. H. Protein fouling of surface-modified polymeric microfiltration membranes. Journal of Membrane Science 116, 47-60 (1996).

123. Kingshott, P. & Griesser, H. J. Surfaces that resist bioadhesion. Current Opinion in Solid State and Materials Science 4, 403-412 (1999).

124. Currie, E. P. K., Gucht, J. V. d., Borisov, O. V. & Stuart, M. A. C. Stuffed brushes: theory and experiment. Pure and Applied Chemistry 71, 1227-1241 (1999).

125. Efremova, N. V., Sheth, S. R. & Leckband, D. E. Protein-induced changes in poly(ethylene glycol) brushes: molecular weight and temperature dependence. Langmuir 17, 7628-7636 (2001).

126. Malmsten, M., Emoto, K. & Van Alstine, J. M. Effect of chain density on inhibition of protein adsorption by poly(ethylene glycol) based coatings. Journal of Colloid and Interface Science 202, 507-517 (1998).

127. Borcherding, H., Hicke, H.-G., Jorcke, D. & Ulbricht, M. Affinity membranes as a tool for life science applications. Annals of the New York Academy of Sciences 984, 470-479 (2003).

128. Ramamoorthy, M. & Ulbricht, M. Molecular imprinting of cellulose acetate-sulfonated polysulfone blend membranes for Rhodamine B by phase inversion technique. Journal of Membrane Science 217, 207-214 (2003).

129. Han, M.-J. Effect of propionic acid in the casting solution on the characteristics of phase inversion polysulfone membranes. Desalination 121, 31-39 (1999).

130. Ulbricht, M., Matuschewski, H., Oechel, A. & Hicke, H.-G. Photo-induced graft polymerization surface modifications for the preparation of hydrophilic and low-protein-adsorbing ultrafiltration membranes. Journal of Membrane Science 115, 31-47 (1996).

131. Kang, G., Liu, M., Lin, B., Cao, Y. & Yuan, Q. A novel method of surface modification on thin-film composite reverse osmosis membrane by grafting poly(ethylene glycol). Polymer 48, 1165-1170 (2007).

132. Hasegawa, T., Iwasaki, Y. & Ishihara, K. Preparation and performance of protein-adsorption-resistant asymmetric porous membrane composed of polysulfone/phospholipid polymer blend. Biomaterials 22, 243-251 (2001).

133. Higuchi, A., Sugiyama, K., Yoon, B. O., Sakurai, M., Hara, M., Sumita, M., Sugawara, S.-i. & Shirai, T. Serum protein adsorption and platelet adhesion on pluronic(TM)-adsorbed polysulfone membranes. Biomaterials 24, 3235-3245 (2003).

134. Reddy, A. V. R., Mohan, D. J., Bhattacharya, A., Shah, V. J. & Ghosh, P. K. Surface modification of ultrafiltration membranes by preadsorption of a negatively charged polymer: I. Permeation of water soluble polymers and inorganic salt solutions and fouling resistance properties. Journal of Membrane Science 214, 211-221 (2003).

135. Ahn, D. S., Jeon, I. S., Jang, S. H., Park, S. W., Lee, S. & Cheong, W. Hydrogen bonding in aromatic alcohol-water clusters: A brief review. Bulletin of the Korean Chemical Society 24, 695-702 (2003).

136. Halperin, A. Polymer brushes that resist adsorption of model proteins: design parameters. Langmuir 15, 2525-2533 (1999).

137. Nath, N., Hyun, J., Ma, H. & Chilkoti, A. Surface engineering strategies for control of protein and cell interactions. Surface Science 570, 98-110 (2004).

138. Lee, H., Rho, J. & Messersmith, P. B. Facile conjugation of biomolecules onto surfaces via mussel adhesive protein inspired coatings. Advanced Materials 21, 431-434 (2009).

139. Glater, J., Hong, S. K. & Elimelech, M. The search for a chlorine-resistant reverse osmosis membrane. Desalination 95, 325-345 (1994).

140. Neil, P. S., Adrian, C. M., Doreen, Y. T., Arlan, D. N., William, B. K. & Alan, R. G. Oxidative degradation of polyamide reverse osmosis membranes: Studies of molecular model compounds and selected membranes. Journal of Applied Polymer Science 90, 1173-1184 (2003).

141. Isaias, N. P. Experience in reverse osmosis pretreatment. Desalination 139, 57-64 (2001).

142. Solvay Advanced Polymers, Inc. http://www.solvayadvancedpolymers.com.

143. Brousse, C., Chapurlat, R. & Quentin, J. P. New membranes for reverse osmosis I. Characteristics of the base polymer: sulphonated polysulphones. Desalination 18, 137-153 (1976).

144. Drzewinski, M. & MacKnight, W. J. Structure and properties of sulfonated polysulfone ionomers. Journal of Applied Polymer Science 30, 4753-4770 (1985).

145. Allegrezza, A. E., Parekh, B. S., Parise, P. L., Swiniarski, E. J. & White, J. L. Chlorine resistant polysulfone reverse osmosis modules. Desalination 64, 285-304 (1987).

146. Vezzani, D. & Bandini, S. Donnan equilibrium and dielectric exclusion for characterization of nanofiltration membranes. Desalination 149, 477-483 (2002).

147. Szymczyk, A. & Fievet, P. Investigating transport properties of nanofiltration membranes by means of a steric, electric and dielectric exclusion model. Journal of Membrane Science 252, 77-88 (2005).

148. Matsuyama, H., Kim, M. M. & Lloyd, D. R. Effect of extraction and drying on the structure of microporous polyethylene membranes prepared via thermally induced phase separation. Journal of Membrane Science 204, 413-419 (2002).

149. http://www.surface-tension.de/.

150. Lee, C. H., Mccloskey, B. D., Lane, O., Freeman, B. D. & McGrath, J. E. Highly chlorine-resistant thin film composite membrane fabrication using a benign solvent for reverse osmosis applications. Unpublished manuscript (2009).

151. Parise, P. L., Allegrezza, A. E. & Parekh, B. S. Chlorine-resistant polysulfone reverse osmosis membrane and module. Ultrapure Water, 54-65 (1987).

152. Temmel, S., Kern, W. & Luxbacher, T. Zeta potential of photochemically modified polymer surfaces. Progress in Colloid and Polymer Science 132, 54-61 (2006).

153. Stakne, K., Smole, M. S., Kleinschek, K. S., Jaroschuk, A. & Ribitsch, V. Characterisation of modified polypropylene fibres. Journal of Materials Science 38, 2167-2169 (2003).

154. Zimmermann, R., Dukhin, S. & Werner, C. Electrokinetic measurements reveal interfacial charge at polymer films caused by simple electrolyte ions. The Journal of Physical Chemistry B 105, 8544-8549 (2001).

155. Kudin, K. N. & Car, R. Why are water-hydrophobic interfaces charged? Journal of the American Chemical Society 130, 3915-3919 (2008).

156. Urase, T., Oh, J.-i. & Yamamoto, K. Effect of pH on rejection of different species of arsenic by nanofiltration. Desalination 117, 11-18 (1998).

157. Vrijenhoek, E. M. & Waypa, J. J. Arsenic removal from drinking water by a "loose" nanofiltration membrane. Desalination 130, 265-277 (2000).

158. Nam, S. Y. & Lee, Y. M. Pervaporation and properties of chitosan-poly(acrylic acid) complex membranes. Journal of Membrane Science 135, 161-171 (1997).

159. Ghazali, M., Nawawi, M. & Huang, R. Y. M. Pervaporation dehydration of isopropanol with chitosan membranes. Journal of Membrane Science 124, 53-62 (1997).

160. Liu, Y.-L., Su, Y.-H., Lee, K.-R. & Lai, J.-Y. Crosslinked organic-inorganic hybrid chitosan membranes for pervaporation dehydration of isopropanol-water mixtures with a long-term stability. Journal of Membrane Science 251, 233-238 (2005).

161. Uragami, T., Kinoshita, H. & Okuno, H. Characteristics of permeation and separation of aqueous alcoholic solutions with chitosan derivative membranes. Angewandte Makromolekulare Chemie 209, 41-53 (1993).

162. Feng, X. & Huang, R. Y. M. Pervaporation with chitosan membranes. I. Separation of water from ethylene glycol by a chitosan/polysulfone composite membrane. Journal of Membrane Science 116, 67-76 (1996).

163. Huang, R. Y. M., Pal, R. & Moon, G. Y. Crosslinked chitosan composite membrane for the pervaporation dehydration of alcohol mixtures and enhancement of structural stability of chitosan/polysulfone composite membranes. Journal of Membrane Science 160, 17-30 (1999).

164. Ito, A., Sato, M. & Anma, T. Permeability of CO_2 through chitosan membrane swollen by water vapor in feed gas. Angewandte Makromolekulare Chemie 248, 85-94 (1997).

165. Gontard, N., Thibault, R., Cuq, B. & Guilbert, S. Influence of relative humidity and film composition on oxygen and carbon dioxide permeabilities of edible films. Journal of Agricultural and Food Chemistry 44, 1064-1069 (1996).

166. Lin, H. & Freeman, B. D. Gas solubility, diffusivity and permeability in poly(ethylene oxide). Journal of Membrane Science 239, 105-117 (2004).

167. Lin, H., Van Wagner, E., Freeman, B. D., Toy, L. G. & Gupta, R. P. Plasticization-enhanced hydrogen purification using polymeric membranes. Science 311, 639-642 (2006).

168. Wang, H., Ugomori, T., Wang, Y., Tanaka, K., Kita, H., Okamoto, K.-I. & Suma, Y. Sorption and pervaporation properties of crosslinked membranes of poly(ethylene oxide imide) segmented copolymer to aromatic/nonaromatic hydrocarbon mixtures. Journal of Polymer Science Part B: Polymer Physics 38, 1800-1811 (2000).

169. Tanaka, K., Kita, H., Okamoto, K.-i., Noble, R. D. & Falconer, J. L. Isotopic-transient permeation measurements in steady-state pervaporation through polymeric membranes. Journal of Membrane Science 197, 173-183 (2002).

170. Prof. Angel Lozano, Institute of Polymer Science and Technology, Department of Macromolecular Chemistry, Madrid, Spain, personal communication.

171. Rowe, B. W., Freeman, B. D. & Paul, D. R. Effect of sorbed water and temperature on the optical properties and density of thin glassy polymer films on a silicon substrate. Macromolecules 40, 2806-2813 (2007).

172. Huang, Y. & Paul, D. R. Effect of molecular weight and temperature on physical aging of thin glassy poly(2,6-dimethyl-1,4-phenylene oxide) films. Journal of Polymer Science Part B: Polymer Physics 45, 1390-1398 (2007).

VITA

Bryan David McCloskey attended the Colorado School of Mines from August, 1999 to May, 2003, and graduated with a B.S. in Chemical Engineering with High Honors. He was recognized as the most outstanding graduating Chemical Engineer in his class. His undergraduate research was performed under the guidance of J. Thomas McKinnon and Andrew M. Herring. He then enrolled in The University of Texas at Austin in August, 2003 to pursue a doctoral degree in Chemical Engineering under the guidance of Benny D. Freeman.

Permanent address: 3407 Apple Ave., Loveland, CO, 80538

This dissertation was typed by Bryan David McCloskey.